DYNAMIC COUPLING OF SOFT-SUSPENSION REACTION WHEEL ASSEMBLY AND SATELLITE ATTITUDE CONTROL SYSTEM

By

Lillian Chen

A Thesis

Presented to

The Faculty of Engineering

The Department of Aerospace Engineering

The University of Auckland

In Partial Fulfilment

of the Requirements for the Degree

Master of Aerospace Engineering

February 2023

ACKNOWLEDGEMENTS

Firstly, the author would like to thank people from the University of Auckland for providing her with great opportunities and assisting her throughout her one-year master's program in Aerospace Engineering.

The author wishes to express her deepest gratitude to her supervisor Professor Guglielmo S. Aglietti for this guidance, advice, encouragement, and insight throughout the study. Without his guidance and support the author could not accomplish what she has achieved on this project.

Special thanks to Mattia Longato and Thomas Thomas Hughes for helping me throughout the project. Their enthusiasm and willingness to provide knowledge on the reaction wheel assemblies and MATLAB programming have given the project a lot of guidance. The meeting and discussions with them helped me resolve a lot of problems and the author highly appreciated their assistance.

Finally, I would like to thank my family, the Kwon family and friends for their constant support and motivation throughout this year of studying. Without them, I would have never finished this thesis.

ABSTRACT

This paper focuses on the investigation of the dynamic coupling effect induced in soft suspension reaction wheel assembly and the relation with the pointing error of the satellite. Different soft suspension parameters are compared against a rigid body reaction wheel to analyse the performance of the satellite. A quaternion feedback controller is further designed to compensate for and minimise the pointing error. The designed controller is evaluated by the performance in the signal noise, rise time, and final output signal.

A mathematical model of the relation between the dynamic of the satellite and the soft suspension reaction wheels is presented. The mathematical model of the gyroscopic effect for a soft suspension reaction wheel is further derived from the dynamic model. Simulations are established according to the mathematical models to enable visualisation of the behaviour of the satellite and reaction wheels. The validity of the simulation is justified by the mathematical model. A soft suspension reaction wheel with moderate stiffness (20 Hz) and a soft suspension reaction wheel with lower stiffness (4 Hz) are simulated, and the results are compared against the simulation results with a rigid body reaction wheel. With the desired output to be the Agi Satellite manoeuvre of $7\,°/sec$ for 30 seconds, the pointing error of each satellite compared against a rigid body reaction wheel configuration is 0.188 degrees and 2 degrees.

The pointing error of the satellite is reduced through the designed quaternion feedback controller with a PID controller. Ziegler-Nichols Closed-Loop tuning method is used to determine the gains for the PID controller. The simulation results indicate that with the controller, the pointing error of the satellite with a lower stiffness is not eliminated, but the error decreased to 0.56 degrees.

Finally, conclusions were taken from the simulation findings, and suggestions for further research were made.

Table of Contents

ACKNOWLEDGEMENTS 1

ABSTRACT 2

LIST OF TABLES 7

LIST OF FIGURES 8

ACRONYMS 11

CHAPTER 1 1

INTRODUCTION 1

1.1 Theoretical Background 1

1.1.1 Small Satellite 1

1.1.2 Pointing Accuracy and Stability of Satellite 1

1.2 Objectives of Research 3

1.3 Outline of the Thesis 4

CHAPTER 2 6

LITERATURE REVIEW 6

2.1 Attitude Control for Small Satellite 6

2.1.1 Thrusters 6

2.1.2 Magnetic Torquers 7

2.1.3 Control Moment Gyros 8

2.2 Reaction Wheel for Attitude Control 8

2.2.1 Reaction Wheels Assemblies 9

2.2.2 Wheel Assembly-Induced Micro-vibrations 10

2.3 Soft-Suspension Reaction Wheel System 11

2.4.1 Soft-Suspension Reaction Wheel 11

2.4.2 Soft Suspension Reaction Wheel Model 12

2.4.3 Dynamic Coupling 13

CHAPTER 3 14
MATHEMATICAL MODELLING 14
3.1 Introduction 14
3.2 Definitions and Notations 15
3.2.1 Rotation Matrix 15
3.2.2 Inertia Matrix 18
3.3 Soft-Suspension Reaction Wheels 19
3.3.1 Reaction Wheel Distribution Matrix 19
3.3.2 Soft-Suspension Reaction Wheel Parameters 20
3.3.3 Soft Suspension Reaction Wheel Stiffness 21
3.4 Equation of Motions 21
3.4.1 Euler Moment Equations 21
3.4.2 Euler Equations with Coriolis Theorem 22
3.4.3 Gyroscopic Effect 23
3.5 Orthogonal 3-wheel Configuration Modelling 24
3.5.1 CASE STUDY 1: Single Wheel Acceleration 24
3.5.2 CASE STUDY 2: Single Wheel Acceleration with Two Constant Wheel Velocity 26
CHAPTER 4 31
MODEL SIMULATION and RESULTS 31
4.1 Introduction to MATLAB/Simulink 31
4.1.1 ODE Solver 32
4.1.2 Step Sizes 33
4.2 Introduction to Simscape Multibody Toolbox 34
4.3 General Structure of the Simspace Multibody Model 34
4.4 Design of Rigid Body Reaction Wheel Satellite Model 36

4.4.1 Simscape Model 36
4.4.2 Mechanics Explorers 38
4.4.3 Design Validation 39
4.5 Design of Soft-Suspension Reaction Wheel Satellite Model 41
4.5.1 Simscape Model 41
4.5.2 Mechanics Explorers 43
4.5.3 Wheel Oscillation Verification 44
4.5.4 Offset Reaction Wheel Placement 47
4.6 Results and Discussions 48
4.6.1 CASE STUDY 1: 20 Hz Soft-Suspension Reaction Wheels 48
4.6.2 CASE STUDY 2: 4 Hz Soft-Suspension Reaction Wheels 50
4.7 Satellite Pointing Accuracy 52
CHAPTER 5 57
CONTROL DESIGN and SIMULATIONS 57
5.1 Quaternion Feedback Controller (PID Controller) 57
5.1.1 Design Method 57
5.1.2 Tuning of Controller 59
5.1.3 Controller Output 61
5.2 Results and Discussions 61
5.2.1 Reference Trajectory 61
5.2.2 Rigid Body Reaction Wheel Satellite Configuration 62
5.2.3 Soft Suspension Reaction Wheel Satellite Configuration 63
Chapter 6 66
CONCLUSION and FUTURE WORK 66
6.1 Conclusion 66
6.2 Recommendations for Future Work 67

BIBLIOGRAPHY 71

APPENDIX 75

Appendix A: Verification of Mathematical Model MATLAB Script .. 75

Appendix B: Validation of Rigid Body Reaction Wheel Simulink Model MATLAB Script 81

Appendix C: Case Study (20 Hz and 4 Hz) MATLAB Script..... 85

Appendix D: Pointing Error Comparison Between Different Reaction Wheel MATLAB Script..... 87

Appendix E: Pointing Error Comparison Between Different Reaction Wheel Test Case 2..... 92

Appendix F: Pointing Error Calculation with Range of Different Frequencies MATLAB Script..... 95

Appendix G: Study of Campbell Diagram MATLAB Script 97

Appendix H: Controller gain Calculation and Simulation MATLAB Script..... 98

LIST OF TABLES

Table 1: Initial condition of Case Study 1: Single Wheel Acceleration 24

Table 2: Initial condition of Case Study 2: Single wheel acceleration with two constant wheel velocity 26

Table 3: Initial condition of the simulation for design validation 39

Table 4: Input frequency compared to the simulated frequency of the reaction wheel 47

Table 5: Initial condition of Case Study 1: 20 Hz Soft-Suspension reaction wheels 49

Table 6: Comparison of wheel velocity and oscillation of satellite body 56

Table 7: The Ziegler-Nichols PID controller parameters from closed-loop experiments [6] 60

LIST OF FIGURES

Figure 1: Effects of micro-vibrations on geometric distortions 2

Figure 2: Propagation of micro-vibrations on satellites 2

Figure 3: Cross-section of a soft suspension reaction wheel assembly 3

Figure 4:Illustration of a thruster in relation to the satellite body [7] 7

Figure 5:Structure of a control moment gyro [2] 8

Figure 6: Structure of a reaction wheel [12] 9

Figure 7:Reaction wheels with a pyramidal layout [2] 10

Figure 8: Structure of a soft suspension reaction wheel at a neutral position [14] 11

Figure 9: Structure of a cantilever-configured soft suspension reaction wheel [13] 12

Figure 10: The dynamic imbalance and static imbalance of the reaction wheel [1] 13

Figure 11: Model of the soft suspension reaction wheel in Simulink 14

Figure 12: The rotation of the satellite in relation to Euler angles 17

Figure 13: Rotation of a point with the defined quaternion 18

Figure 14: A standard orthogonal 3-wheel configuration 20

Figure 15: The structure of the soft suspension reaction wheel used in the thesis [13] 21

Figure 16:Input profile of Case Study 1: Single wheel acceleration 25

Figure 17: Satellite behaviour of Case Study 1: Single wheel acceleration 26

Figure 18: Input profile of Case Study 2: Single wheel acceleration with two constant velocity wheels 27

Figure 19: Satellite behaviour of Case Study 2: Single wheel acceleration with 2 constant velocity wheels 28

Figure 20: Gyroscope effect for reaction wheel 1 in each axis 29

Figure 21: Gyroscope effect for reaction wheel 2 in each axis 29

Figure 22: Gyroscope effect for reaction wheel 3 in each axis 30

Figure 23: Simulink library components for block model creation 32

Figure 24: Configuration parameters function in Simulink 33

Figure 25: Elements of the current Simscape library 34

Figure 26: Overall configuration of the Simspace multibody model of the satellite and reaction wheels 35

Figure 27: Satellite sub-system of the Simscape model 36

Figure 28:Shafts sub-system of the Simscape model 36

Figure 29: Rigid body reaction wheel sub-system of the Simcape model 37

Figure 30:Block design of the reaction wheel 38

Figure 31: Input profile sub-system of the Simscape model 38

Figure 32: Mechanics Explorer of the developed rigid body reaction wheel satellite configuration 39

Figure 33: Angular displacement of the rigid model and mathematical model 40

Figure 34: Simulation results of the satellite acceleration 41

Figure 35: Simscape model of soft suspension reaction wheel configuration 42

Figure 36:MATLAB script to calculate the parameters for the simulation 43

Figure 37: Block parameters of the gimbal joint 43

Figure 38: Mechanics Explorer of the developed soft suspension reaction wheel satellite configuration 44

Figure 39: Satellite model with corresponding reaction wheel placement **Error! Bookmark not defined.**

Figure 40:The simulation input profile for each reaction wheel 46

Figure 41: Simulation result of the angular displacement of each wheel (20 Hz) 46

Figure 42: Mechanics Explorer of the developed offset reaction wheel satellite configuration 47

Figure 43: Difference in angular displacement between different reaction wheel placement 48

Figure 44: Model orientation of the 20 Hz soft suspension configuration at the end of simultion period **Error! Bookmark not defined.**

Figure 45: Input rpm profile from signal builder 50

Figure 46: Simulation results of angular displacement of each wheel (20 Hz) 50

Figure 47: Model orientation of the 4 Hz soft suspension configuration at the end of simultion period **Error! Bookmark not defined.**

Figure 48: Simulation results of angular displacement of each wheel (4 Hz) 51

Figure 49: Simulation results of difference in angular displacement of the satellite with soft suspension reaction wheels (4 Hz, 20 Hz, 200Hz) with rigid body reaction wheels 53

Figure 51:Campbell diagram for a 4 Hz soft suspension reaction wheel model 55

Figure 52: Overall Simulink model of the satellite system with a quaternion feedback controller 57

Figure 53: Controller sub-system of the control design model 58

Figure 54: Actuator sub-system of control signal conversion of the control system model 59

Figure 55: Input profile sub-system of the control system model 61

Figure 56:PID controller performance evaluation between simulation results and reference trajectory of the satellite (Rigid body) 63

Figure 57: PID controller performance evaluation between simulation results and reference trajectory of the satellite (Soft suspension) 64

Figure 58: PID controller performance evaluation between simulation results and reference trajectory of the satellite (Rigid body and soft suspension) 64

ACRONYMS

ACS	Attitude Control System
CAD	Computer-Aids Design
CMG	Control Moment Gyro
CoM	Center of mass
COTS	Commercial-off-the -shelf
DC	Direct Current
DoF	Degrees of Freedom
Eq.	Equation
LEO	Low Earth Orbit
LQR	Linear Quadratic Regulation
MPC	Model Predictive Control
ODE	Ordinary Differential Equations
PID	Proportional Integral Derivative
P-POD	Poly-PicoSatellite Orbital Deployer
rpm	revolutions per minute
RWA	Reaction wheel assembly

CHAPTER 1

INTRODUCTION

This chapter briefly introduces information about soft-suspension reaction wheel assembly in small satellites. The importance of the effect of dynamic coupling in relation to the pointing error of the satellite is presented. Furthermore, the objective of this Master's thesis is introduced. Finally, the outline of the thesis is given.

1.1 Theoretical Background

1.1.1 Small Satellite

Small satellites are developed to provide affordable access to space for research and remote sensing purposes. The standardised aspects of small satellites enable accessibility to commercial off-the-shelf (COTS) components and mass-produced components, significantly reducing the cost. Small satellite is defined for all satellites with a launch mass of less than 1000 kg, while further sub-classifications depend on the range in which the small satellite corresponds [7]. For example, a small satellite with a 10-100 kg launch mass is classified as a microsatellite. This classification method provides a good indication of the launch costs of the satellite.

With the growth in technology, sensors, actuators, and propulsion has decreased in size with higher performance. These characteristics enable the small satellite to perform applications in which larger satellites perform mainly around the Low Earth Orbit (LEO) at an altitude of 160 km to 2000 km [5]. This range is primarily used by commercial use for transportation, communication, observation, and resupply. Replacing large satellites with small satellites allows scalable and flexible missions since small satellites can be produced and launched in relatively short terms and at lower costs.

1.1.2 Pointing Accuracy and Stability of Satellite

The stability and accuracy of the satellite are significantly impacted by the micro-vibrations of the satellite, especially in the field of earth observation and space astronomy. For example, Figure 1 demonstrates the effects of satellite micro-

vibrations on the quality of an image captured by the telescope onboard the satellite, ALSAT-1B. The distortions of the image can be observed as zigzag patterns on geometrically straight features from an image taken from ALSAT-1B. Thus, it is essential to increase the satellite structure stability by minimising the micro-vibration of the satellite for satellites carrying highly sensitive payloads such as telescopes, cameras, and sensors.



Figure 1: Effects of micro-vibrations on geometric distortions

Micro-vibration is defined as the low-level mechanical disturbances affecting payload performance (typically occurring at frequencies from 1 Hz to 1000 Hz). A range of equipment on the satellite acts as micro-vibrations sources which can generate low-level mechanical vibration. High-speed rotation devices such as reaction wheel assemblies (RWAs) and momentum wheel assemblies (MWAs) generate crucial micro-vibrations which affect the stability of the satellite. The instrument's performance is impacted by the micro-vibrations produced by these sources, which are transmitted via the satellite structure and excite the instrument's structure or other components. Thus, controlling the induced micro-vibration from the RWAs is important to achieve the desired satellite performance. The relation between the micro-vibration transmission process is illustrated in Figure 2.



Figure 2: Propagation of micro-vibrations on satellites

To minimise the micro-vibration generated by the RWAs, a cantilever configured Wheel Assembly with a soft-suspension system is used. A soft-suspension reaction wheel assembly incorporates a spring structure that suspends the rotor and motor shown in Figure 3. This configuration is able to attenuate the undesired mechanical disturbance transfer to the satellite structure. A wheel supported by a soft-suspension system provides both rotational and translational support to the system. The soft-suspension wheel can be used as a passive system that filters the micro-vibrations produced by the motor.

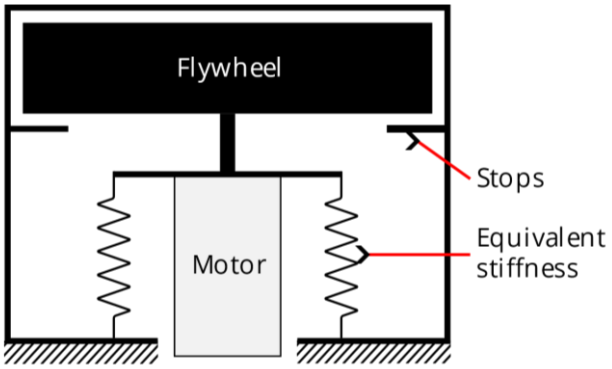


Figure 3: Cross-section of a soft suspension reaction wheel assembly

The introduction of the soft-suspension results in a dynamic coupling condition between the attitude control system and the satellite. The presence of dynamic coupling means there are attitude control system uncertainties which can affect the stability and accuracy of the satellite. Point accuracy has increased significantly over the last decade as satellite instruments requiring a higher level of accuracy have been employed. The performance of the satellite is significant for high-level pointing accuracy missions such as optical/imaging, which are high-accuracy-required missions. Additionally, minimising the pointing error is essential for inter-satellite laser communications. Misalignment between the transmitter and the receiver causes a highly vulnerable link between long-distance inter-satellite laser communication [16].

1.2 Objectives of Research

The main objective of this thesis is to provide a methodology to model the dynamic coupling of the soft-suspension reaction wheel and simulate the model with a real-world scenario to further interpret the pointing error caused by the dynamic coupling effect. In order to address the pointing error issue derived from

the dynamic coupling effect, an investigation of a controller to compensate for this issue is developed. In particular, the focus of this thesis is on the modelling of the soft-suspension RWAs and the design of a controller to compensate for the effect of dynamic coupling.

In order to achieve the goal, the research methodology followed the three steps:

I. Dynamic coupling effect analysis; in this part of the work, the mathematical model of the soft-suspension RWAs is developed to characterise the theoretical behaviour of the satellite manoeuvre.

II. Model development and simulation; in this part of the work, the author developed the model of a standard orthogonal 3-wheel configuration satellite. Different cases with typical satellite manoeuvre profiles are tested and further evaluated the performance with the effect of soft-suspension RWAs. The impact of the dynamics coupling can be determined by comparing the pointing error of the soft-suspension RWAs with the rigid-body RWAs.

III. Controller design of the soft-suspension RWAs; in this part of the work, different controller methodologies are studied. The final design of a quaternion feedback controller with a PID controller is developed and optimised to improve the accuracy of the soft-suspension RWAs.

1.3 Outline of the Thesis

The outline of the dissertation is as follows:

Chapter 1, the current chapter, is the introduction which presents the background, motivation, and objectives of the thesis work. More in detail, following from the introduction presented in the current chapter, in Chapter 2, soft-suspension reaction wheel system studies in the literature are reviewed.

Chapter 3 provides definitions and notations to describe the various notations used throughout the report and some fundamental definitions are presented. Mathematical models are then derived to provide a representation of the satellite with kinematics and dynamics equations. Moreover, reaction wheel assembly configurations with case studies are mentioned.

Chapter 4 includes the simulation and results of the satellite body with soft-suspension reaction wheels assembly. The results are also compared against the rigid reaction wheel assembly model to determine the pointing error of the soft-suspension reaction wheel assembly model.

In Chapter 5, a control system is implemented in the model to minimise the pointing error of the soft-suspension reaction wheel assembly model. A quaternion feedback controller with a PID controller is designed, tuned, and integrated with the designed model in Chapter 4. The simulation output is compared against the reference trajectory to determine the accuracy of the designed controller.

The final chapter, chapter 6 (Conclusions and Future Work), summarises the work presented in the dissertation and provides further directions for this work. The thesis concludes by recounting the main aspects of the work done by the author and the research team and the new perspectives that the present research work has opened in the field.

CHAPTER 2

LITERATURE REVIEW

In this chapter, the different types of attitude control for satellites are introduced, in particular the reaction wheel attitude control. Furthermore, the properties of a soft-suspension reaction wheel are presented. Lastly, the dynamic coupling effect with the reaction wheel assembly is discussed.

2.1 Attitude Control for Small Satellite

The development of an attitude control system for small spacecraft is an area of interest in which NASA does intense research due to the increased usage of small satellites for various missions/payloads [18]. The high pointing accuracy of the small satellites is required for missions such as a three-axis stabilised satellite required to point the instruments to the desired location, and a small communication satellite is required to have high pointing accuracy to ensure precise antenna location. With the current implemented attitude control devices used for larger satellites are needed to be further developed to minimise the pointing error.

The standard tolerance for pointing error is less or equal to 1 degree for a spin or three-axis stabilised satellite [14]. An attitude control system (ACS) generates torque to the spacecraft to maintain the required orientation and minimise the pointing error [18]. An ACS is designed to compensate for the undesired angular rotations caused by the errors and uncertainties in the alignment of the components within the body of the satellite. The ACS should further eliminate small perturbation torques caused by magnetic, gravitational and atmospheric drag [17]. Different actuators are used as attitude control devices for small satellites and are mainly classified into reaction-type actuators and momentum exchange devices [10].

2.1.1 Thrusters

Thrusters eject mass to create a force in which the thruster vector that did not pass through the spacecraft's centre of mass (CoM) generates a torque in the spacecraft's body. The amount of torque the thruster produces can be adjusted depending on the force and the moment arm which is determined by the placement

of the thruster. This is illustrated in Figure 4, where a thruster with force F with a moment arm r gives a torque T on the satellite body [9].

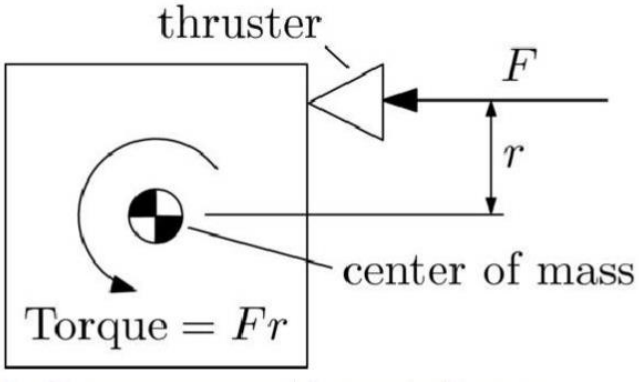


Figure 4:Illustration of a thruster in relation to the satellite body [9]

Due to this configuration, a thruster can only generate torque in a single axis and a single direction. Thus, the standard configuration is coupled thrusters on each of the three axes to ensure the controllability and stabilisation of the whole system.

2.1.2 Magnetic Torquers

Magnetic torquers are built from electromagnetic coils where the rotational asymmetric magnetic field is created. A magnetic dipole is created by controlling the current flow through the coils [9]. Since the magnet is attached to the spacecraft, the magnetic force from the magnetic dipole is exerted into the surrounding magnetic field (Earth magnetic field), causing a magnetic reverse force resulting in the torque in the spacecraft body [9]. The generated torque can be calculated using the formula $\tau = m \times B$, where m is the magnetic dipole generated by the magnetic torque, and B is the Earth's magnetic field vector.

A three-coil assembly with three perpendicular coils is typically used as a magnetic torquer configuration. The configuration creates an equalisation of the rotational symmetry of the generated magnetic field. With the configuration, it means the orientation of the Earth's magnetic field with respect to the spacecraft does not impact the total torque produced by the magnetic torquer since the total torque can be controlled by applying different current densities on the three different coils.

Due to the weak Earth's magnetic field, the amount of torque generated by a magnetic torquer is limited to achieve rapid and large manoeuvres, high magnetic

flux densities are required meaning high current is required, which can cause other issues such as overheat of the spacecraft [9]. Thus, the total torque that can be provided with a magnetic torquer is limited and can support a small amount of controllability. Magnetic torquer cannot be used for precise attitude control due to insufficient ability for accurate attitude control and stabilisation. To overcome this issue, magnetic torquers are often used incorporated with a reaction wheel to minimise the inaccuracy of attitude control.

2.1.3 Control Moment Gyros

A control moment gyro (CMG) is a spinning rotor in combination with one or more motorised gimbals to achieve a tilt in the angular momentum of the rotor shown in Figure 5 [2]. When an inclination in the rotor, the change in angular momentum generates a gyroscopic torque in the spacecraft and rotates the body. The tilt of the rotor axis is not dependent on the spin speed of the rotor, meaning that the torque produced by the CMG is not dependent on the rotational speed of the rotor.

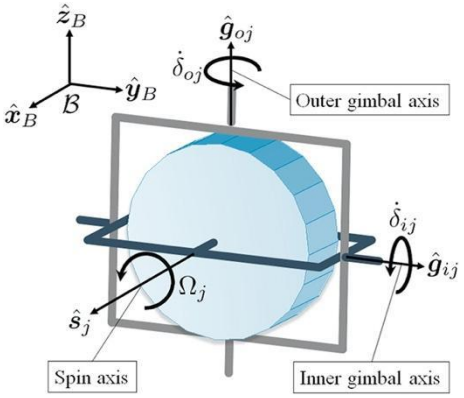


Figure 5:Structure of a control moment gyro [2]

The most commonly used CMG utilises a single gimbal. When the gimbal rotates and changes the direction of the rotor's angular momentum, a counter torque is created on the spacecraft body to oppose the torque generated by the CMGs [2]. Thus, causing the spacecraft body to rotate and attitude control through controlling the torque generated by the CMGs.

2.2 Reaction Wheel for Attitude Control

A reaction wheel is a type of actuator used to control the attitude and pointing of satellites, especially for precise rotation [17]. The typical structure of a

reaction wheel is shown in Figure 6, in which a brushless DC motor drives the flywheel, which is mounted on a shaft supported with bearings [16]. Since reaction wheels rotate a spacecraft only around its centre of mass meaning it provides angular control of the spacecraft and does not affect the linear motion of the spacecraft. The housing cover provides protection for the components.

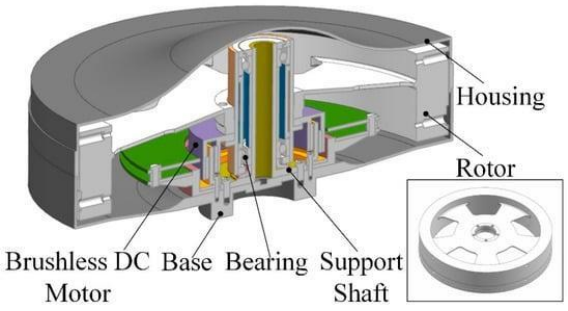


Figure 6: Structure of a reaction wheel [12]

The reaction wheel operates based on the conservation of angular momentum law [10]. The nominal speed of a reaction wheel typically operates around several thousand revolutions per minute (rpm) and can spin both counter-clockwise and clockwise. The change in rotational speed of the reaction wheel causes the spacecraft to counter-rotate proportionally to conserve the angular momentum [10]. Through this operation mechanism, the reaction wheel is operated without requiring positioning thrusters or external applicators of torque. This means no additional resources are required to power the actuator, significantly reducing the satellite payload.

2.2.1 Reaction Wheels Assemblies

Three or more reaction wheels are often equipped within a spacecraft, forming a reaction wheel assembly (RWAs). An assembly of four is typically used for redundancy. This is for the purpose of active redundancy as well as increasing the maximum available torque and momentum [2]. The most used reaction wheel configuration is the pyramidal layout in which the four reaction wheels are arranged, shown in Figure 7 [2]. This layout is suitable for the Earth-pointing spacecraft, which is required to point on-board instruments towards the Earth's surface.

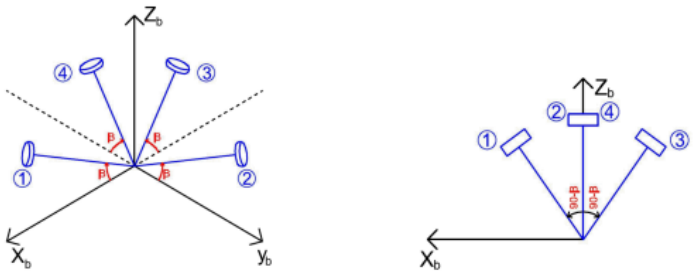


Figure 7:Reaction wheels with a pyramidal layout [2]

A six-wheel layout is implemented to operate satellites which require large inertia (meteorological satellites) or platforms with high pointing accuracy [2]. The six-wheel RWAs enable even distributed spin axes, thus, minimising disturbances caused by reaction wheel imbalances.

2.2.2 Wheel Assembly-Induced Micro-vibrations

During the operation of RWAs, continuous high amplitude and high-frequency micro-vibrations are induced. The micro-vibrations can be induced from three main reaction wheel structural-related factors: mass imbalances of the flywheel, including static and dynamic mass imbalances in which both generate micro-vibrations at a fundamental frequency of the angular speed; bearing irregularities caused by lubricant dynamics and irregularities in the balls, races, and cage of the bearing; motor irregularities such as DC motor noise from ripple and cogging [23].

Through multiple experiments, the frequency and the magnitude of the micro-vibrations have a correlation with the angular speed of the spinning flywheel [17]. Thus, when the RWAs operate at critical speeds, resonances occur, causing the amplified response of micro-vibrations. The magnitude of the amplified micro-vibrations can cause critical damage to the flywheel and the whole spacecraft.

The total excitations of micro-vibrations in RWAs are caused by harmonic excitations and broadband excitations [23]. When applied linear assumption, the excitations can be superimposed as the total input excitations to the RWA structural model [23]. Through this, predictions can be made for the generated micro-vibrations in the system for further analysis and control of the micro-vibration minimisation.

2.3 Soft-Suspension Reaction Wheel System

2.4.1 Soft-Suspension Reaction Wheel

The standard RWAs are rigidly designed in which the mechanical structure of the reaction wheels is sized to resist the forces applied during launch. The rigid reaction wheel provides sufficient stiffness to enable the resonant frequency which achieves the requirements of the spacecraft [22]. A soft-suspension reaction wheel assembly incorporates a spring structure that suspends the rotor and motor. The configuration of a soft-suspension reaction wheel at a neutral position is shown in Figure 8 [21].

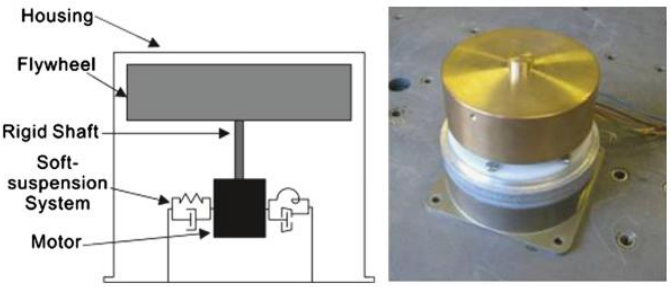


Figure 8: Structure of a soft suspension reaction wheel at a neutral position [21]

During the launch of the spacecraft, the deflection causes the gaps between the flywheel and the housing to close until contact between the two components. The deflection is determined by the stiffness of the soft suspension system which is investigated and optimised in the study with more detail by Zhang, Z. (2013). This minimises the direct load applied to the housing and the overall structure of the spacecraft. Thus, with the implementation of soft-suspended RWAs, the required load support during the launch is minimised for the design of the bearings and the shaft for the reaction wheels [22]. During the operation of the spacecraft, unwanted mechanical disturbances described in *section 2.2.2* are attenuated through the soft suspended RWAs structure.

The introduction of the soft suspension system results in a dynamic coupling condition between the attitude control system and the satellite. An increase in the requirement for high pointing accuracy for satellites is needed. Thus, it is essential to gain an understanding of the effect of soft suspension on pointing accuracy.

2.4.2 Soft Suspension Reaction Wheel Model

Through simplification of the structure, the cantilever configured soft suspension reaction wheel in the hard-mounted boundary condition is shown in Figure 9 [20]. The model represents the given structural modes of the RWA and includes the gyroscopic effects of the flywheel.

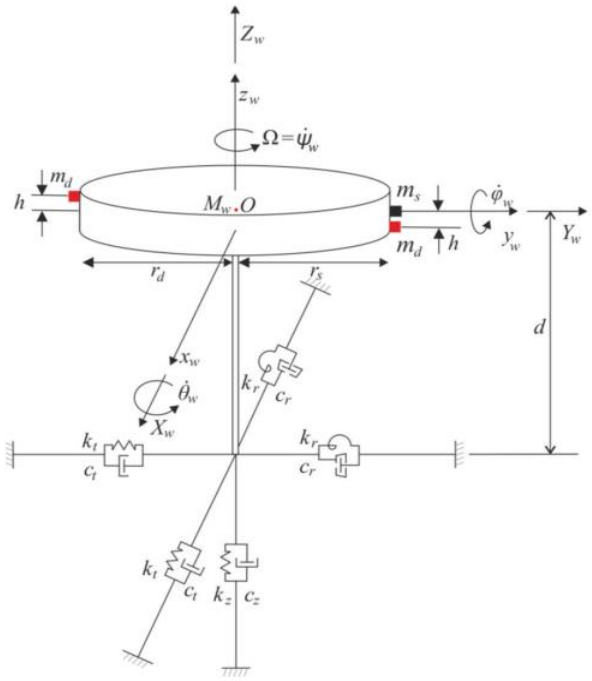


Figure 9: Structure of a cantilever-configured soft suspension reaction wheel [20]

At the CoM of the flywheel, the inertial frame, $X_wY_wZ_w$, and the body frame, $x_wy_wz_w$ coincide. The rotation of the body occurs about the three axes $\theta_w, \varphi_w,$ and ψ_w. By assuming constant angular velocity, Ω, $\Omega = \dot{\psi}_w$. The mass of the flywheel is defined as M_w and the rigid shaft is assumed to be massless with a length d to the soft-suspension system.

Due to the cantilevered configuration, the RWA is assumed to be axisymmetric about the shaft where the flywheel is modelled at one side of the suspension system. The system is modelled as a combination of five DoFs, including two pairs of linear spring and dashpot and two pairs of torsional spring and dashpot. The asymmetry of the system means the linear spring stiffness, k_t, is the same in the two-radial translational DoFs, as well as the torsional spring stiffness, k_r, and dashpot damping coefficients, c_t and c_r [20].

2.4.3 Dynamic Coupling

In fixed RWAs, the attitude control axis of the reaction wheel assembly is fixed with respect to the satellite axis. The inclusion of a soft suspension allows the rotor torque axis to deviate from the satellite axis and causes imbalances in the reaction wheel [1]. This results in non-direct torque and an internal force and torque on the spacecraft. Hence the problem of a non-static coupling of applied torque is introduced. The asymmetric mass distribution along the reaction wheel spin axis indicates the dynamic imbalance and produces an internal disturbance torque onto the spacecraft. Figure 10 illustrates the inequalities geometrically [1].

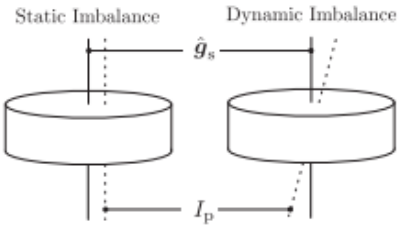


Figure 10: The dynamic imbalance and static imbalance of the reaction wheel [1]

Having a dynamic coupling between the RWAs and the satellite body results in an on-direct application of torque, resulting in point accuracy and pointing stability problems. Dynamic coupling introduces attitude control system uncertainty; thus, modelling allows the prediction of soft-suspension effect on RWAs offset.

CHAPTER 3

MATHEMATICAL MODELLING

The orientation of the satellite and its mathematical model can be derived in different frames including the gyroscopic effect of the soft-suspension reaction wheel. This chapter presents some definitions and notations used throughout the thesis. Furthermore, a mathematical model of the dynamics and kinematics of satellites is derived in this chapter. Also, the satellite's environment is described in detail.

3.1 Introduction

The dynamic equations for a spacecraft with reaction wheels are derived in this part, with careful consideration given to the underlying assumptions on the wheel geometry, inertia, and attachment to the spacecraft bus. As depicted in Figure 11, it is assumed that a rigid satellite has three soft-suspension reaction wheels attached to it. The rigid satellite is represented by the grey cube and each of the reaction wheel are the hollowed yellow cylinder. Every wheel has a mounting arrangement that allows it to rotate freely about one of its principal axes, which passes through its mass centre. In this project, it is assumed that the mass distribution of each wheel is symmetric about its axis of rotation.

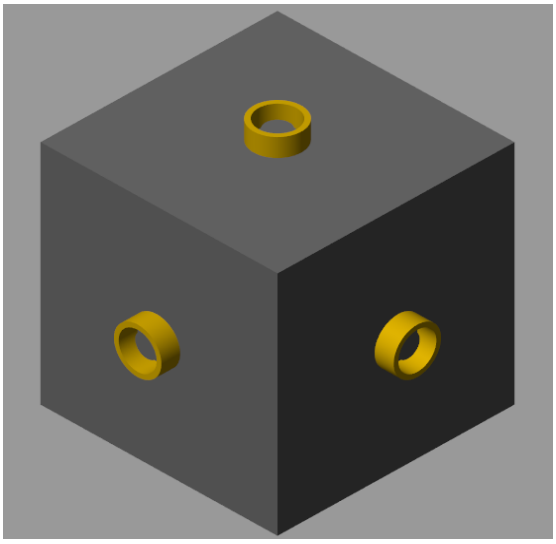


Figure 11: Model of the soft suspension reaction wheel in Simulink

3.2 Definitions and Notations

3.2.1 Rotation Matrix

A rotation matrix can be described as a transformation matrix that transforms a vector into a rotated vector while maintaining fixed coordinate axes. These matrices rotate a vector by an angle in the anticlockwise direction. A square matrix with real entities is what a rotation matrix is. This indicates that the number of rows and columns will always be equal.

The rotation matrix R from frame a to b is denoted, R_a^b. Rotation of a vector from one frame to another frame can be given using R_a^b as:

$$v^{to} = R_{from}^{to} v^{from}$$

(1)

Additionally, rotation matrices have an orthogonal structure and a determinant of 1. Assume that R is a square matrix. Then, and only then, will R be a rotation matrix if $R^T = R^{-1}$ and $|R| = 1$.

$$R_B^A = (R_A^B)^{-1} = (R_A^B)^T$$

(2)

$$R_B^A R_A^B = 1_{3x3}$$

(3)

The direction of the satellite can be described using a rotation matrix R_B^A, where R_B^A represent:

$$R_B^A = [c_{11}\ c_{12}\ c_{13}\ c_{21}\ c_{22}\ c_{23}\ c_{31}\ c_{32}\ c_{33}\ ]$$

(4)

The column vectors are cosines of the angles between the two frames. Each of the element c_{ij} is named directional cosines, and column vectors can be arranged as:

$$c_1 = [c_{11}\ c_{21}\ c_{31}\ ] \quad c_2 = [c_{12}\ c_{22}\ c_{32}\ ] \quad c_3 = [c_{13}\ c_{23}\ c_{33}\ ]$$

(5)

Moreover, the rotation matrix is orthogonal and because of the orthogonality c_1, c_2, and c_3 are orthonormal.

$$c_1 \times c_2 = c_3 \quad c_2 \times c_3 = c_1 \quad c_3 \times c_1 = c_2$$

(6)

3.2.1.1 Euler Angles

The Euler Angles are a typical collection of angles that characterise the body frame of a spacecraft in relation to the inertial frame. A vector in the inertial frame is transformed into the body frame using a series of three specific rotations. Using roll (ϕ), pitch (θ) and yaw (ψ) angles, three parameters can represent the attitude. The x, y and z axis can be defined as ϕ, θ and ψ respectively, in a frame-to-frame rotation, which are the Euler Angles, Θ.

$$\Theta = [\phi \; \theta \; \psi \;]$$

(7)

Thus, the rotation matrices can be defined as:

$$R_{x,\phi} = [1\ 0\ 0\ 0 \;\; cos\ cos\ \phi \;\; -sin\ sin\ \phi \;\; 0 \;\; -sin\ sin\ \phi \;\; cos\ cos\ \phi \;\;]$$

(8)

$$R_{y,\theta} = [cos\ cos\ \theta \;\; 0 \;\; sin\ sin\ \theta \;\; 0\ 1\ 0\ \theta \;\; 0 \;\; cos\ cos\ \theta \;\;]$$

(9)

$$R_{z,\psi} = [cos\ cos\ \psi \;\; \psi \;\; 0 \;\; sin\ sin\ \psi \;\; cos\ cos\ \psi \;\; 0\ 0\ 0\ 1\ ]$$

(10)

The rotation matrix consists of a rotation ψ (yaw) about the z-axis, then a rotation θ (pitch) about the y-axis and followed by a rotation ϕ (roll) about the x-axis, which is shown in Figure 12.

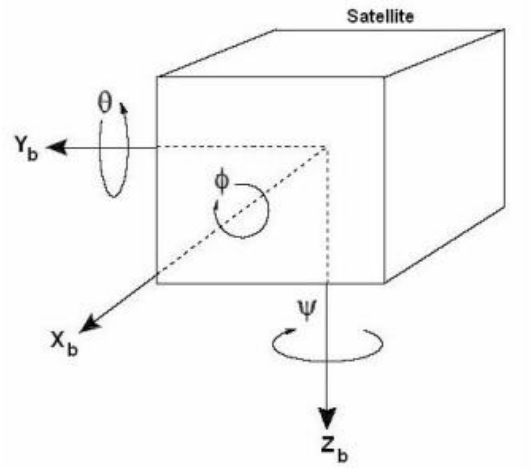


Figure 12: The rotation of the satellite in relation to Euler angles

3.2.1.2 Quaternions

Quaternions are four parameter representations derived from the Euler axis and Euler angle. It consists of a vector $\vec{q} = (q_1, q_2, q_3)$ and a scalar part $q_0 = cos\, cos\, \frac{\varphi}{2}$, where φ is the rotation angle. The vector is often assembled with the scalar part into a 4D vector:

$$q_1 = e_1\, sin\, sin\, \frac{\varphi}{2}\,, q_2 = e_2\, sin\, sin\, \frac{\varphi}{2}, q_3 = e_3\, sin\, sin\, \frac{\varphi}{2}$$

(11)

$$\tilde{q} = (q_0, q_1, q_2, q_3)$$
$$= \left(cos\, cos\, \frac{\varphi}{2}, e_1\, sin\, sin\, \frac{\varphi}{2}\,, e_2\, sin\, sin\, \frac{\varphi}{2}\,, e_3\, sin\, sin\, \frac{\varphi}{2}\right), \quad 0 \leq \varphi \leq 2\pi$$

(12)

The magnitude of $\tilde{q}$ is 1 since:

$$q^T q = {q_0}^2 + {q_1}^2 + {q_2}^2 + {q_3}^2 = 1$$

(13)

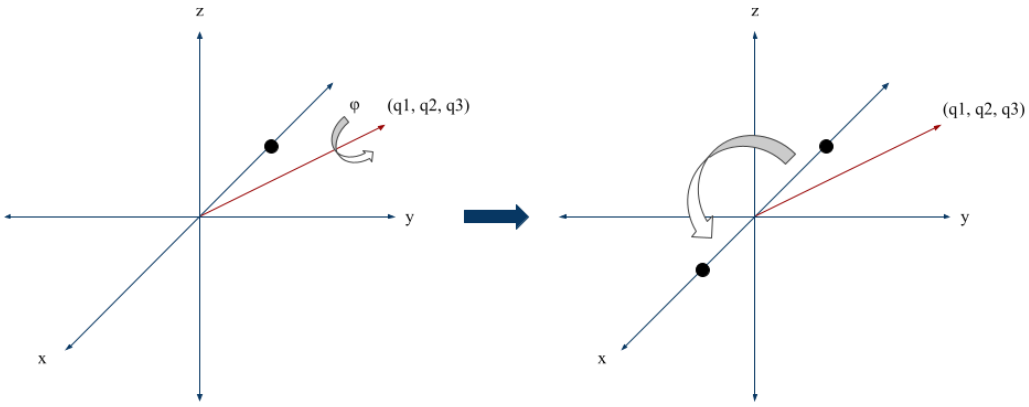


Figure 13: Rotation of a point with the defined quaternion

The rotation matrix using direct transformation can be written in the form of a quaternion:

$$R = cos\ cos\ \varphi\ I + (1 - cos\ cos\ \varphi\ )\hat{e}\hat{e}^T - sin\ sin\ \varphi\ \hat{e}^x$$

(14)

$$R = [q_0{}^2 + q_1{}^2 - q_2{}^2 - q_3{}^2\ 2(q_1q_2 + q_0q_3)\ 2(q_1q_3 - q_0q_2)\ 2(q_2q_1 - q_0q_3)\ q_0{}^2 - q_1{}^2 + q_2{}^2 - q_3{}^2\ 2(q_2q_2 + q_0q_1)\ 2(q_3q_2 + q_0q_2)\ 2(q_3q_2 + q_0q_1)\ q_0{}^2 - q_1{}^2 - q_2{}^2 + q_3{}^2\ ]$$

(15)

3.2.2 Inertia Matrix

The inertia of the satellite can be defined as:

$$I_s = [I_x\ -I_{xy}\ -I_{xz}\ -I_{yx}\ I_y\ -I_{yz}\ -I_{zx}\ -I_{zy}\ I_z\ ]$$

(16)

Where:

$$\rho = mass\ of\ density, V = volume$$

$$I_x = \int\ (y^2 + z^2)\rho dV\ , I_y = \int\ (x^2 + z^2)\rho dV\ , \qquad I_z = \int\ (x^2 + y^2)\rho dV$$

(17)

$$I_{xy} = \int\ xy\rho dV\ , I_{xz} = \int\ xz\rho dV\ , I_{yz} = \int\ yz\rho dV$$

(18)

$$I_{xy} = I_{yx},\ I_{yz} = I_{zy},\ I_{xz} = I_{zx}$$

(19)

If the axes of the body frame coincide with the principal axes of inertia, the inertia matrix can be simplified to:

$$I_s = \begin{bmatrix} I_x & 0 & 0 \\ 0 & I_y & 0 \\ 0 & 0 & I_z \end{bmatrix}$$

(20)

The small satellite inertia matrix parameters are $I_x = I_y = I_z = 2.0833\ kgm^2$. Diagonal terms of inertia matrix are more significant than other components of inertia. This means that we can assume the off-diagonal terms are neglectable.

The inertia of the reaction wheel can be calculated using the following equations 21, 22, and 23:

$$I_x = \frac{1}{12} m(3(r_{outer}^2 + r_{inner}^2) + h^2)$$

(21)

$$I_y = \frac{1}{12} m(3(r_{outer}^2 + r_{inner}^2) + h^2)$$

(22)

$$I_z = \frac{1}{2} m(r_{outer}^2 + r_{inner}^2)$$

(23)

The equations are established with the assumption that the reaction wheel is a hollow cylinder. The inner radius and the outer radius with the mass of the reaction wheel are used to calculate the inertia of the z-axis. To calculate the inertia in the x-axis and y-axis, the height of the reaction wheel is also taken into account for the calculation.

3.3 Soft-Suspension Reaction Wheels

3.3.1 Reaction Wheel Distribution Matrix

The distribution matrix of reaction wheels has n columns, each of which corresponds to one reaction wheel and is determined only by the configuration of

the reaction wheel assembly. The distribution of reaction wheel torques on the satellite's axis of rotation is represented by each column vector. A standard orthogonal 3-wheel configuration is used throughout the project, which is shown in Figure 14.

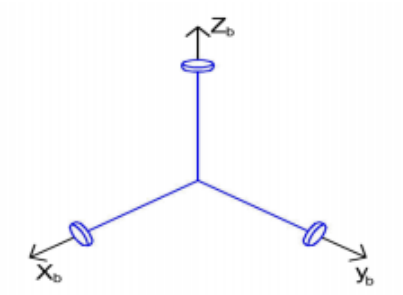


Figure 14: A standard orthogonal 3-wheel configuration

The distribution matrix of a standard orthogonal 3-wheel configuration can be defined.

$$A = [1\ 0\ 0\ 0\ 1\ 0\ 0\ 0\ 1\ ] \quad (24)$$

The moment acting on the satellite body can be defined as where T1, T2, and T3 represent the torque produced by each reaction wheel.

$$[T_x\ T_y\ T_z\ ] = A_{3x3}[T_1\ T_2\ T_3\ ] \quad (25)$$

3.3.2 Soft-Suspension Reaction Wheel Parameters

The soft-suspension reaction wheel used for the mathematical modelling is configured as illustrated in Figure 15 [20]. The soft-suspension reaction wheel is constructed with the web-spring model with a frequency of 20 Hz. The base of the reaction wheel is fixed to represent the hard-mounted boundary condition.

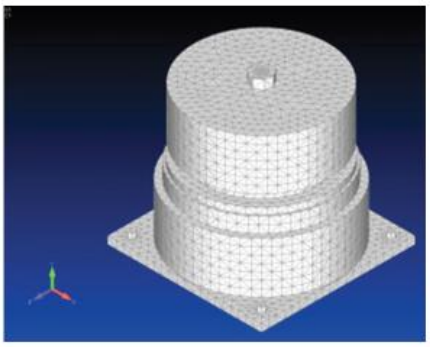




Figure 15: The structure of the soft suspension reaction wheel used in the thesis [20]

Off-the-shelf components are used within the reaction wheel assembly, in which the parameters are modelled accordingly to the datasheets provided by the manufacturers. The chosen motor produces maximum torque of 0.6 Nm in both counter-clockwise and clockwise directions. The flywheel is able to generate a maximum of 3000 revolutions per minute [3]. The mass of the reaction is assumed to be 0.5 kg and cylindrical shaped with a radius of 0.05m. The satellite is assumed to be the standard small satellite with a mass of 50 kg and a dimension of 0.5m x 0.5m x 0.5m [3].

3.3.3 Soft Suspension Reaction Wheel Stiffness

The stiffness of the reaction wheel is based on the desired frequency for the reaction wheel. The stiffness is dependent on the inertia of the reaction wheel in both the local reaction wheel x-axis and y-axis, I_x and I_y. Due to the symmetric shape of the reaction wheel, $I_x = I_y$, meaning the stiffness is the same for both the local reaction wheel x-axis and y-axis. The relation between the stiffness and the frequency is defined with Equation 26.

$$stiffness = (2\pi \times frequency)^2 \times I_x$$

(26)

3.4 Equation of Motions

3.4.1 Euler Moment Equations

The Euler Moment Equation describes how applied moments can affect the spacecraft body. Equation 27 is Euler's Moment Equation in vector form. When a moment is exerted on the spacecraft, the momentum changes.

$$M = \dot{h}_{body} + \omega_{body} \times h_{body}$$

(27)

By assuming the spacecraft body to be rigid, h can be expressed in terms of inertia and angular velocity. This is because by assuming a rigid body, any change in the momentum is directly proportional to the change in angular velocity. The inertia matrix is stated in *section 3.2.2*. The Euler Moment Equations can be simplified in the form of:

$$M = I\dot{\omega} + \omega \times I\omega$$

(28)

When the body reference frame is aligned with the principal axes, then the products of inertia are zero. Equation 28 can be further reduced into three equations in terms of the body frame, x, y, and z-axis.

$$M_x = I_x\dot{\omega}_x + \omega_y\omega_z(I_z - I_y)$$

(29)

$$M_y = I_y\dot{\omega}_y + \omega_x\omega_z(I_x - I_z)$$

(30)

$$M_z = I_z\dot{\omega}_z + \omega_x\omega_y(I_y - I_x)$$

(31)

3.4.2 Euler Equations with Coriolis Theorem

The orientation of the satellite is determined by the acceleration of the satellite, which the torque exerted by the RWA generates. To find the total angular momentum of the satellite with reaction wheel configuration, Equation 32 is used.

$$\underline{H} = I_G\underline{\omega} + A\underline{H_\omega}$$

(32)

I_G is the moment of inertia matrix of the spacecraft and $\underline{\omega}$ is the angular velocity of the spacecraft. $\underline{H_\omega}$ is a vector where the length of the vector corresponds to the number of wheels in which $\underline{H_\omega} = [I_{w1}\ \omega_{w1}\ ;\ I_{w2}\ \omega_{w2}\ \ldots\ I_{wn}\ \omega_{wn}\ ]$ and I_w the inertia of the reaction wheel and ω_w is the angular velocity of the reaction wheel. A is the reaction wheel distribution matrix mentioned in *section 3.3.1*.

The mathematical model of the reaction wheel and spacecraft using Euler's equation is derived using the Coriolis theorem and the total angular momentum. Euler's equation is shown in Equation 33, which consists of a change in the total angular momentum relative to the observer and a cross product of the angular velocity of the spacecraft and the total angular momentum from Equation 35. The total angular momentum equals zero if no external torque is produced.

$$\frac{d\underline{H}}{dt} = \left(\frac{dH}{dt}\right)_{rel} + \underline{\omega} \times \underline{H} = 0$$

(33)

Where:

$$\left(\frac{dH}{dt}\right)_{rel} = I_G\underline{\dot{\omega}} + A\underline{\dot{H_w}}$$

(34)

$$\underline{\omega} \times \underline{H} = \underline{\omega} \times I_G\underline{\omega} + \underline{\omega} \times A\underline{H_w}$$

(35)

Rearranging Euler's equation in terms of angular acceleration gives Equation 36.

$$\underline{\dot{\omega}} = (-\underline{\omega} \times I_G\underline{\omega} - \underline{\omega} \times A\underline{H_w} - A\underline{\dot{H_w}})/I_G$$

(36)

The derivation of the angular acceleration of the spacecraft enables the calculation of the spacecraft's orientation at a specific time.

3.4.3 Gyroscopic Effect

The gyroscopic effect of each reaction wheel is calculated with the free gyro Eulerian equation. The torque, T, generated in each axis is determined by the following equations:

$$T_x = I_w\dot{\omega}_{wx} + \omega_s \times I_w\omega_{wx}$$

(37.1)

$$T_y = I_w\dot{\omega}_{wy} + \omega_s \times I_w\omega_{wy}$$

(37.2)

$$T_z = I_w\dot{\omega}_{wz} + \omega_s \times I_w\omega_{wz}$$

(37.3)

The equation consists of the vector of the angular velocity of the satellite, ω_s, cross product with the wheel angular momentum, $I_w\omega_w$ with the product of the inertia of the reaction wheel and the angular acceleration of the reaction wheel.

3.5 Orthogonal 3-wheel Configuration Modelling

The derived mathematical models are used in MATLAB (Appendix A) for a different test case to obtain results for the behaviour of each reaction wheel and the spacecraft. Different profiles of wheel accelerations are created as input for the mathematical model to determine the acceleration of the spacecraft.

3.5.1 CASE STUDY 1: Single Wheel Acceleration

The first test case investigates the behaviour of the spacecraft with the acceleration of a single reaction wheel while other wheels remain stationary. In this test case, the single reaction wheel is accelerated to $0.01\,rad/s^2$ for 60 seconds with a constant speed of 120 seconds which minimises any steady error and overshoot results. The reaction wheel is then decelerated at $0.02\,rad/s^2$ for 30 seconds twice with an interval 60 seconds in between. With another interval of 60 seconds, the reaction wheel is accelerated at $0.01\,rad/s^2$ for 60 seconds. With the created profile shown in Figure 16, the predicted behaviour of the satellite should be in the opposite direction. Also, the angular displacement of the satellite should be zero meaning that the satellite rotates back to the original starting orientation. The initial condition of the simulation is defined in Table 1, and the simulation period is 60 seconds.

Table 1: Initial condition of Case Study 1: Single Wheel Acceleration

	Value	Unit
Wheel 1 acceleration	0.01	rad/s^2
Wheel 2 acceleration	0	rad/s^2
Wheel 3 acceleration	0	rad/s^2
Satellite acceleration	0	rad/s^2
Wheel 1 velocity	0	rad/s
Wheel 2 velocity	0	rad/s
Wheel 3 velocity	0	rad/s
Satellite velocity	0	rad/s^2
Wheel 1 displacement	0	rad
Wheel 2 displacement	0	rad
Wheel 3 displacement	0	rad
Satellite displacement	0	rad

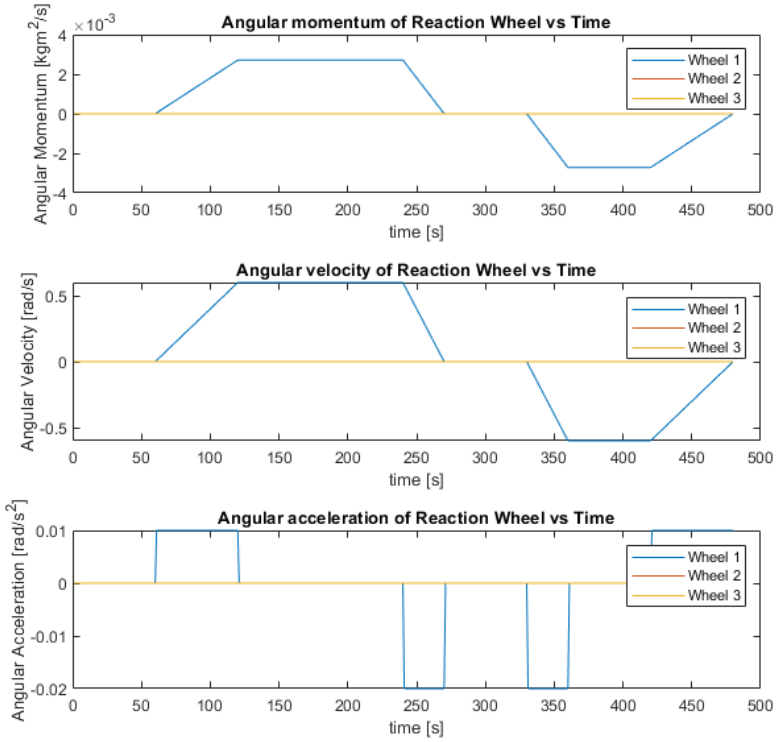


Figure 16:Input profile of Case Study 1: Single wheel acceleration

The spacecraft's behaviour is shown in Figure 17. The angular acceleration of the spacecraft performs the same as the prediction, where it is in the opposite direction comparing the reaction wheel. Additionally, the satellite did return to the original angular displacement, which matches the prediction. The gyroscopic effect was not investigated for this case study because only a single reaction wheel is utilised. This means the dynamic coupling effect is not applicable to the case.

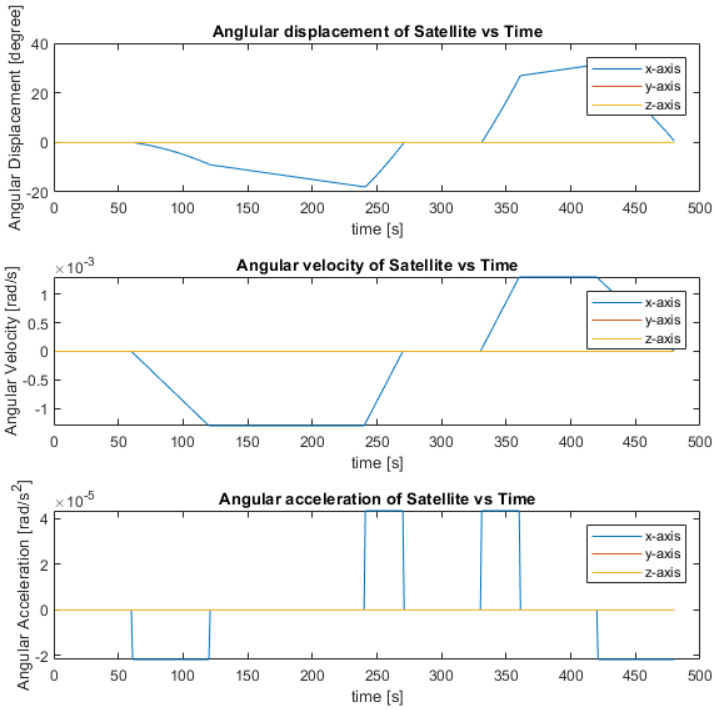


Figure 17: Satellite behaviour of Case Study 1: Single wheel acceleration

3.5.2 CASE STUDY 2: Single Wheel Acceleration with Two Constant Wheel Velocity

The second test case investigates the spacecraft's behaviour with a single reaction wheel's acceleration while other reaction wheels operate at a constant velocity. The single reaction wheel 1 is accelerating at 0.01 rad/s^2 while the other two reaction wheels, wheel 2 and wheel 3, operate at a constant velocity of 5 rad/s. The initial condition of the simulation is defined in Table 2, and the simulation period is 60 seconds. The angular acceleration is shown in the third graph in Figure 18.

Table 2: Initial condition of Case Study 2: Single wheel acceleration with two constant wheel velocity

	Value	Unit
Wheel 1 acceleration	0.01	rad/s^2
Wheel 2 acceleration	0	rad/s^2
Wheel 3 acceleration	0	rad/s^2
Satellite acceleration	0	rad/s^2
Wheel 1 velocity	0	rad/s
Wheel 2 velocity	5	rad/s
Wheel 3 velocity	5	rad/s

Satellite velocity	0	rad/s
Wheel 1 displacement	0	rad
Wheel 2 displacement	0	rad
Wheel 3 displacement	0	rad
Satellite displacement	0	rad

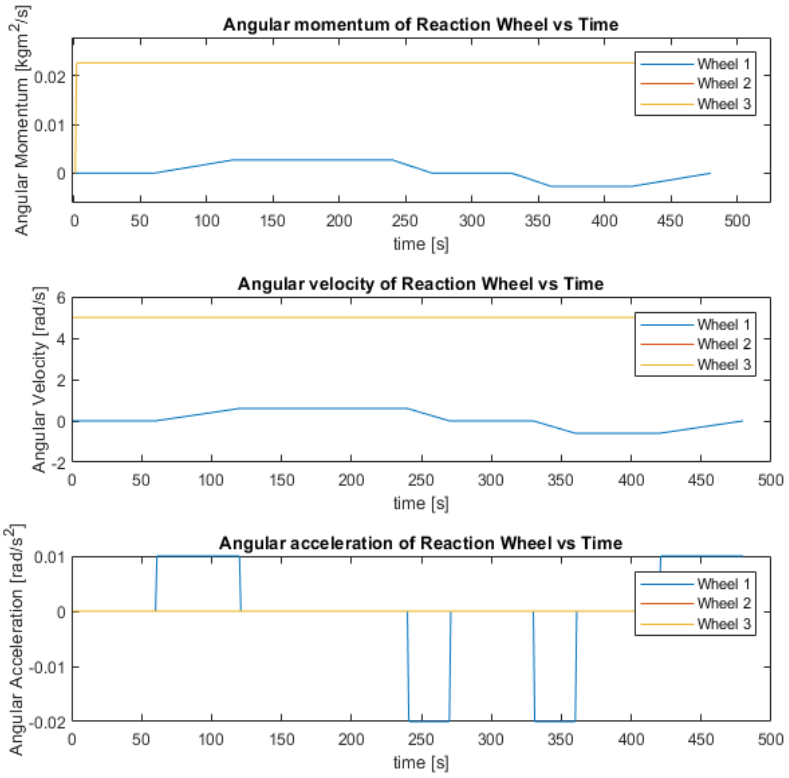


Figure 18: Input profile of Case Study 2: Single wheel acceleration with two constant velocity wheels

The result is shown in Figure 19 where the acceleration of one reaction wheel while two other reaction wheels remain constant velocity. The results show that the two reaction wheels operating at constant velocity have the same magnitude for acceleration, velocity, and displacement, but in the opposite direction. Compared to the first case, it is shown in the result that a single reaction wheel acceleration acting on the x-axis affects the acceleration of the satellite in all three axes when the two other reaction wheels are operating at constant velocity. The results also indicate that the constant angular velocity of the other two reaction wheels has an impact on the magnitude of the acceleration of the satellite with the acceleration of the reaction wheels remaining in the same profile as the first case. Different combination of the angular acceleration of the reaction wheels were tested

as well as creating profiles with ramp-up and ramp-down angular acceleration and all gives matches the predicted results. These simulation result verifies the equation derived in *section 3.4.2*.

The angular displacement of the satellite in the x-axis did not return to the original orientation like the result from study case 1. This is because the effect on the acceleration of satellites creates an overall positive acceleration in the x-axis. Thus, the displacement of the satellite will not return to the origin in the x-axis.

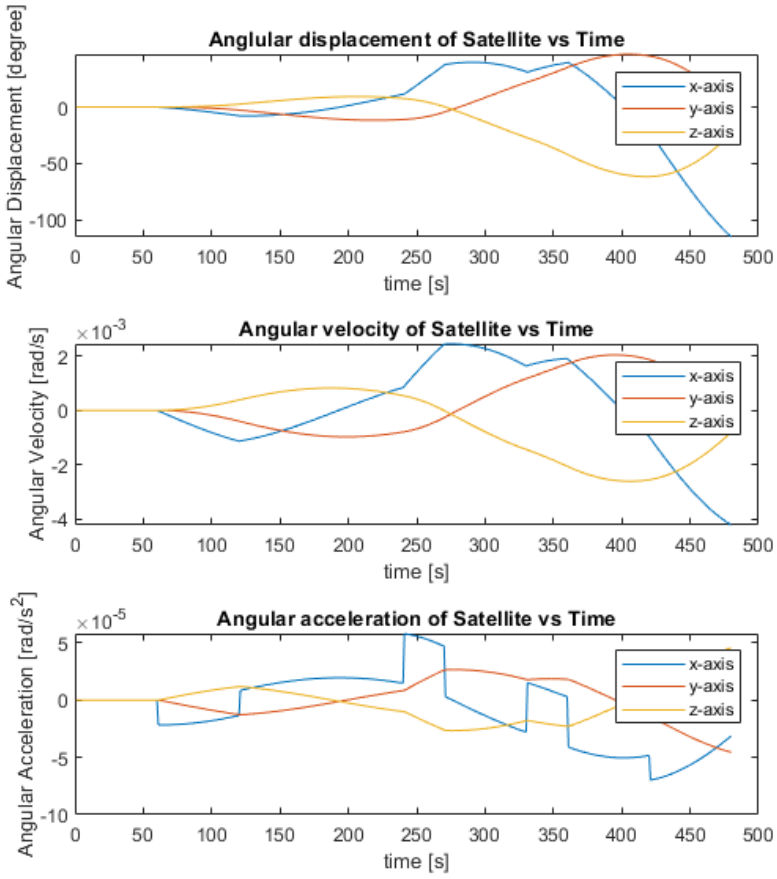


Figure 19: Satellite behaviour of Case Study 2: Single wheel acceleration with 2 constant velocity wheels

Investigations are also carried out for each reaction wheel to gain an understanding of the gyroscopic effect on each reaction wheel when only a single reaction wheel is accelerating and two reaction wheels are at constant angular velocity. The momentum experienced by each wheel in the axis in which it is placed has the same profile as the angular acceleration input.

According to the results, torques are experienced by each reaction wheel. The two reaction wheels rotating at a constant angular velocity experience the same amount of torque but in opposite directions due to the placement of the wheels. The shape of the torque is similar to the form of the angular velocity of the satellite body. This validates the gyroscopic effect equation stated in Equation 37. The torque experienced by the accelerated reaction wheel has a similar profile as the angular momentum calculated in Figure 18 with shifts in the y-axis. It is assumed that the torque on the accelerating wheel is not affected by the gyroscopic effect in the rotating direction. This is shown in Figure 20 where the in-plane axes of the rotation experience torque.

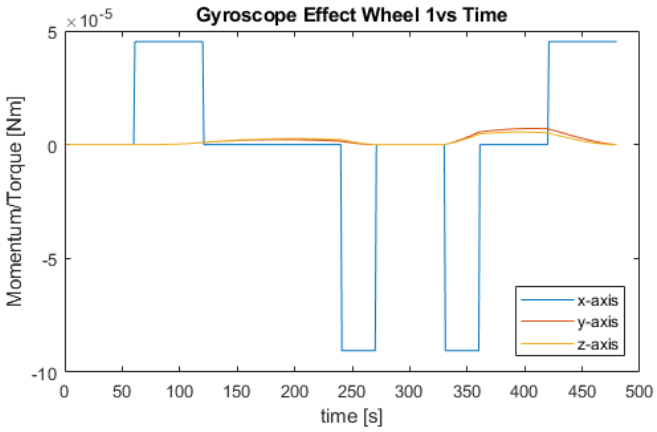


Figure 20: Gyroscope effect for reaction wheel 1 in each axis

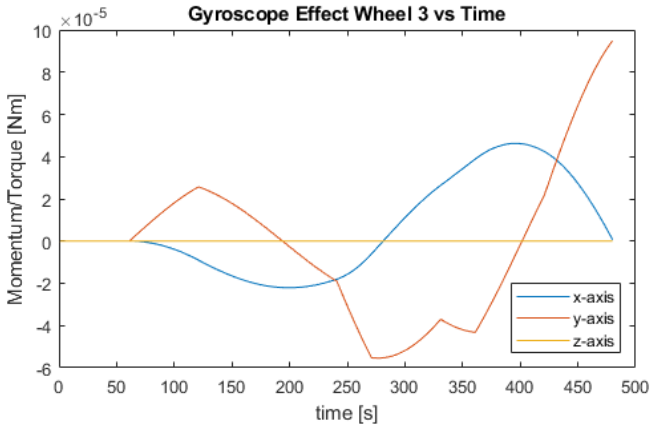


Figure 21: Gyroscope effect for reaction wheel 2 in each axis

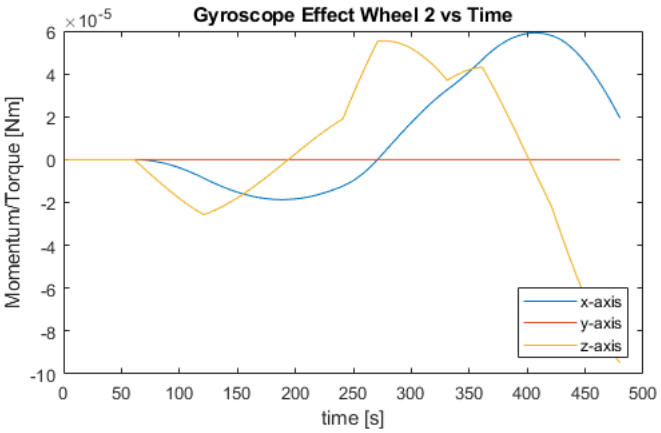


Figure 22: Gyroscope effect for reaction wheel 3 in each axis

CHAPTER 4

MODEL SIMULATION and RESULTS

The mathematical model in Chapter 3 is further validated through the simulation of the satellite and RWAs. This is achieved through MATLAB and Simulink. This chapter explains the model developed for both the rigid reaction wheel and the soft-suspension reaction wheel. Different case studies are tested to gain an understanding of the behaviour of the satellite. Further validation of the models is established by comparing the simulation results against the results of the mathematical model derived in Chapter 3. The pointing error of the soft-suspension reaction is further investigated to determine the feasibility of the soft-suspension reaction wheels.

4.1 Introduction to MATLAB/Simulink

Simulink, a product of Mathworks, offers an interactive, graphical environment for the modelling, simulation, and analysis of dynamical systems based on block diagrams. Simulink is frequently used in conjunction with MATLAB to model physical systems using both textual and graphical programming. Simulink has an extensive library of parts that can be used to create block diagram models of real-time systems based on information flow, as seen in Figure 23. The Simulink library's components can be "dragged and dropped" into the model window.

Simulink gives users access to several functions, including event-based modelling, modelling of physical systems, model-based design verification and validation in embedded systems, and real-time testing. Block diagrams and bond graphs, which are examples of signal flow-based modelling, are useful for conceptualising Multiphysics systems, but they are insufficient for creating working prototypes. The simulation is used to validate and test the Soft-suspension reaction wheel configuration for the small Satellite to validate that the dynamic coupling effect does not significantly impact the desired satellite performance.

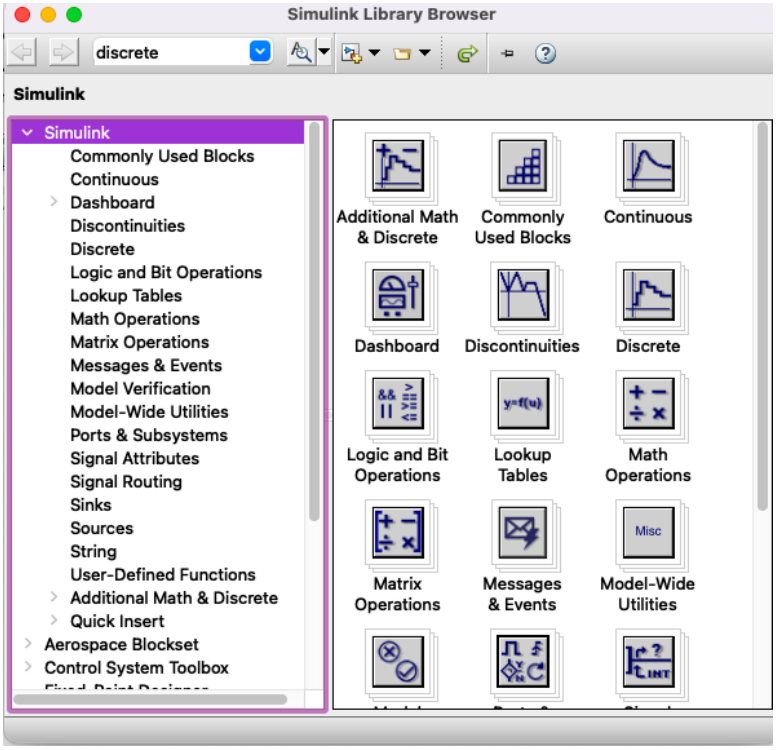


Figure 23: Simulink library components for block model creation

4.1.1 ODE Solver

Simulation of Simulink models involves numerical integration of ordinary differential equations (ODEs) sets. Because of the diversity of the dynamic system behaviour of different models, some solvers are more suitable and efficient than others at solving a particular model. Two different types of solvers, variable-step and the fixed-step solver, can be chosen to simulate the model. A variable-step solver can modify their step sizes during the simulation. A fix-step solver takes the same size during the simulation.

A variable-step solver ODE45 was chosen for the designed model, which is the standard solver for ordinary differential equations (ODEs). The solver is based on an explicit Runge-Kutta (4, 5) formula, the Dormand-Prince pair. ODE 45 is designed to solve the general equation of:

$$\frac{dx}{dt} = f(t,x), \qquad x(t_0) = x_0$$

(39)

Where t is the independent variable, x is a vector of dependent variables to be found and $f(t,x)$ is the function of t and x. The one-step solver means ode45

estimates $y(t_n)$ using the solution at the immediately preceding time point, $y(t_{n-1})$, and the values of the derivative at multiple points between t_n and t_{n-1}.

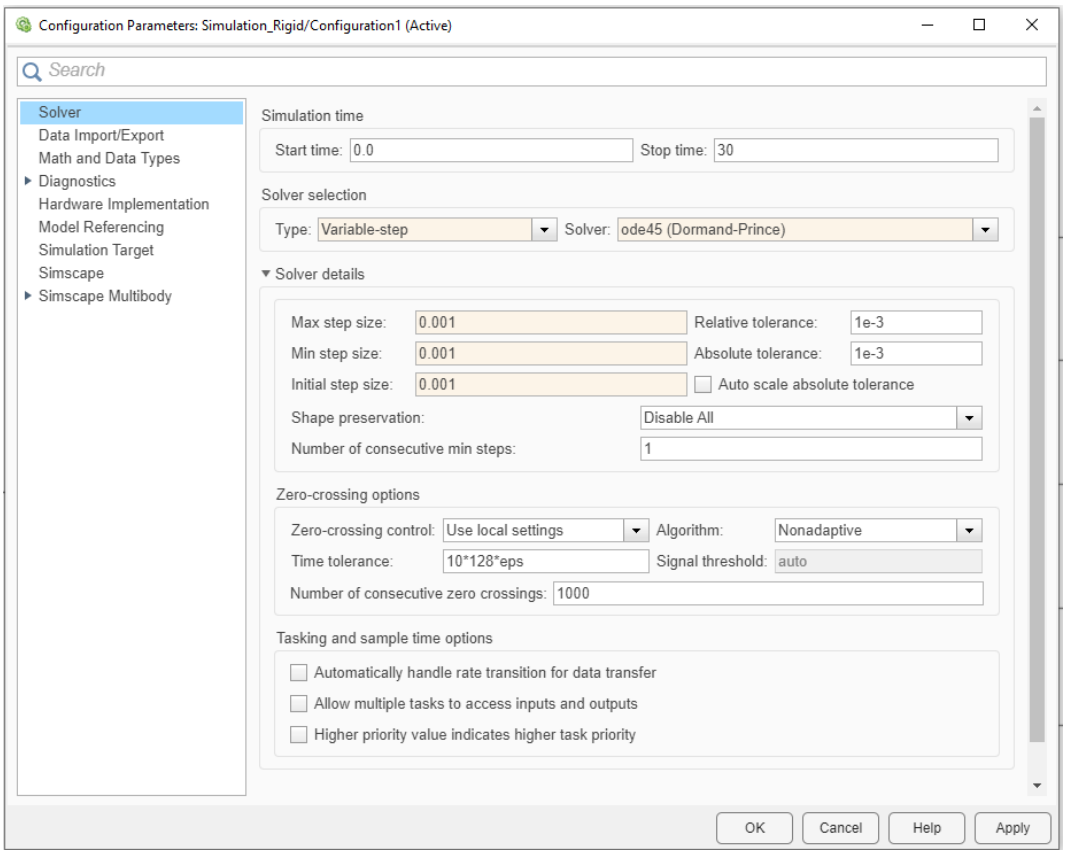


Figure 24: Configuration parameters function in Simulink

To define the solver in Simulink, the *Configuration Parameters* function is shown in Figure 24. Firstly, the solver is categorised by the type, in which a Variable-step type is chosen for ODE 45. By further selecting ODE 45 in the solver selection section, the ODE solver used to analyse the created model is defined.

4.1.2 Step Sizes

Initially, a variable-step simulation is used to gain reference results which are further used as the baseline of the step size for the simulation model. Tuning is required to increase the accuracy of the simulation result through a fix-step simulation.

Discontinuous or rapid changes in the simulation system require small step sizes to capture the changes in the dynamics accurately. The step size to analyse the designed simulation model is defined using the Configuration Parameters function shown in Figure 24. The step size of 0.001 is set to a fixed value for the maximum,

minimum, and initial step sizes. The maximum step size chosen for this project was 0.001 s which ensures a high accuracy result for micro-vibration determination of the reaction wheels and satellite body.

4.2 Introduction to Simscape Multibody Toolbox

The Mathworks suite's Simscape simulation platform enables the modelling of physical systems based on the energy flow paradigm. As a result, it is possible to simulate a multibody structure without its transfer function by combining the body's essential parts into a comparable physical network. To conduct a co-simulation of the entire system-level model, the physical component-based models in the Simscape environment can be combined with the signal-flow-based modelling in Simulink. Figure 25 presents the elements of the current Simscape library.

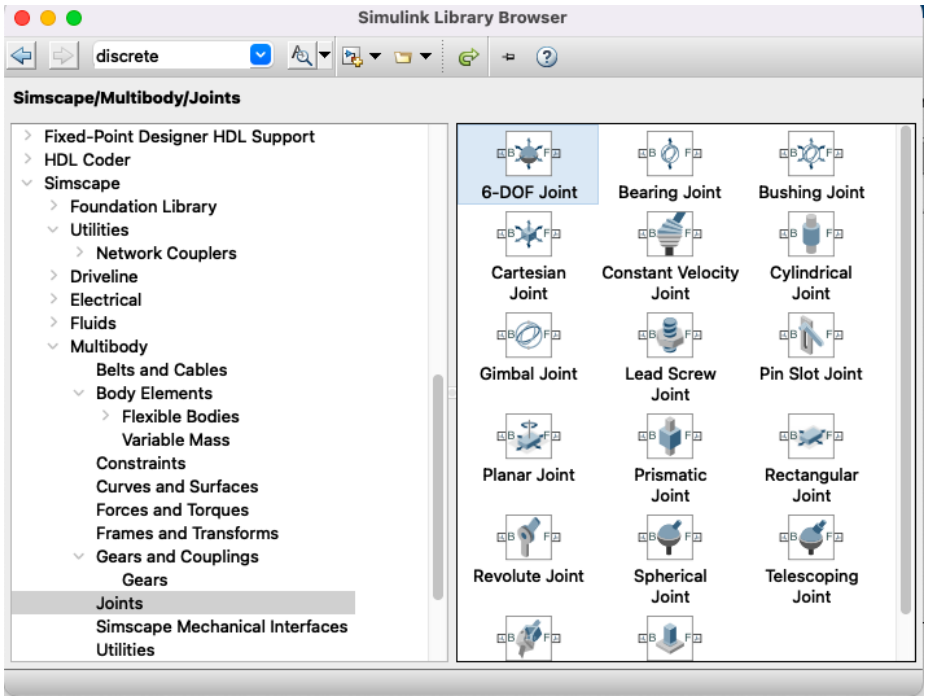


Figure 25: Elements of the current Simscape library

4.3 General Structure of the Simspace Multibody Model

The general configuration of the Simspace Multibody Model is shown in Figure 26. The model consists of the satellite sub-system and the reaction wheel sub-system and the definition of the properties of the model. The properties of the model are defined with three function blocks: the global reference frame of the model is determined using the world frame, the frame is inertial and at absolute rest;

the model parameters are solved using the solver configuration; the mechanism configuration block provides mechanical and simulation parameters to the model such as defining the gravity and linearisation delta which is the perturbation value for calculating the numerical partial derivatives. These blocks are connected to the satellite sub-system since the movement of the satellite body is of interest. The multibody block has port B and port F which correspond to the base and follower frame respectively, and the motion of the follower frame relative to the base frame defines the joint direction.

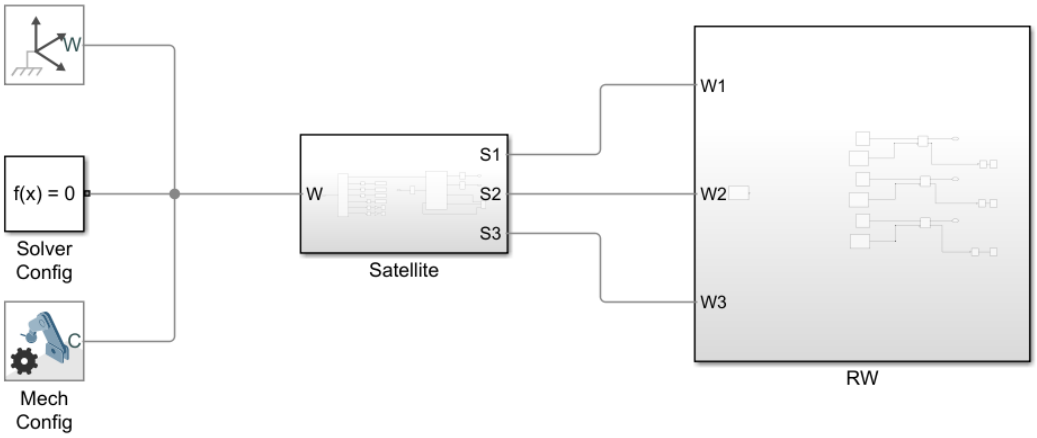


Figure 26: Overall configuration of the Simspace multibody model of the satellite and reaction wheels

The satellite sub-system (Figure 27) incorporates the 6-DOF joint, the global reference point for the Simscape model. The joint has three translational and three rotational degrees of freedom. The base frame of the joint is connected to the world frame block, and the follower frame is connected to the multibody body element of a brick which represents a small satellite with a dimension of $0.5 \times 0.5 \times 0.5\ m^3$. Three frames are created with the small satellite block to connect to the corresponding shafts of the reaction wheels. Additionally, three balanced masses identical to the RWAs are designed to minimise the effects of unbalanced masses affecting the pointing error results. The results of the satellite are obtained through the output of the 6-DOF joint with the sensing function, the simulation results of the angular position, angular velocity, and angular acceleration of the joint can be further exported to the MATLAB workspace with the workspace block.

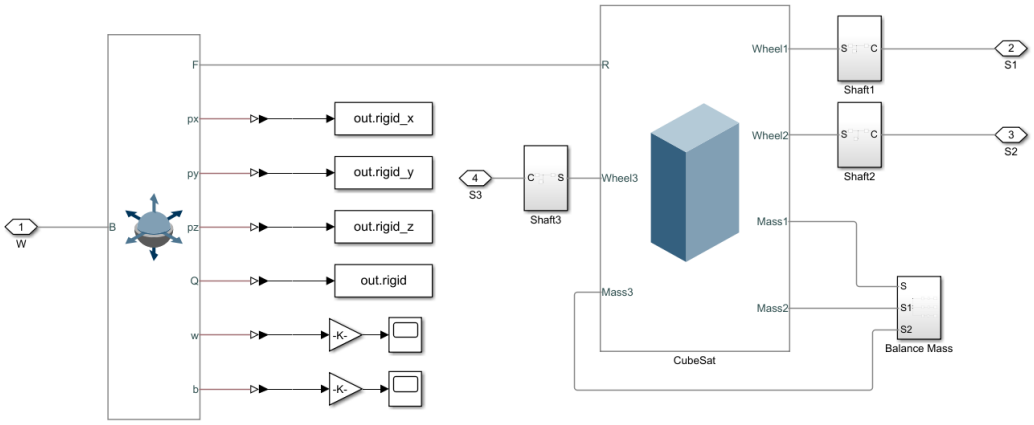


Figure 27: Satellite sub-system of the Simscape model

Rigid transformation blocks are used between the connection of the shafts and the small satellite to ensure the axis is aligned in the corresponding direction shown in Figure 28. In the example, the reaction wheel has a transformation in the z-axis translation for an offset of 0.025 m. The shafts are further connected to the designed reaction wheel models, which are discussed in *section 4.4* and *section 4.5*.

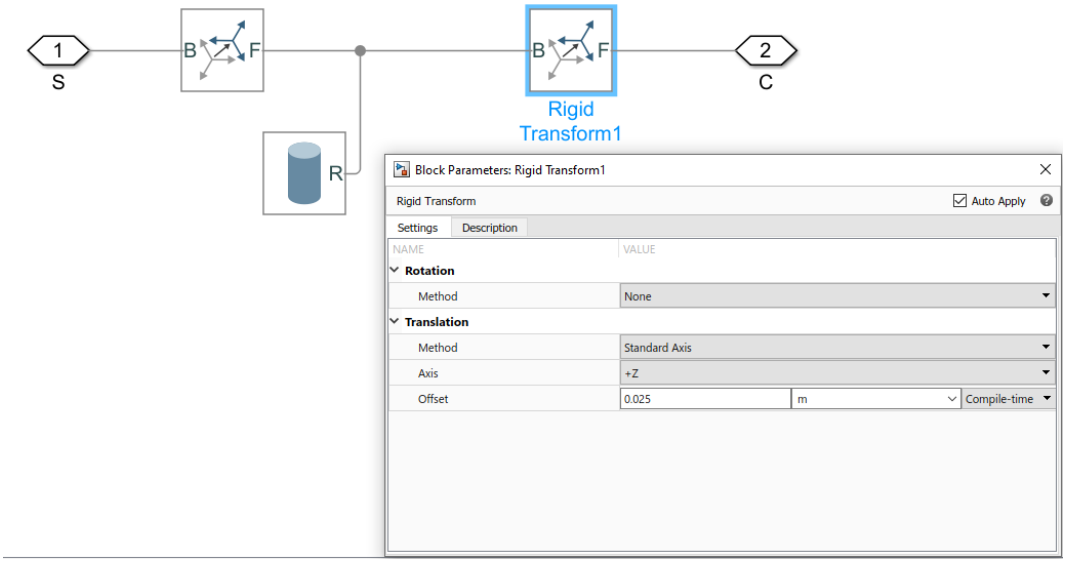


Figure 28:Shafts sub-system of the Simscape model

4.4 Design of Rigid Body Reaction Wheel Satellite Model

4.4.1 Simscape Model

The developed Simscape model of the orthogonal 3-wheel configuration of a rigid body reaction wheel is shown in Figure 29. The design of the rigid body

reaction wheel model operates with a revolute joint. A revolute joint has one rotational degree of freedom represented by one revolute primitive. This characteristic is suitable to represent a rigid body reaction wheel in which it is constrained to rotational movement in a singular axis. The joint constrains the base frame and the follower frame to coincide in the z-axes of both frames, meaning that the follower x-axis and y-axis will rotate around the z-axis. The base frame is the reaction wheel, and the follower frame is the shaft connecting the reaction wheel to the satellite body. The parameters inside the revolute joint are set to default settings since no extra constraints are required for the design of a rigid reaction wheel.

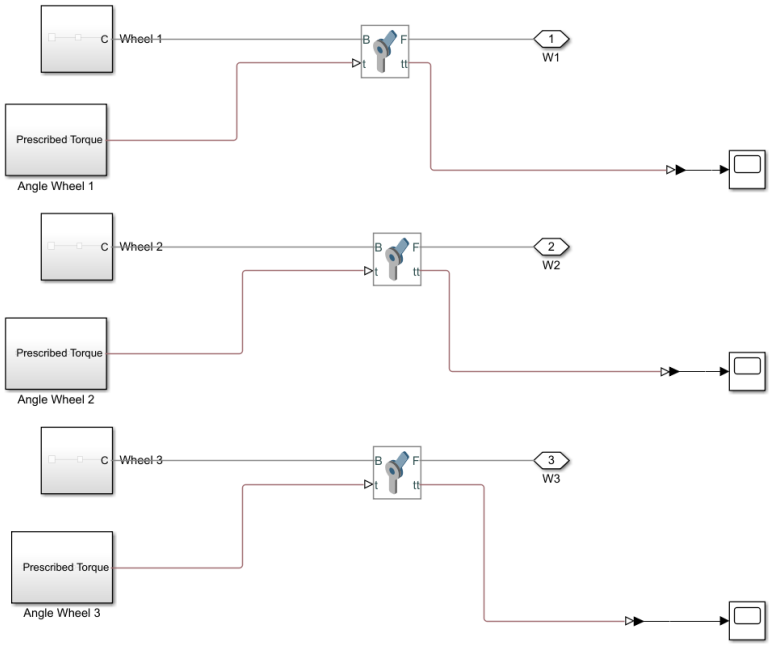


Figure 29: Rigid body reaction wheel sub-system of the Simcape model

The design of the reaction wheel body uses the revolved solid block where the cross-section is defined using the coordinates from the origin [0, 0] on the cross-sectional XZ plane. The given mass of the standard reaction wheel of 0.5 kg, the moment of inertia of the reaction wheel, is calculated by Simulink. This is derived values are further validated with the equation derived from *section 3.2.2* inertia matrix.

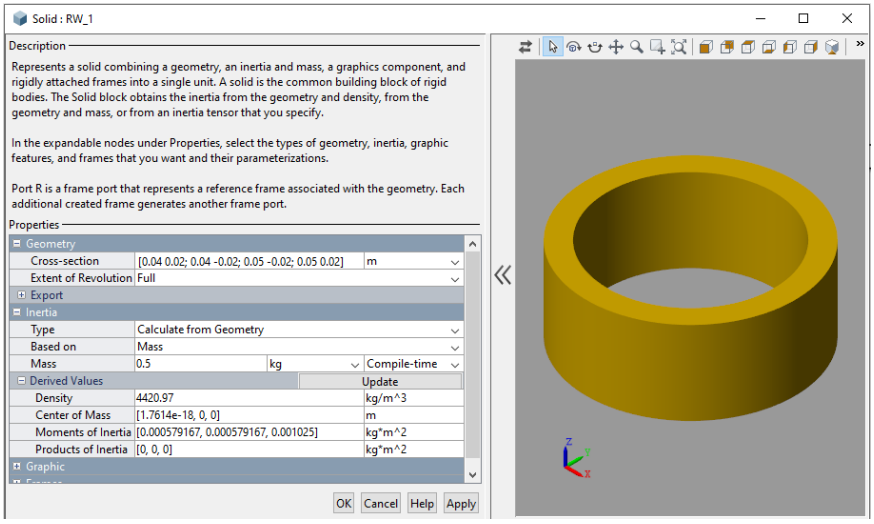


Figure 30:Block design of the reaction wheel

The reaction wheel movement is established through a signal builder block and creates a profile of the desired RPM output of the reaction wheel. The RPM profile is further converted to radians per second and derived to obtain the angular acceleration of the reaction wheel. The torque is obtained by multiplying the angular acceleration with the moment of inertia of the reaction wheel. Saturation blocks are used throughout the conversion to ensure the output values are within the range of the standards of the reaction wheel used.

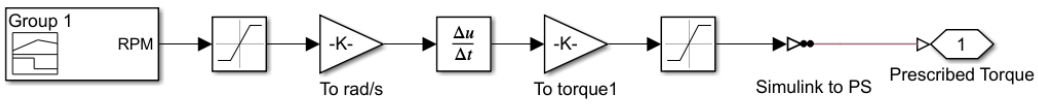


Figure 31: Input profile sub-system of the Simscape model

4.4.2 Mechanics Explorers

The Mechanics Explorers of the rigid reaction wheels with the satellite structure are shown in Figure 32. Mechanism explorer shows the behaviour of the satellite and the reaction wheels for each time step. In Figure 32 the green axis represents the y-axis, the red axis represents the x-axis, and the blue axis represents the z-axis. The coordinate of the satellite body is set to be the global coordinate, and the subsystem coordinate of each wheel is defined as a frame and is shown in Figure 32.

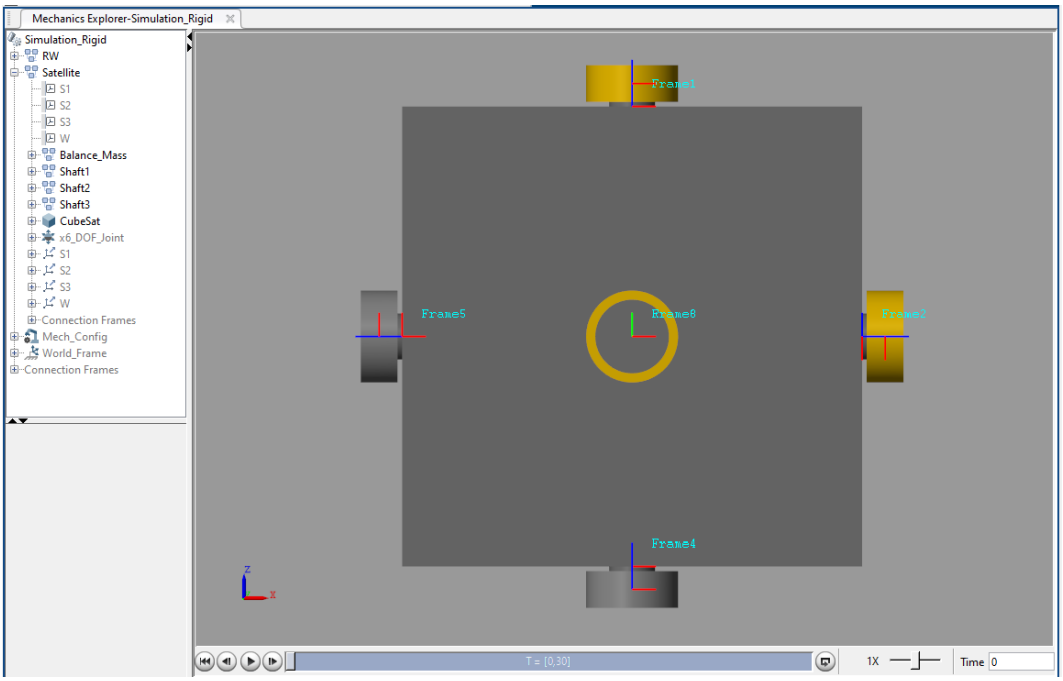


Figure 32: Mechanics Explorer of the developed rigid body reaction wheel satellite configuration

By running the simulation, the trajectory of the satellite matches the input profile of the reaction wheel motion. It was also observed that the axis of the reaction wheels was aligned with the shafts in which they were connected. This means there is no angle displacement of the axis which is caused by the gyroscopic effect. The results complement the prediction of no axis displacement. The rigid reaction wheel does not allow flexibility in the joint, so there should be no displacement between the reaction wheels and the shafts.

4.4.3 Design Validation

The designed Simscape model is further validated by comparing the output results of the satellite movement with the results obtained from the mathematical model in *section 3.5.1*. Both the mathematical model and the designed Simscape model have the same input profile of a ramp-up velocity from 0 to 2000 rpm in the period of 10 seconds. The initial condition of the simulation is defined in Table 3 with a simulation period of 30 seconds. The angular displacement of the satellite is compared against each other to validate the designed Simscape model.

Table 3: Initial condition of the simulation for design validation

	Value	Unit
Wheel 1 acceleration	20.94	rad/s^2
Wheel 2 acceleration	0	rad/s^2

Wheel 3 acceleration	0	rad/s^2
Satellite acceleration	0	rad/s^2
Wheel 1 velocity	0	rad/s
Wheel 2 velocity	0	rad/s
Wheel 3 velocity	0	rad/s
Satellite velocity	0	rad/s
Wheel 1 displacement	0	rad
Wheel 2 displacement	0	rad
Wheel 3 displacement	0	rad
Satellite displacement	0	rad

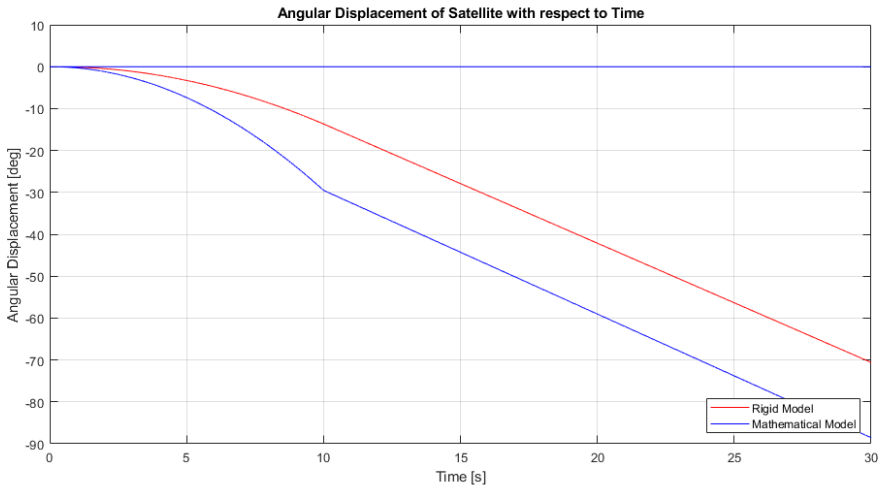


Figure 33: Angular displacement of the rigid model and mathematical model

By comparing the angular displacement of the rigid model against the mathematical model, it indicates the displacement of the rigid model is less than the theoretical results. This means the results obtained from the Simscape model will not represent the theoretical behaviour of the satellite in relation to the reaction wheels. Investigations were carried out to determine the cause of the contradiction between the Simscape and mathematical models.

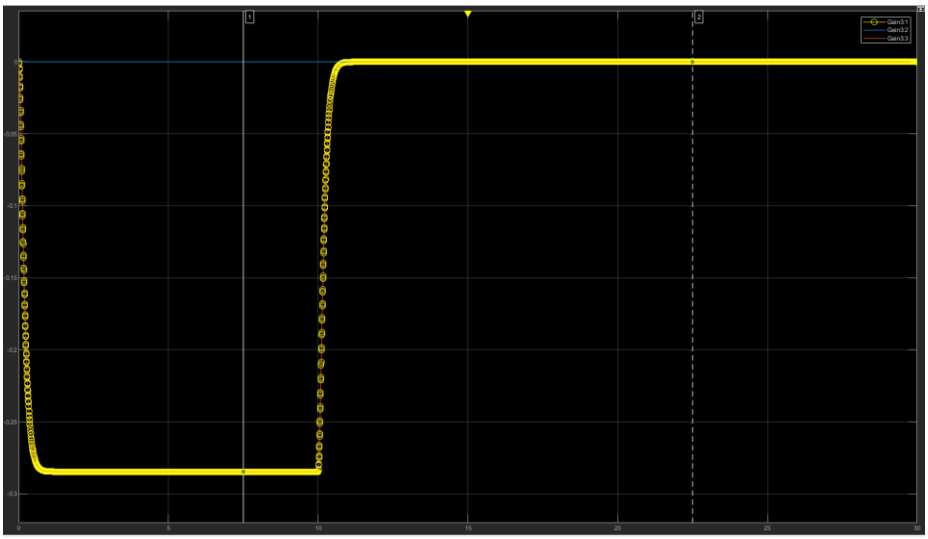


Figure 34: Simulation results of the satellite acceleration

Through investigations, it was found that the acceleration of the satellite has a ramp-up period, shown in Figure 34. This means the time for the model to achieve the desired acceleration is not instant. Therefore, with the given period of time for acceleration (10 seconds), the satellite would not reach the desired acceleration meaning the final angular displacement achieved will be less than the theoretical angular displacement. However, this result is considered more realistic in the real-life scenario than the theoretical results. This is because, in practice, the reaction wheel has a mechanical time constant, which is required for an unloaded motor to reach 63.2% of its no-load speed [6]. According to the datasheet from the motor used throughout the project, it has a mechanical time constant of 3.18 milliseconds [12].

4.5 Design of Soft-Suspension Reaction Wheel Satellite Model

4.5.1 Simscape Model

The developed Simscape model of the orthogonal 3-wheel configuration of a soft-suspension reaction wheel is shown in Figure 35. The design of the soft-suspension reaction wheel model operates with a gimbal joint. The gimbal joint block is highlighted in red which has three rotational degrees of freedom represented by the three revolute primitives, while the translational behaviour is constrained. Using the gimbal joint allows the three primitive axes to remain mutually unaligned, with the constraints of the origins of the two frames being coincident. The property of the joint satisfied the characteristic of a soft-suspension reaction wheel. The z-axis of the joint is constrained to ensure the reaction wheel

only has spring stiffness in the x and y axes. The base frame port, *B*, is connected to the reaction wheel, and the follower frame, *F*, is connected to the shaft creating a connection between the reaction wheel to the satellite body. The inputs and outputs on the gimbal joint are defined with the ports connecting to the joint block. The torque applied to the joint is set to an input and connected through the port *tx*. To understand the changes to the reaction wheel with the given input, the output of the joint is exported through port *qy*, *wy*, and *tt* which corresponds to angular displacement, angular velocity and time which are connected to the scope block for further analysis.

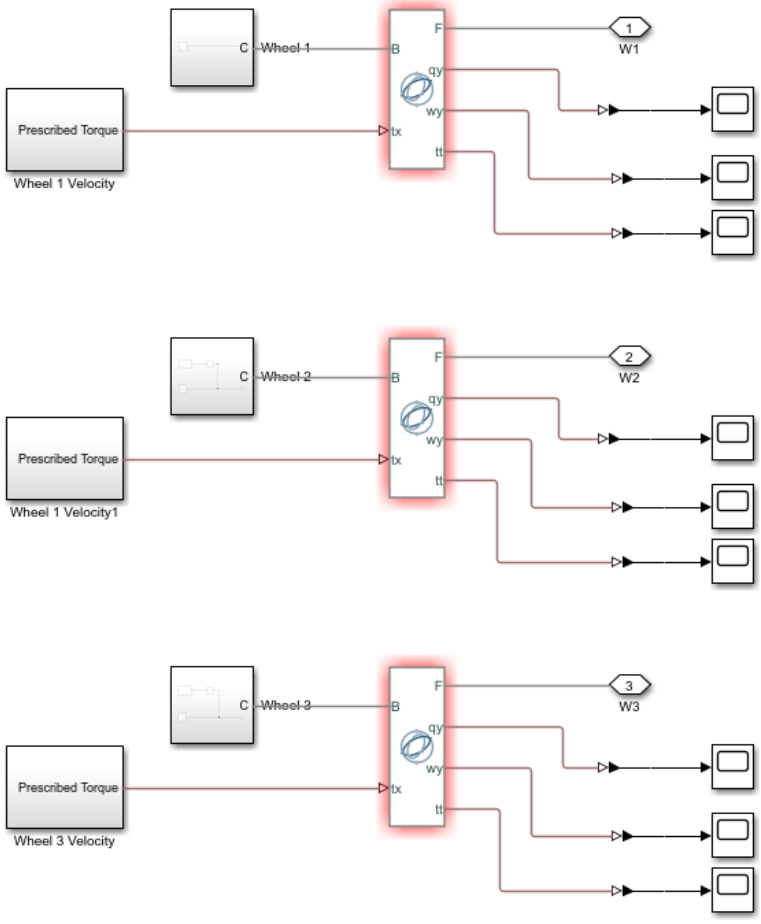


Figure 35: Simscape model of soft suspension reaction wheel configuration

The parameters of the gimbal joints are initialised using MATLAB scripts, the example in Figure 36 is the initialisation of a 4 Hz Soft-suspension reaction wheel with a damping coefficient of 0.01 Ns/m. Figure 37 shows the block parameters of the gimbal joint. The spring stiffness and damping coefficient value are defined as variables *s* and *d* respectively. In the design of the soft-suspension

reaction wheel, the x-axis is constrained to be the rigid axis for the general rotational motion of the reaction wheel. This is because the rotation of the follower frame follows the order of the x-axis, y-axis, and z-axis and the rotational motion is prioritised compared to the dynamic coupling effect caused by the soft-suspension configuration. Thus, the plane in which the y-axis and z-axis create soft suspension characteristics.

```
% Simunlate the 20Hz Soft-Suspension RW Configuration
f = 20;
s = (f*2*pi)^2 * Iw_xy; % Formula converting frequency to spring stiffness
d = 0.01;
```

Figure 36:MATLAB script to calculate the parameters for the simulation

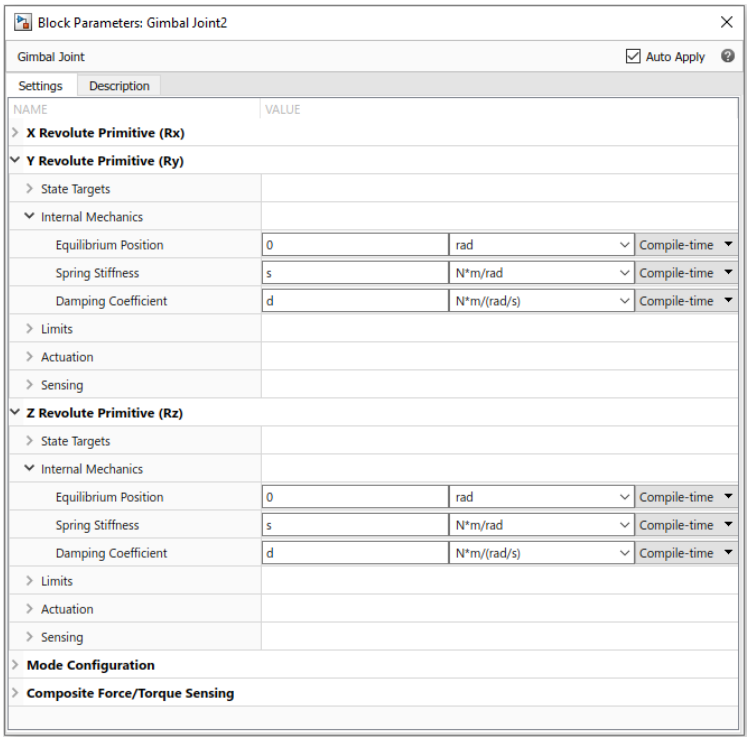


Figure 37: Block parameters of the gimbal joint

The wheel configuration of the designed soft suspension reaction wheel model is identical to the wheel design in *section 4.4.1*. Additionally, the reaction wheel movement is established through the same methodology as the method used in *section 4.4.1*.

4.5.2 Mechanics Explorers

The Mechanics explorers of the soft suspension reaction wheels with the satellite structure are shown in Figure 38. The behaviour of the satellite and the reaction wheels are analysed with each time step. In Figure 38 the green axis

represents the y-axis, the red axis represents the x-axis, and the blue axis represents the z-axis. The coordinate of the satellite body is set to be the global coordinate, and each wheel's subsystem coordinate is shown in Figure 38.

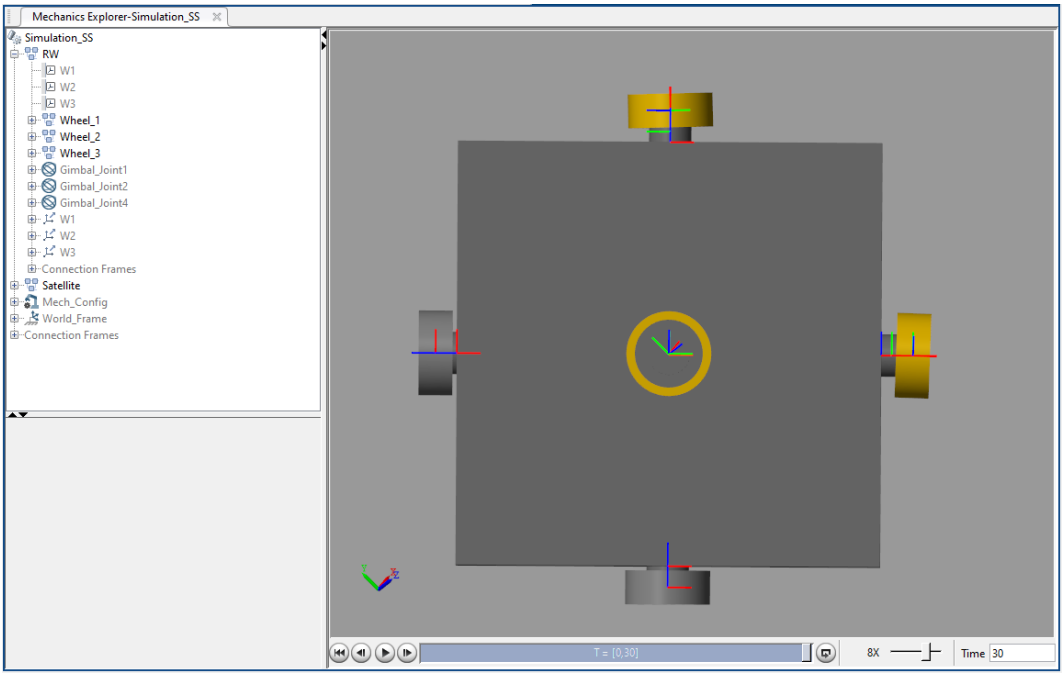
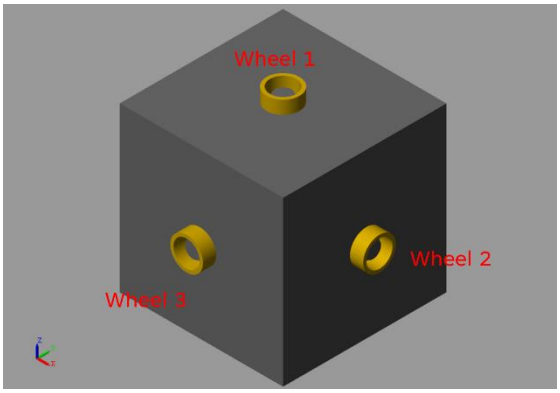


Figure 38: Mechanics Explorer of the developed soft suspension reaction wheel satellite configuration

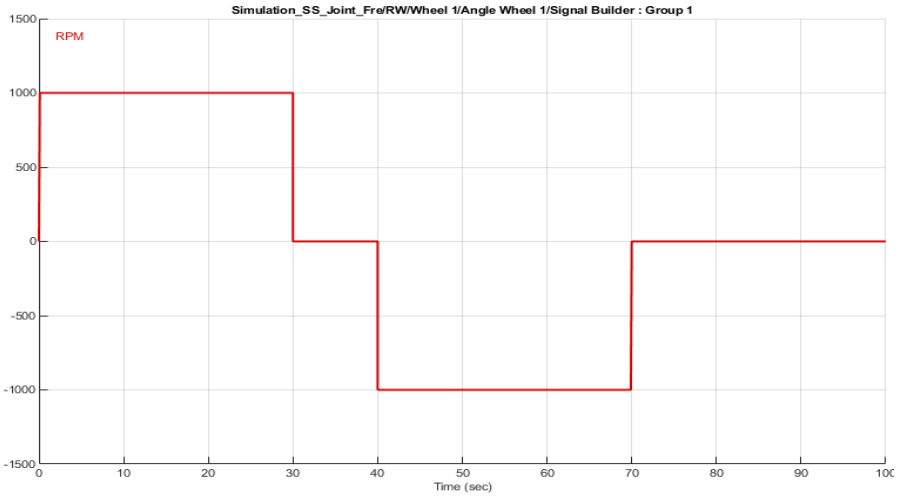
The model is simulated for 30 seconds with the parameters of a 20 Hz soft suspension reaction wheel with a damping coefficient of 0.01 Ns/m. It was observed that the axes of the reaction wheels were not aligned with the shafts in which they were connected. The tilt in the axes means the gyroscopic effect has an effect on the reaction wheels. The impact on the wheels of whether it has an effect on the pointing accuracy of the satellite is further investigated in *section 4.7*. The results of this simulation complement the prediction of the model since the inclusion of a soft suspension allows the rotor torque axis to deviate from the satellite axis and causes imbalances of the reaction wheel.

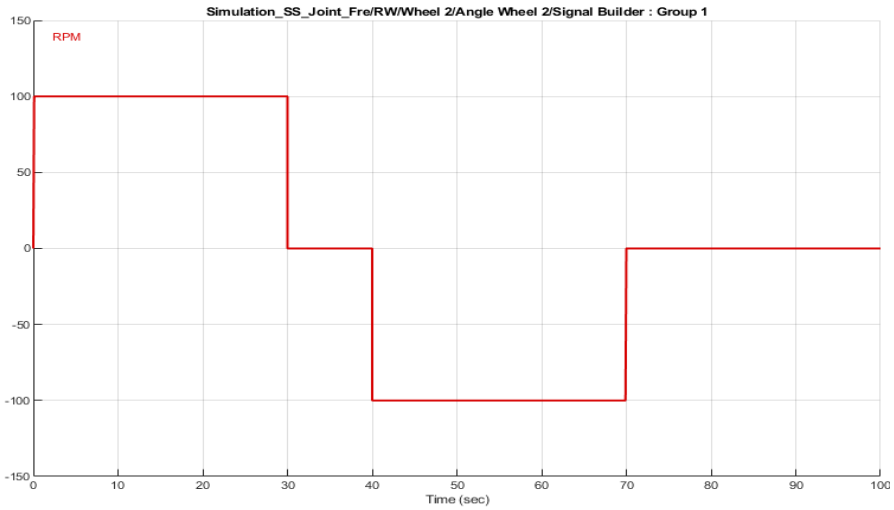
4.5.3 Wheel Oscillation Verification

Two types of validations are verified for the designed Simspace model for the soft-suspension reaction wheels configuration. The oscillation period of the soft suspension wheel is investigated because a soft-suspension system means there is a correlation between the frequency designed for the soft-suspension system and the period of the oscillation. Thus, the period of the oscillation and the derived frequency should match the frequency of the soft-suspension reaction wheel.



To validate the design of the reaction wheel, different frequencies of the spring stiffness are tested by simulating the model. The oscillation of the simulation results is observed, and the actual frequency is calculated to validate the initial frequency. The simulation condition (Figure 40) utilises excitation on wheel 1 and wheel 2 which are indicated in Figure 39, with step inputs with a variation of ±1000 rpm and ±100 rpm, while wheel 3 has a constant 0 rpm shown in the graphs from Figure 40:





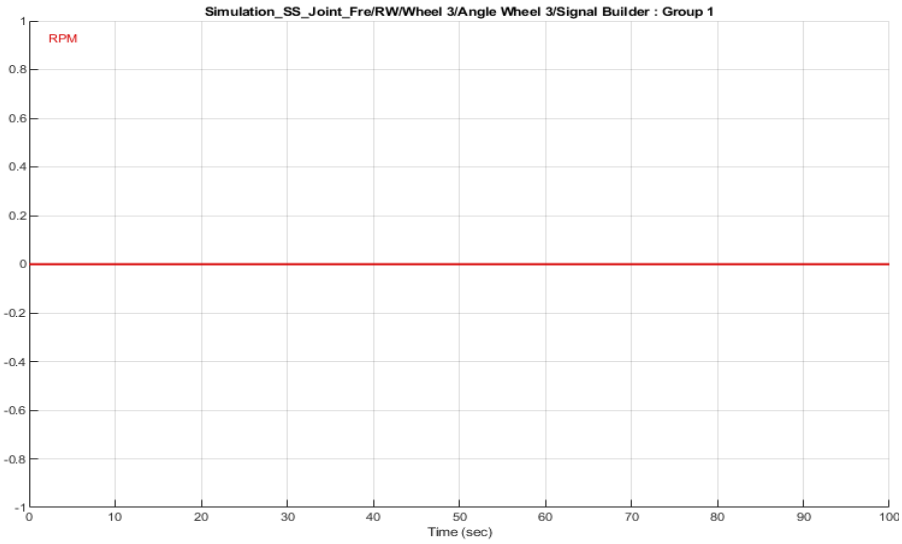


Figure 40:The simulation input profile for each reaction wheel

Below is an example of the 20 Hz soft suspension reaction wheel configuration result. The simulated result is a damped harmonic oscillation with a period of approximately 0.05 seconds in wheel 3, in which the corresponding frequency is the reciprocal of the period giving an actual frequency of 20 Hz. For both wheel 1 and wheel 2 there is not angular displacement in the reaction wheels. This is identical to the spring stiffness parameter initialised for the system, thus, validating the simulation model with the theoretical model.



Figure 41: Simulation result of the angular displacement of each wheel (20 Hz)

Further investigations are carried out with different spring stiffness to ensure the performance of the model is valid with other parameters. The results are shown in Table 4. Through the repeating process of verifying the regularity and

flexibility of the model, the results indicate that the simulated frequency of the oscillation matches the parameters initialised.

Table 4: Input frequency compared to the simulated frequency of the reaction wheel

Results

Inertia	5.79E-04	kgm^2	Ramp up Time	0.001
Simulation Velocity	1.00E+03	rpm		

Desire Frequency [Hz]	Stiffness [Nm/rad]	Period [s]	Actual Frequency [Hz]	Amplitude [rad]
0.05	5.72E-05	2.01E+01	0.0499	1.52E-01
0.1	2.29E-04	9.99E+00	0.1001	7.59E-02
1	2.29E-02	9.99E-01	1.001	5.46E-03
10	2.29E+00	1.00E-01	10	1.88E-05
20	9.15E+00	5.00E-02	20	2.37E-06
30	2.06E+01	3.40E-02	29.41	6.56E-07

4.5.4 Offset Reaction Wheel Placement

Further testing is done to determine the effect of reaction wheel placement on the gyroscopic effect of the soft suspension reaction wheel. The purpose of the test is due to the general placement of the reaction wheels on a satellite body which is not aligned at the centre of the satellite body. Figure 42 shows the mechanic explorer display of offsetting all three reaction wheels to the corner of the satellite body. The initial condition is the same as *section 4.5.3* defined in Figure 40.

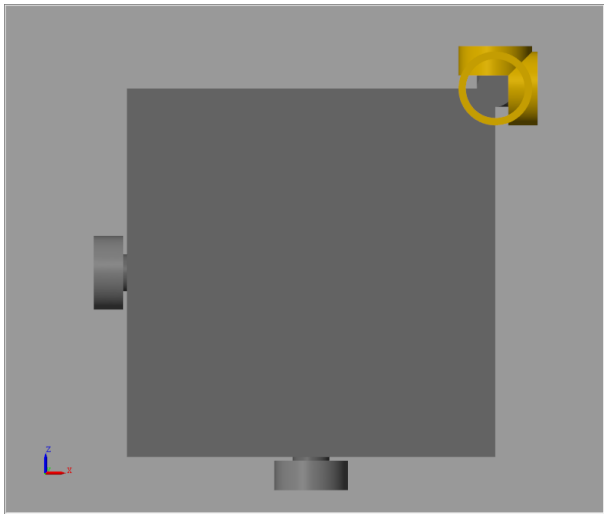


Figure 42: Mechanics Explorer of the developed offset reaction wheel satellite configuration

The model depicted in Figure 42 is compared against the configuration used in *section 4.5.3.1* with the same input for each reaction wheel. MATLAB calculates the angular displacement difference between the two models (Figure 43). The angular difference of the satellite body between the two models was found to be approximately 3.5 degrees at maximum in the y-axis. The angular displacement

difference is approximately 0.14 degrees at maximum for both the x direction and z direction.

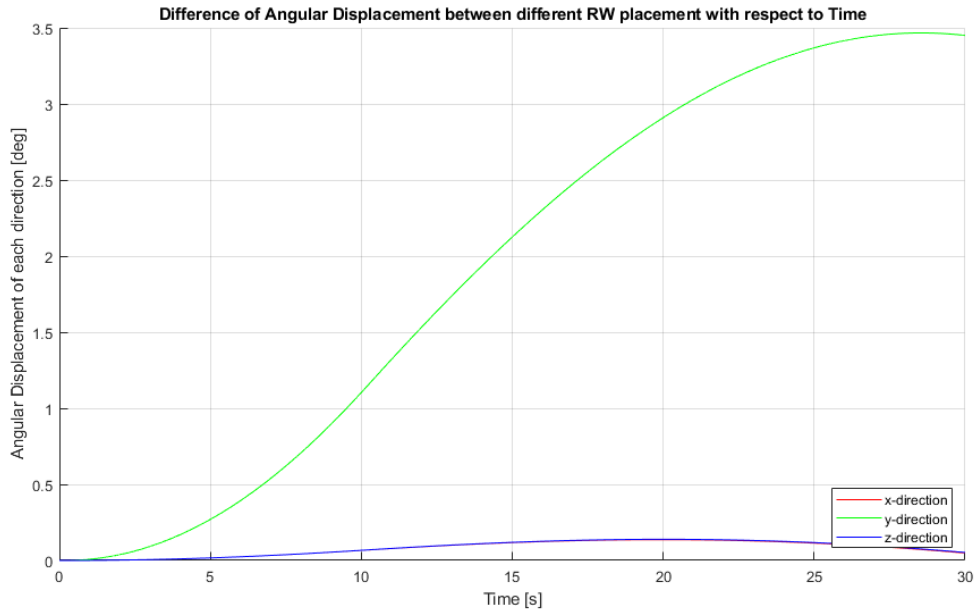


Figure 43: Difference in angular displacement between different reaction wheel placement

4.6 Results and Discussions

Two different cases are studied with the developed real-time simulation model in *section 4.5.1*. The first study case is a simulation of a 20 Hz soft-suspension RWAs which is used throughout the project. The second case studies soft-suspension RWAs with a lower frequency meaning the reaction wheels are less rigid and have higher flexibility compared to the first case study. Both cases have a damping coefficient of 0.01 Ns/m. A profile of a typical Agile Satellite manoeuvre moment for each wheel is used as an input for both case studies. The tilting moment caused by the gyroscope effect is analysed, which is determined by the angular displacement of the wheels.

4.6.1 CASE STUDY 1: 20 Hz Soft-Suspension Reaction Wheels

A 20 Hz soft suspension reaction wheel is investigated as a baseline for the stiffness of the reaction wheel throughout the project. In order to obtain results of the behaviour of the 20 Hz soft suspension reaction wheel, an input profile which generates an excitation moment for the wheel is implemented to wheel 1 and wheel 2 using signal builder shown in Figure 45. The model is simulated for 30 seconds, and the final orientation of the satellite configuration is shown in Figure 44. The

initial condition of the simulation is defined in Table 5. By analysing Figure 44 there is no displacement in the alignment of the reaction wheel axes with the satellite axes.

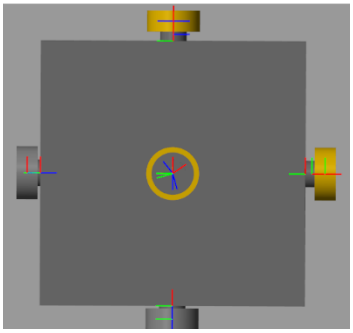


Figure : Model orientation of the 20 Hz soft suspension configuration at the end of simultion period

Table 5: Initial condition of Case Study 1: 20 Hz Soft-Suspension reaction wheels

	Value	Unit
Spring stiffness	9.15	N/m
Damping coefficient	0.01	Ns/m
Wheel 1 acceleration	0	rad/s^2
Wheel 2 acceleration	0	rad/s^2
Wheel 3 acceleration	0	rad/s^2
Satellite acceleration	0	rad/s^2
Wheel 1 velocity	267.04	rad/s
Wheel 2 velocity	267.04	rad/s
Wheel 3 velocity	0	rad/s
Satellite velocity	0	rad/s^2
Wheel 1 displacement	0	rad
Wheel 2 displacement	0	rad
Wheel 3 displacement	0	rad
Satellite displacement	0	rad

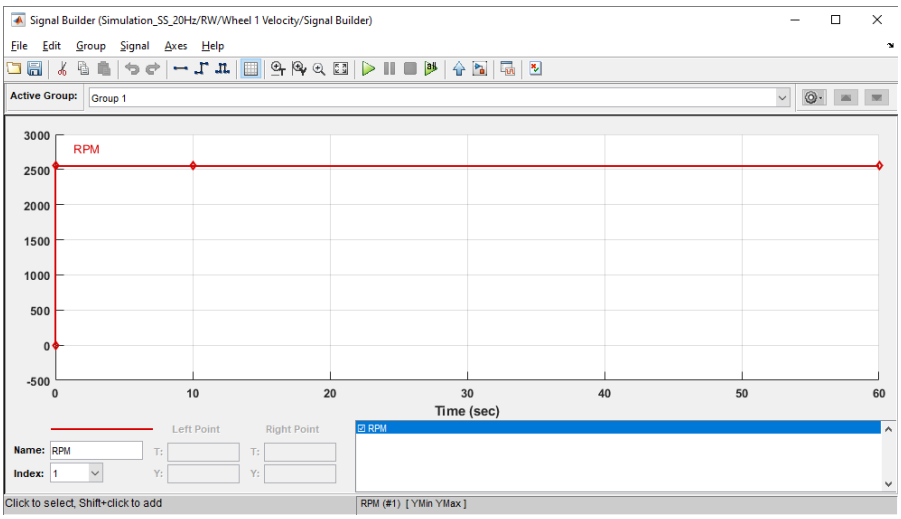


Figure 45: Input rpm profile from signal builder

The angular displacement of each wheel in the reaction wheel local coordinate y-axis is analysed because it represents the movement in the plane in which the soft suspension is applied. It is shown that wheel 1 has a significantly greater magnitude in angular displacement compared to the other two wheels. Small oscillations are observed on all wheels, caused by the rocking effect generated by the dynamic coupling of the reaction wheels.

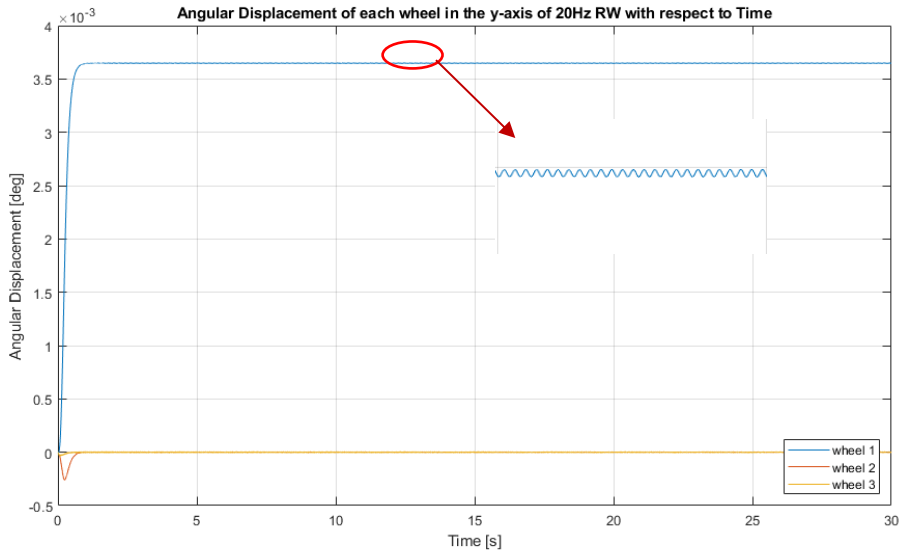
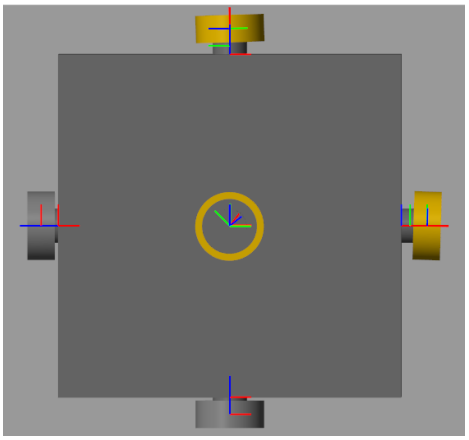


Figure 46: Simulation results of angular displacement of each wheel (20 Hz)

4.6.2 CASE STUDY 2: 4 Hz Soft-Suspension Reaction Wheels



Another case study investigates reaction wheels with less stiff soft suspension structures. The same input profile (Figure 45) is used to simulate the model for 30 seconds. The initial condition of the simulation is identical to the initial state in *section 4.6.1* defined in Table 5. By observing the orientation of the model after the simulation, there is misalignment between the reaction wheels and the satellite body. This means that the dynamic coupling causing the reaction wheels to experience a gyroscopic effect has a more significant effect on the less stiff soft suspension reaction wheel in comparison to the relative magnitude of the 20 Hz soft suspension reaction wheel.

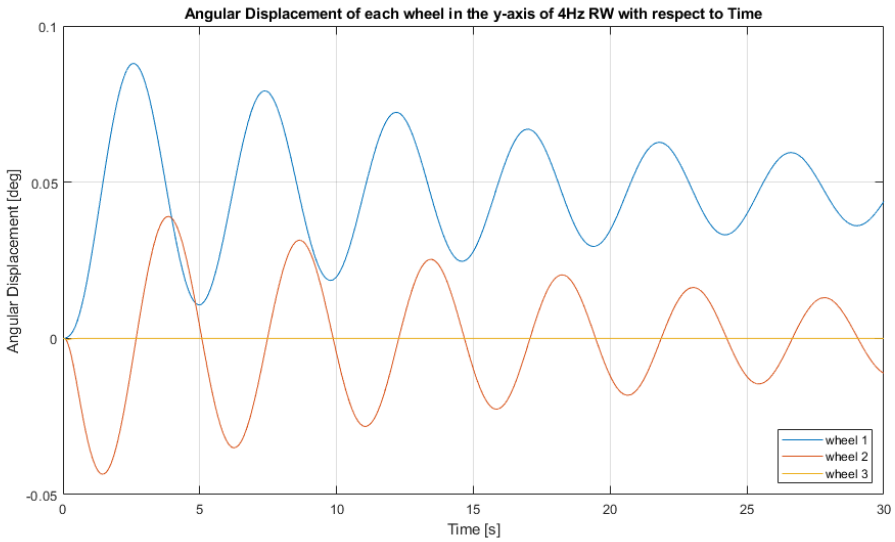


Figure 48: Simulation results of angular displacement of each wheel (4 Hz)

Detailed investigations are carried out to gain an understanding of a soft suspension reaction wheel with a lower stiffness by analysing the angular displacement of each wheel on the y-axis. It is shown that the magnitude of the angular displacement of wheel 1 is greater than the angular displacement in the other reaction wheels. Additionally, it is observed that there is a phase difference in the oscillation between wheel 1 and wheel 2 but with the same oscillation period. This is caused by the configuration of the reaction wheels on the satellite body. Since the x-axis and y-axis are on the same plane, the direction of the rotation of the reaction wheels determined the amplitude of the oscillation.

It is also observed that the oscillation amplitude for both wheel 1 and wheel 2 decreases with time. This is caused by the defined damping coefficient of 0.01 Ns/m from the designed soft suspension reaction wheel. With the implementation of the damping coefficient, the amplitude of the amplitude-frequency curve decreases. Thus, the system becomes more stable with the reduced amplitude meaning the effect of the oscillation affecting the movement of the reaction wheel body is minimised over time.

Comparing the results against the 20 Hz soft suspension model, the magnitude of the angular displacement is significantly larger, and the oscillation period is longer. This is justifiable since the frequency is inversely proportional to the oscillation period $f = \frac{1}{T}$. Thus, the oscillation period is longer with lower stiffness (lower frequency). With a lower stiffness, the overall structure in the soft

suspension plane of the reaction wheel is more flexible, increasing the tolerance of the displacement in the soft suspension plane.

4.7 Satellite Pointing Accuracy

A comparison of the accuracy performance between a rigid reaction wheel configurated satellite system and a soft suspension reaction wheel configurated satellite system is investigated. A commonly used manoeuvre profile is used to simulate the movement of the reaction wheels and further observe the behaviour of the satellite. An Agi Satellite manoeuvre of a constant angular velocity of $7\ °/sec$ for a period of 30 seconds for two reaction wheels is chosen for the simulation. Three different soft suspension reaction wheel parameters are compared, 20 Hz, which is the baseline of the soft suspension reaction wheel, 200 Hz, which has more similar characteristics to a rigid reaction wheel, and 4 Hz, which is considered a more flexible structure. From Figure 49, it is shown that the stiffness of the reaction wheel is exponentially related to the difference in angular displacement of the satellite compared to a rigid body reaction wheel. The maximum angular displacement for the 20 Hz soft suspension reaction wheel is approximately 0.188 degrees, whereas, for the 4 Hz soft suspension reaction wheel, the maximum angular displacement reaches 2 degrees.

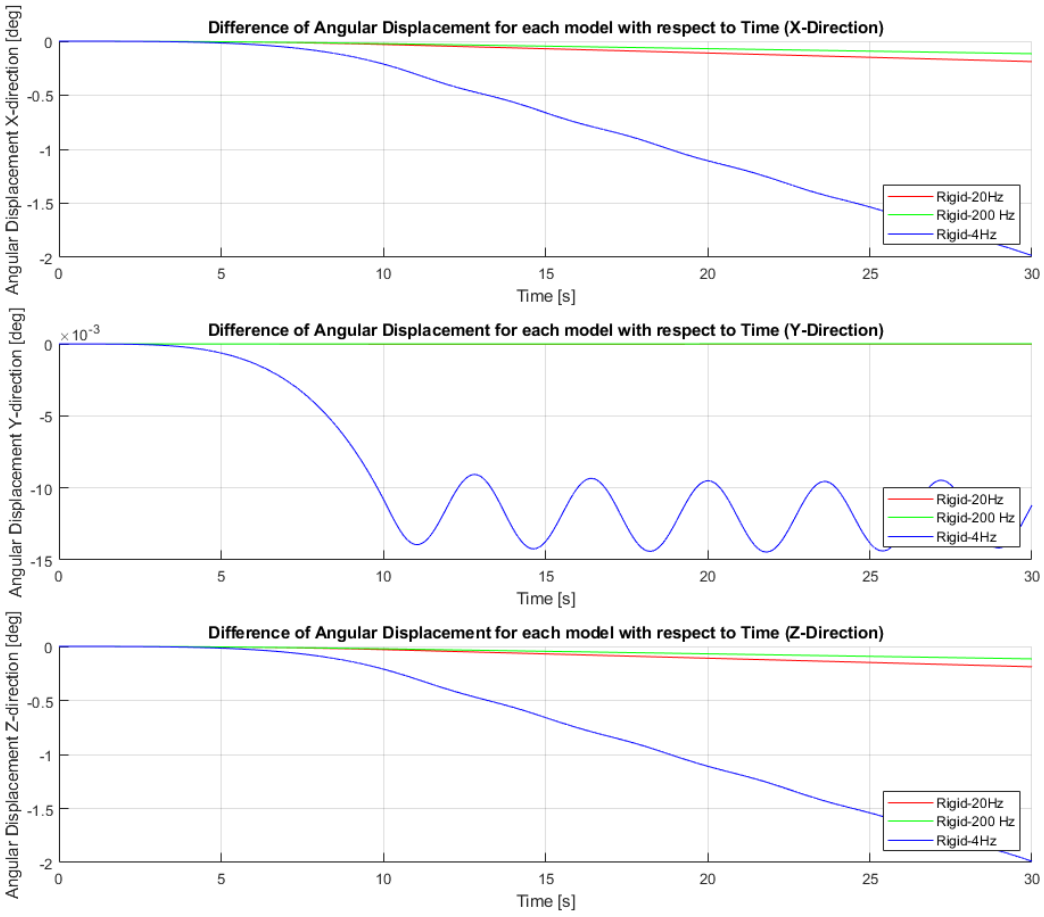


Figure 49: Simulation results of difference in angular displacement of the satellite with soft suspension reaction wheels (4 Hz, 20 Hz, 200Hz) with rigid body reaction wheels

Additionally, another test case shown in Appendix E is used to demonstrate the accuracy of the designed model further. The simulation utilises the same MATLAB script in Appendix D. However, instead of modelling the simulation to manoeuvre a constant angular velocity of $7\ °/sec$ for two reaction wheels, a ramp-up speed to the angular velocity of $7\ °/sec$ in 10 seconds for two reaction wheels was chosen. With the slower ramp-up angular velocity, it is shown in the result that the angular difference between the rigid body reaction wheel and all soft suspension reaction wheels is minimal and can be considered negligible. The angular difference has significantly decreased by comparing the result to the test case shown in Figure 49, which has a relatively higher ramp-up angular velocity.

Further investigations are carried out where the difference in angular displacement in each direction of the rigid body reaction wheel is compared against different frequencies ranging from 1 Hz to 40 Hz with a step of 1 Hz. The results

are shown in Figure 50, and the calculations are shown in Appendix F. It is concluded that the less stiffness (lower frequency) of the soft suspension reaction wheels, the larger the pointing error. For example, according to the results a soft suspension reaction wheel with a frequency of 1 Hz has a pointing accuracy approximately 25 degrees. With the same reaction wheel input profile, an exponential relation between the angular displacement and the stiffness of the reaction wheels can be concluded. Thus, it can be concluded that lowering the stiffness of the reaction wheels can significantly impact the pointing accuracy of the satellite.

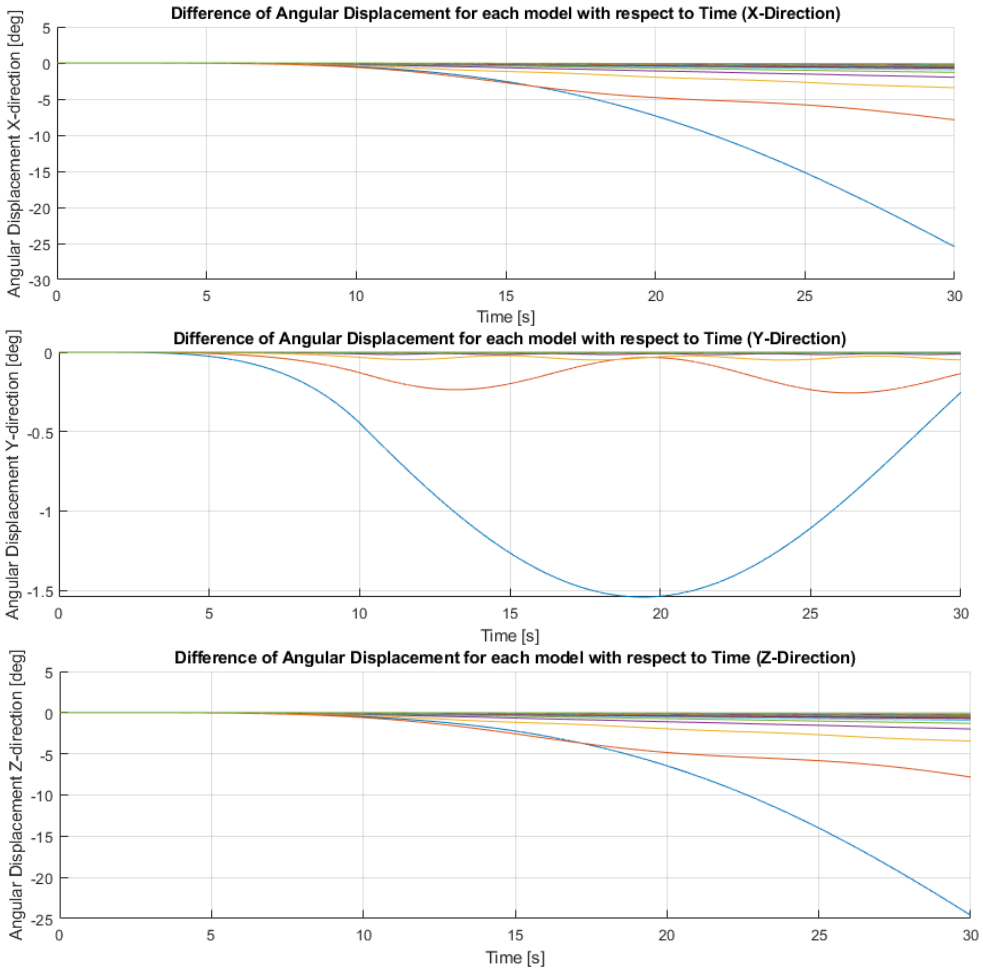


Figure: Simulation results of difference in angular displacement of the satellite with soft suspension reaction wheels (1-40 Hz) with rigid body reaction wheels

Unexpected oscillations are observed in the simulation results in which the period differs depending on the angular velocity of the soft suspension wheels. The amplitude of the oscillation significantly impacts the performance of the satellite at lower stiffness. This was suspected to be caused by the resonance with eigenfrequencies of vibration. To investigate whether this factor causes the

oscillation Campbell diagram is used. A Campbell diagram represents the vibration frequencies of a system at various operating rpm [18]. The formula to calculate the natural frequency and further derive the Campbell diagram is stated in Equation 40 [20]. Ω is the angular velocity in which the reaction wheels are rotating, and ω is the eigenfrequencies. I_z is the vertical inertia of the wheel and I_r is the inertia in the radial direction. Since the reaction wheel is symmetric, k_t and k_r are the stiffness of the wheel which are equal. M_w is the mass of the reaction wheel and d is the diameter of the shaft in which the wheel is connected to the satellite body.

$$\omega^4 - \Omega\frac{I_z}{I_r}\omega^3 - \left(\frac{k_t}{M_w} + \frac{k_r + k_t d^2}{I_r}\right)\omega^2 + \Omega\frac{k_t I_z}{M_w I_r}\omega + \frac{k_t k_r}{M_w I_r} = 0 \quad (40)$$

This solution of the equation provides four structural modes for the reaction wheel and by calculating with a range of angular velocity, the Campbell diagram of the reaction wheel can be obtained. To verify the assumption that the resonance with the eigenfrequencies causes the oscillation, the 4 Hz soft suspension reaction wheel is used as an example. The Campbell diagram for the model is derived (Figure 51).

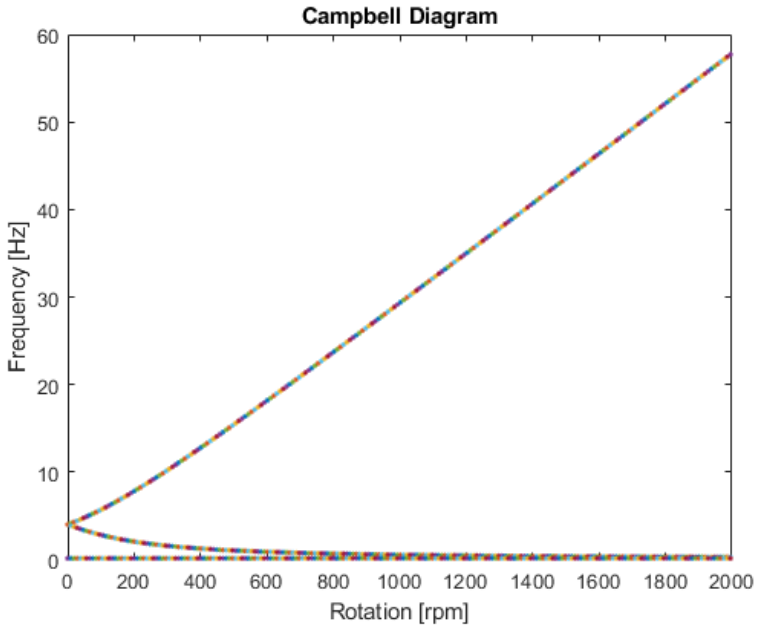


Figure 51:Campbell diagram for a 4 Hz soft suspension reaction wheel model

Different angular velocities are tested with the Simspace model to obtain the corresponding oscillation frequencies. The frequencies are compared against the

Campbell diagram derived from the MATLAB script (Appendix G), shown in Table 6. It was found that the second natural frequency is the exact frequency in which the vibration frequency of the satellite body. Thus, it can be concluded that the effect of eigenfrequency of the soft suspension reaction wheels causes the oscillation in the manoeuvre of the satellite body.

Table 6: Comparison of wheel velocity and oscillation of satellite body

Wheel RPM vs Oscillation of Satellite Body (4 Hz)				
Wheel RPM [rpm]	*Wheel Natural Frequency [Hz]*	*Oscillation Period [s]*	*Oscillation Frequency [Hz]*	*Amplitude [deg]*
2550	*0.1360, 0.2218, 72.219*	*4.474*	*0.223513634*	*0.01535*
2000	*0.1361, 0.2768, 57.847*	*3.591*	*0.278473963*	*0.004884*
1500	*0.1361, 0.3680, 43.511*	*2.751*	*0.36350418*	*0.001196*
1000	*0.1361, 0.5497, 29.291*	*1.867*	*0.53561864*	*0.00015678*
500	*0.1361, 1.0354, 15.462*	*0.991*	*1.009081736*	*0.002831959*
10	*0.1361, 3.866, 4.141*	*NA*	*NA*	*NA*
0	*0.1361, 4, 4*	*0*	*NA*	*0*

CHAPTER 5

CONTROL DESIGN and SIMULATIONS

The pointing error investigated and discussed in Chapter 4 raises the problem of the accuracy and performance of the satellite. A control system is designed in this chapter to compensate for and minimise the pointing error. A PID controller is designed using the Ziegler-Nichols close-loop PID tuning method. A comparison between the reference trajectory and the trajectory of the controller is carried out. The performance of the controller is evaluated by further comparing the trajectory of the rigid body reaction wheel configuration and soft-suspension reaction wheel configuration. Analyses and discussions on the obtained responses are given in this chapter.

5.1 Quaternion Feedback Controller (PID Controller)

5.1.1 Design Method

A quaternion feedback controller is used to control the movement of the reaction wheels and manoeuvre the satellite body. The controller minimises the satellite's pointing error caused by the dynamic coupling effect from the reaction wheels. The designed controller is developed in Simulink to obtain simulation results and validate the feasibility of the controller in which the overall structure is shown in Figure 52.

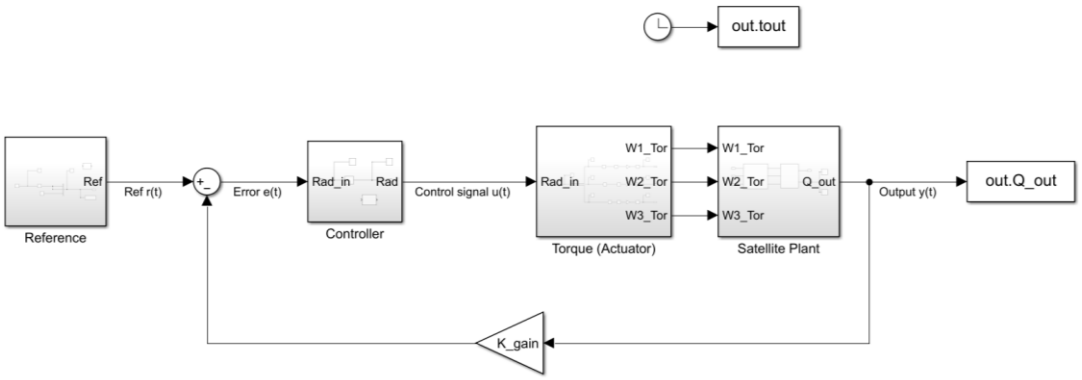


Figure 52: Overall Simulink model of the satellite system with a quaternion feedback controller

The *Reference* subsystem is where the reference trajectory of the simulation is defined through inputs from the workspace in MATLAB. The input is further

used as the reference point for the control system. The Controller subsystem is used to control the Torque (actuator) subsystem to provide the Satellite Plant subsystem with the desired actuation for the plant to output the desired trajectory of the satellite body. The controller block is described by a control law, which has a relationship between the error, e(t), and the control signal, u(t), as indicated in Figure 53. The error in the trajectory of the satellite is calculated by comparing the difference between the output of the Satellite Plant and the reference trajectory.

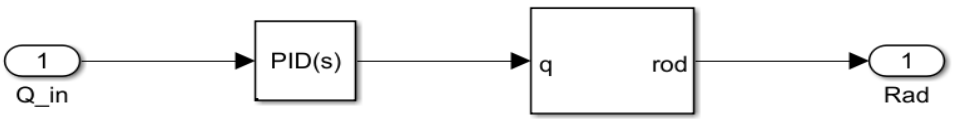


Figure 53: Controller sub-system of the control design model

The configuration of the designed control system is a standard reference tracking control system which uses a Proportional-Integral-Derivative (PID) controller illustrated in Figure 53. The PID controller takes the quaternion of the feedback system as an input and outputs the control signal with the tuned gains (Kp, Ki, and Kd), which is discussed in *section 5.1.2*. The control signal is decomposed in terms of radians using the *Quaternions to Rodrigues* block in which a 4-by-1 quaternion determines three elements of the Rodrigues vector.

However, due to the nonlinearity of the Satellite system, a PID controller can be tuned to operate around a specific equilibrium point where the linearity is valid. The performance of the controller degrades when operating above the equilibrium point. To overcome this issue, the implementation of gain-scheduling is utilised in which the *Gain (K_gain)* block is used in the referencing tracking loop of the controller.

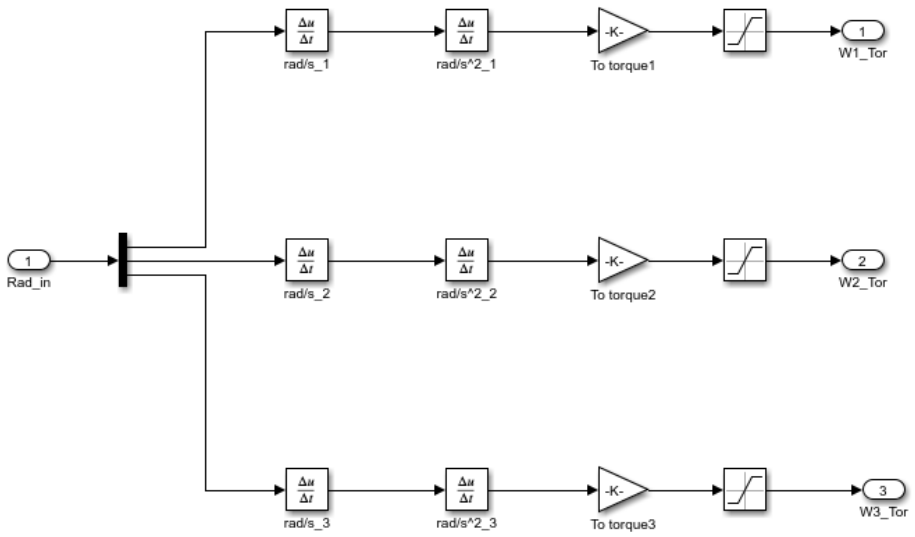


Figure 54: Actuator sub-system of control signal conversion of the control system model

The *Torque (Actuator)* subsystem takes the control signal, *u(t)*, from the PID controller as the input. The vector of the control signal is extracted to separate signals which each corresponds to the torque required to be generated by each reaction wheel. The process of converting the control signal to the required torque for each reaction wheel is shown in Figure 54.

5.1.2 Tuning of Controller

Proportional-Integral-Derivative (PID) Controller is used as the reference tracking control system controller. A PID controller follows the control law stated in Equation 41 where the output of the control law is the control signal.

$$u(t) = K_P e(t) + K_I \int_0^t e(\tau)d\tau + K_D \frac{d}{dt} e(t) \quad (41)$$

where K_P, K_I and K_D are the proportional, integral, and derivative gains, respectively [9]. The proportional controller element ($K_P e(t)$) is an amplifier with an adjustable gain. The integral controller element $K_I \int_0^t e(\tau)d\tau$ increases the Type Number of the system by 1, thus, eliminating the steady-state error of the system. The integral term also increases the order of the closed-loop system, decreasing the stability of the system. The derivative term $K_D \frac{d}{dt} e(t)$ provides damping to the

close-loop system, reducing the overshoot and settling time and stabilising the unstable plant.

Adjusting the gain affects the response of the controller to changes in the input between each time step. When tuning the proportional gain, increasing the value increases the response on the output to bring the output closer to the desired output. The derivative gain limits the output value to prevent overshooting a specific output.

To tune the gains (K_P, K_I and K_D) the Ziegler-Nichols Closed-Loop tuning method is used with the ultimate gain technique for the PID controller. The tuning process is achieved by experimentally testing the plant's behaviour in a closed-loop system with a Proportional controller. The value of K_P is increased until the system exhibits a sustained oscillation meaning it is marginally stable. The value of the K_P at the instant is the value of the ultimate gain, K_u, and the period of the sustained oscillation is the ultimate period, T_u. Table 7 shows the relation of the ultimate gain and ultimate period with each controller type and the corresponding values of the gains (K_P, K_I and K_D) [9].

Table 7: The Ziegler-Nichols PID controller parameters from closed-loop experiments [9]

Controller Type	K_P	K_I	K_D
P	$0.5K_u$	-	-
PI	$0.45K_u$	$\frac{0.54K_u}{T_u}$	-
PID	$0.6K_u$	$\frac{1.2K_u}{T_u}$	$0.075K_uT_u$

Through repetitive experiments of simulating different K_P values, the ultimate gain, K_u, is determined to be 32 with an ultimate period, T_u, of 0.45 seconds. The gains for the PID controller are calculated using the MATLAB script in Appendix H, where the gains are defined in terms of the ultimate gain and ultimate period. The final values of the K_P, K_I and K_D are 19.2, 85.33 and 1.08, respectively.

5.1.3 Controller Output

The output of the tuned controller is used to adjust the error between the desired trajectory of the spacecraft and the actual trajectory of the spacecraft. The output acts as a gain which modifies the actuator of the system which are the reaction wheels. The gain changes the applied torque for each of the reaction wheels and adjusts the torque accordingly to the difference between the actual trajectory of the spacecraft and the desired trajectory. For example, when the actual trajectory is less than the desired trajectory, the output of the controller will have gains which increase the torque value of the reaction wheels for the next time step and vice versa.

5.2 Results and Discussions

5.2.1 Reference Trajectory

To compare the performance of the designed controller in *section 5.1*, the controller is tested by comparing the simulation results against the reference trajectory. The reference trajectory for the control system is defined using the following model (Figure 55). The angular velocity of the satellite is defined with the signal source of the *Ramp* and *Constant* blocks. The simulation period is 10 seconds, and the Agile satellite manoeuvre is used as the simulation profile in both the x-axis and y-axis of the satellite. A common manoeuvre profile with an Agile satellite of increasing $7\,°/second$ is chosen. Thus, the Ramp parameter, slope, is defined as $0.122\,rad/second$. The reference angular velocity is integrated to obtain the reference angular displacement of the satellite which is converted into the quaternion form.

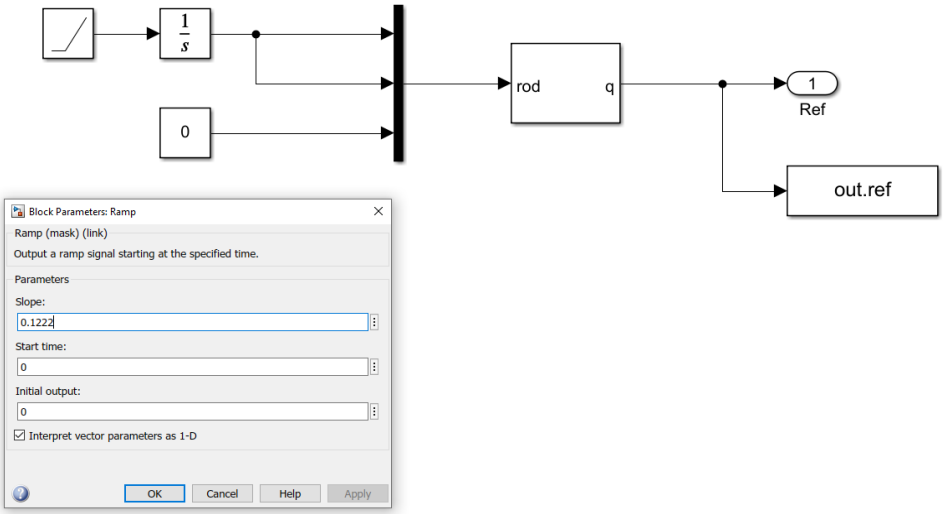


Figure 55: Input profile sub-system of the control system model

5.2.2 Rigid Body Reaction Wheel Satellite Configuration

The performance of the Quaternion feedback controller is evaluated using the satellite model with rigid body reaction wheels. The reference profile of the desired satellite manoeuvre is described in *section 5.2.1*. The performance of the quaternion feedback controller is evaluated by determining the final angular displacement the satellite travelled in comparison to the reference angular displacement. Additionally, the trajectory of the simulation is analysed to determine the processing time, overshoot, and noise compared against the reference trajectory. The simulation result is shown in the graph from Figure 56, with a comparison with the reference trajectory.

By analysing the results, it is found that the performance of the quaternion feedback controller has the final angular displacement of the simulation result achieving approximately the same result as the reference angular displacement. The reference angular displacement at the end of the 10 seconds is -350.08 degrees, whereas the angular displacement from the simulation is -351.6 degrees, which gives a difference of 1.52 degrees. The processing time of the controller is found to be approximately 0.0057 seconds. Then by analysing the graph, the simulated results have a slower rise time compared to the reference angular displacement. The results from the simulation do not indicate generated or amplified noise from the controller, and the results do not have overshoot which are desirable characteristics

for a controller. Overall, the result from the simulation shows that the performance of the controller instantly achieves the desired trajectory with limited process time.

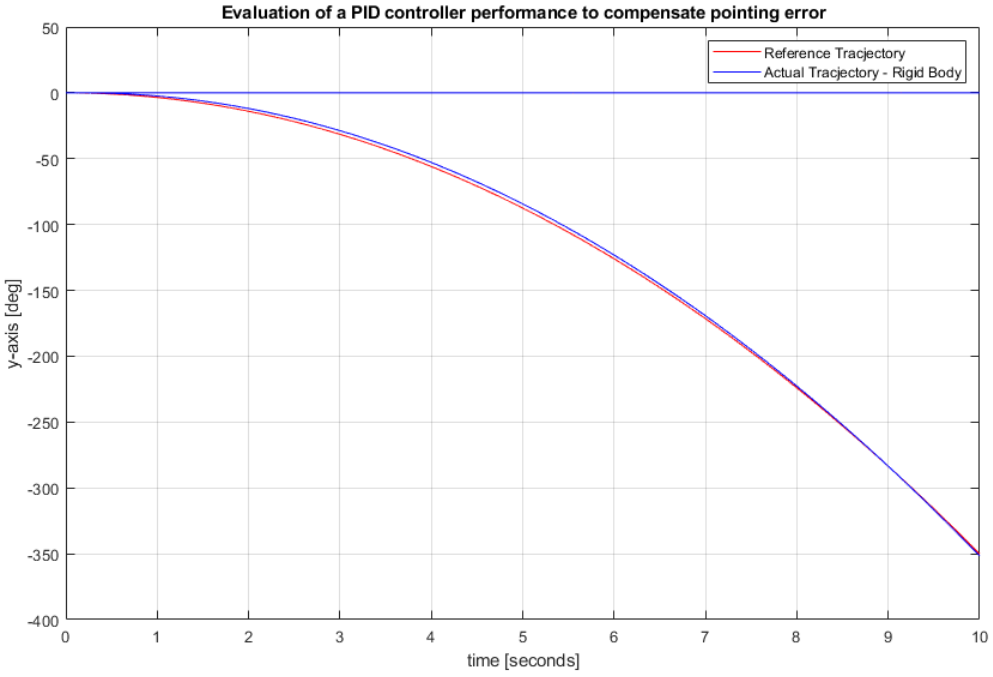


Figure 56:PID controller performance evaluation between simulation results and reference trajectory of the satellite (Rigid body)

5.2.3 Soft Suspension Reaction Wheel Satellite Configuration

The performance of the Quaternion feedback controller is further tested with the soft suspension reaction wheel satellite configuration. Soft suspension reaction wheels system has a higher uncertainty in the stability compared to the rigid body reaction wheels. Thus, the simulation results can determine the designed controller's ability to compensate for higher uncertainties within the plant system.

The results obtained from the soft suspension reaction wheel simulation are similar to the results from *section 5.2.2*. The final angular displacement of the simulation results achieves approximately the same as the reference angular displacement. The angular displacement of the soft suspension reaction wheel and the end of the simulation is 351.04 degrees, which is a 0.56 degrees difference from the reference angular displacement. The processing time of the controller is found to be the same as the rigid body reaction wheel simulation of 0.0057 seconds. By analysing the graph (Figure 57), the actual trajectory from the simulation has a similar result to the rigid body reaction wheel simulation, where the rise time is

lower compared to the reference angular displacement. No induced or amplified noise is observed from the results, and no overshoot of the results can be determined. Thus, the performance of the quaternion feedback controller can be concluded to be adaptable to different reaction wheel configurations and compensate for the pointing errors generated from the dynamic coupling effect of the soft suspension reaction wheels.

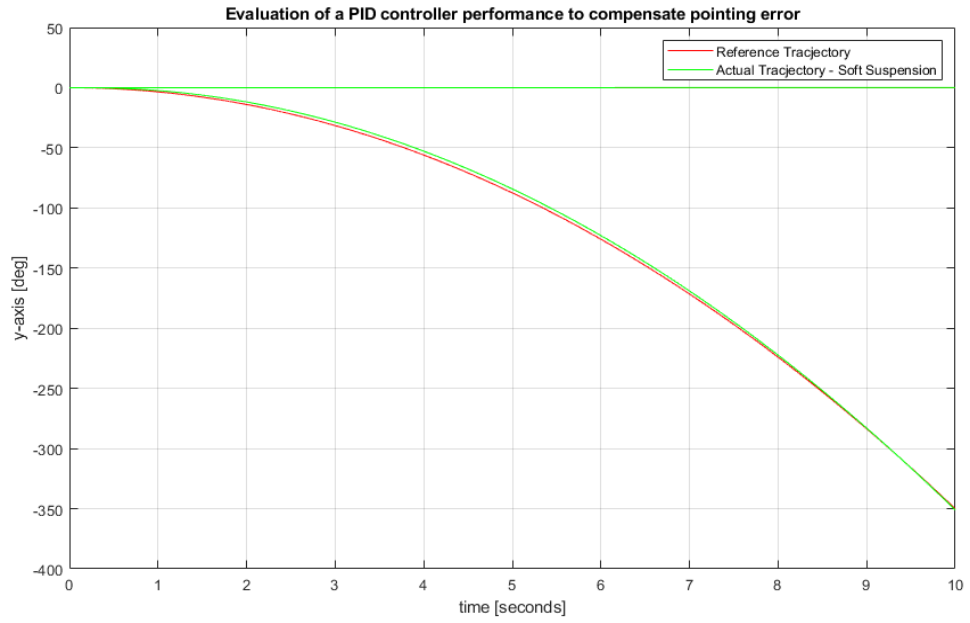


Figure 57: PID controller performance evaluation between simulation results and reference trajectory of the satellite (Soft suspension)

The results for both simulations towards the end of the simulation time are specifically analysed against the reference trajectory. It is found that the angular displacement from both simulations has a similar trajectory except for a slight difference in the angular displacement for less than 0.5 degrees at any time given.

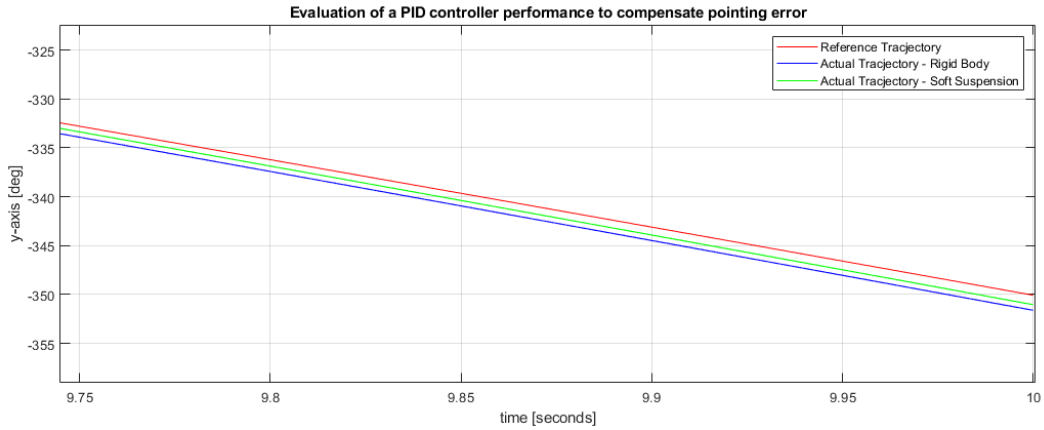


Figure 58: PID controller performance evaluation between simulation results and reference trajectory of the satellite (Rigid body and soft suspension)

By investigating Figure 58, it is shown that the rigid body simulation has a more significant difference in angular displacement with the reference trajectory compared to the soft suspension simulation. This means the performance of the controller was able to compensate for less of the error through the control system giving an output with a higher error. The result was opposite to the prediction as the rigid body expected to have a smaller error in angular displacement than the soft suspension reaction wheel since the initial angular displacement error is smaller, which is proven in *section 4.7*. This indicates that the designed quaternion feedback controller has an increased performance with an increased error signal.

Chapter 6

CONCLUSION and FUTURE WORK

Evaluation of the difference in performance between a rigid body reaction wheel and a soft suspension reaction wheel is modelled and the obtained results are analysed. This chapter summarises and concludes the results and findings obtained in previous chapters. Recommendations and suggestions are given for future work.

6.1 Conclusion

The requirement of high structure stability for small spacecraft for the mission has been in high demand with developed highly sensitive payloads such as cameras, telescopes, and sensors. The micro-vibrations of the satellite significantly impact the stability and accuracy of the spacecraft. The main micro-vibration source of a spacecraft is the high-speed rotation devices such as reaction wheel assemblies (RWAs). The development of a soft suspension system minimises the micro-vibration but introduces uncertainty into the system due to the dynamic coupling effect between the reaction wheels.

With the main objective of this project is to develop a methodology to model the dynamic coupling effect. Additionally, the pointing error of the satellite with the soft suspension reaction wheel assembly configuration is determined. The pointing error is addressed by designing a controller. In particular, the focus of this thesis is on the modelling of the soft-suspension RWAs and the design of a controller to compensate for the effect of dynamic coupling.

Investigation of the relationship between the satellite body and the reaction wheels was achieved. The mathematical model is derived using Euler's Equation with Coriolis Theorem with the understanding of the relation of the reaction wheel with respect to the satellite. The gyroscopic effect on each reaction wheel induced by the dynamic coupling effect between each reaction wheel and the satellite body is further discussed.

The simulation of both the rigid body reaction wheel and the soft suspension reaction wheel is developed in accordance with the developed mathematical model. This enables visualisation of the model at each time step and easier access to the

input for the system for testing and validation purposes. The result of the simulation is compared against the theoretical results obtained from the mathematical model to verify the designed simulation models. Detailed analyses of the motion of the satellite are accomplished by studying the results and observing the trends by changing the parameters for the soft suspension structure, such as the stiffness and damping coefficient.

With the developed simulation models, the pointing error of the satellite is further investigated. Two different soft suspension reaction wheel models were compared against the rigid body reaction wheel models. One model is 20 Hz, the baseline frequency used for the soft suspension design throughout the project, and 4 Hz, demonstrating a configuration with a more flexible structure. With the input profile of a manoeuvre of 7 degrees/second, it was found that the pointing error of the standard soft suspension reaction wheel structure (20 Hz) is 0.188 degrees. In contrast, the more flexible structure (4 Hz) has a pointing error of 2 degrees.

A quaternion feedback controller is designed to eliminate the pointing error of the satellite. The PID controller implemented in the controller system is tuned using the Ziegler-Nichols Closed-Loop tuning method. An additional gain was required for the control system in the feedback loop due to the nonlinearity of the satellite plant. The results from the simulation show that with the implementation of the control system the pointing error of the satellite was minimised to 0.56 degrees for the soft suspension reaction wheel structure. Compared to the pointing error without the designed controller, the pointing error of the satellite can be concluded to be improved. It is also concluded that the controller is better at regulating larger error signals and performs better when the initial error signal is high.

6.2 Recommendations for Future Work

The recommendations for future work can be categorised into three main areas:

- The detailed structural design of the satellite body and reaction wheel placement using CAD software (i.e. ADAMS and Autodesk Investor).
- Improved/Alternative controller design to minimise pointing error of the satellite to less than 0.01 degrees.

- Experiments of testing the designed controller with applications to gain evidence of the reliability and practicality of the controller designed in this thesis.

They are briefly introduced as follows:

- Detailed satellite body structure design with accurate reaction wheel placements.

Although the current satellite body and reaction wheel models used for the simulation process, adequately represent the industry-employed small satellite, the model can still be further improved. The current structure of the satellite body and the configuration of the reaction wheels are simplified, such as the location of the reaction wheels and the internal structure of the satellite. These factors can have an effect on the dynamic coupling effect of the reaction wheels. The developed mathematical model developed in Chapter 3 has the assumption that three reaction wheels are aligned with the XYZ axes of the satellite, and the small satellite is assumed to be a solid cube. With a more detailed model of the satellite structure and reaction wheel configuration, the relation between the inertia and moments of the satellite can be different to the theoretical equations derived in Chapter three.

An alternative reaction wheel configuration should be implemented to further investigate the satellite behaviour instead of the current orthogonal 3-wheel configuration. For example, a pyramidal reaction wheel layout can be tested since it is the most commonly used assembly where the four reaction wheels are designed for redundancy.

The detailed structural design of the satellite body and the reaction wheel can be created using Computer-Aided Design (CAD) software such as ADAMS or AutoCAD Inventor. Brief research for the feasibility of ADAMS was carried out in the initial stages of the project. Due to the time constraints, simplicity and compatibility between ADAMS and MATLAB the proposal was changed to using one software, MATLAB. However, with a more detailed design, ADAMS has the benefit of multibody dynamics simulation, such as building the relationship between different bodies and joints with inputs such as forces, moments, and velocity to be defined by the system.

- Improvement of the controller design.

To improve the efficiency, feedback linearisation or Lyapunov-based control can be performed to directly overcome the issue of the non-linearity of the satellite system. In this thesis, the presented controller design utilises a quaternion feedback controller with a PID controller to minimise the pointing error for the manoeuvre of the designed satellite. With the results from the simulation, it is found that the pointing error of the satellite is not eliminated with the implemented controller meaning improvements in the controller design can be achieved from the current method. For optimal control of the satellite system, a state-space approach that determines the control variable (the quaternion of the satellite) and further minimises the cost function using methods such as Linear Quadratic Regulation (LQR) or Model Predictive Control (MPC) instead of the PID controller. Additionally, to compensate for the non-linear behaviour of the satellite the gain-scheduling method is used in the project which is tuned according to the experiment results.

Apart from one single controller to control the angular displacement of the satellite, multiple controllers can be implemented in the satellite to control the actuators (torque). Increasing controller numbers means applying the single-tuning method to multiple controllers. This enables the fine-tuning process for individual controllers depending on the specific error signal and minimises the overall error for the output. However, multiple controllers mean the processing time will be longer than a single controller. Thus, calculating the equilibrium between the two and the feasibility are to be investigated and validated.

- In practice test applications of the designed controller.

The quaternion feedback controller introduced in the thesis has been only simulated in MATLAB. In practice, the accuracy of the designed controller would differ from the simulation results. This is because the simulation operates at ideal conditions (i.e. no friction in the reaction wheels and a steady voltage supply). Thus, it is necessary to verify the quaternion feedback controller developed in this thesis using in-practice test applications to obtain experimental results.

With the results obtained from the practical tests, the disturbances that were not accounted for in this thesis and caused uncertainty in the system can be further

modelled and integrated into the design to improve the model's accuracy in the practical situation. Applying the simulation to in-practice test applications verifies the theoretical model derived for the soft suspension reaction wheel structure. This further validates the reliability of the designed Simulink model for the soft suspension reaction wheel.

BIBLIOGRAPHY

[1] Addari, D., Aglietti, G. S., & Remedia, M. (2017). Experimental and numerical investigation of coupled microvibration dynamics for satellite reaction wheels. *Journal of Sound and Vibration*, *386*, 225–241. https://doi.org/10.1016/j.jsv.2016.10.003

[2] Canuto, E., Novara, C., Massotti, L., Carlucci, D., & Montenegro, C. P. (2018). Orbit and attitude actuators. *Spacecraft Dynamics and Control*, 463–520. https://doi.org/10.1016/b978-0-08-100700-6.00009-x

[3] Chin, J., Coelho, R., Foley, J., Johnstone, A., Nugent, R., Pignatelli, D., Pignatelli, S., Powell, N., & Puig-Suari, J. (2017, October). *CubeSat 101: Basic concepts and processes for first-time CubeSat developers*. NASA CubeSat Launch Initiative. https://smdepo.org/download/0ca0e4a9526a5

[4] DOUGHERTY, H. J., LEBSOCK, K. L., & RODDEN, J. J. (1971). Attitude Stabilization of synchronous communications satellites employing narrow-beam antennas. *Journal of Spacecraft and Rockets*, *8*(8), 834–841. https://doi.org/10.2514/3.59732

[5] Elburn, D. (2019, May 31). *FAQs-LEO Economy*. NASA. https://www.nasa.gov/leo-economy/faqs

[6] Glueck, E. (2022, January 15). *Introduction to motor constants for fractional horsepower gearmotors - bodine - gearmotor blog*. Bodine. https://www.bodine-electric.com/blog/bodine-gearmotor-constants/#:~:text=Mechanical%20Time%20Constant%20(Tm)%20%E2%80%94,is%20usually%20expressed%20in%20milliseconds

[7] Kramer, H. J., & Cracknell, A. P. (2008). An overview of small satellites in remote sensing. *International Journal of Remote Sensing*, *29*(15), 4285–4337. https://doi.org/10.1080/01431160801914952

[8] MORK, H. (1971). Synthesis and design of a gimbaled reaction wheel attitude stabilization package (grasp). *Guidance, Control and Flight Mechanics Conference*. https://doi.org/10.2514/6.1971-950

[9] Ogata, K. (2016). Chapter 8, PID Controllers and Modified PID Controllers. In *Modern Control Engineering* (pp. 567–647). essay, Pearson.

[10] R., de R., Anton H. ;Damaren, Christopher;Forbes, James. (n.d.). Chapter 26. In *Spacecraft Dynamics and control*. essay, John Wiley & Sons, Incorporated.

[11] Schweber, B. (2022, March). *Reaction wheels ensure satellites maintain the right attitude: Part 1*. Microcontroller Tips. https://www.microcontrollertips.com/reaction-wheels-ensure-satellites-maintain-the-right-attitude-part-1-faq/

[12] *Series 4221 ... BXT R*. Dr. Fritz Faulhaber GmbH & Co. KG. (n.d.). https://www.faulhaber.com/en/products/series/4221bxtr/

[13] Siahpush , A., & Sexton, A. (1987). Conference Proceedings, 1st Annual USU Conference on Small Satellites. *A Study for Semi-Passive Gravity Gradient Stabilization of Small Satellites*.

[14] Siahpush, A., Utah, L., & Gleave, J. (1988). *A BRIEF SURVEY OF ATTITUDE CONTROL SYSTEMS FOR SMALL SATELLITES USING MOMENTUM CONCEPTS*.

[15] *Small satellites 101*. NanoAvionics. (2023, January 31). https://nanoavionics.com/small-satellites-101/

[16] Song, T., Wang, Q., Wu, M.-W., Ohtsuki, T., Gurusamy, M., & Kam, P.-Y. (2017). Impact of pointing errors on the error performance of Intersatellite Laser Communications. *Journal of Lightwave Technology*, *35*(14), 3082–3091. https://doi.org/10.1109/jlt.2017.2705132

[17] Teodoro, A. C., & Duarte, L. (2022). Chapter 10 - The role of satellite remote sensing in natural disaster management. In *Nanotechnology-based Smart Remote Sensing Networks for Disaster Prevention* (pp. 189–216). essay, ELSEVIER - HEALTH SCIENCE.

[18] Wikimedia Foundation. (2021, December 4). *Campbell diagram*. Wikipedia. https://en.wikipedia.org/wiki/Campbell_diagram

[19] Yin, X., Xu, Y., Sheng, X., & Shen, Y. (2019, November 18). *Signal denoising method using AIC–SVD and its application to micro-vibration in reaction wheels*. MDPI. https://www.mdpi.com/1424-8220/19/22/5032

[20] Zhang, Z. (2013). *Development and validation of microvibration models for a satellite reaction wheel assembly* (thesis). Original typescript.

[21] Zhang, Z., S. Aglietti, G., & Ren, W. (2013). Coupled microvibration analysis of a reaction wheel assembly including gyroscopic effects in its accelerance. *Journal of Sound and Vibration*, *332*(22), 5748–5765. https://doi.org/10.1016/j.jsv.2013.06.011

[22] Zhou, W.-Y., Aglietti, G. S., & Zhang, Z. (2011). Modelling and testing of a soft suspension design for a reaction/momentum wheel assembly. *Journal of Sound and Vibration*, *330*(18–19), 4596–4610. https://doi.org/10.1016/j.jsv.2011.03.028

[23] Bialke, B. Microvibration Disturbance Fundamentals for Rotating Mechanisms, 34th AAS Annual Guidance and Control Conference, Breckenridge, CO. USA, 2011

APPENDIX

Appendix A: Verification of Mathematical Model MATLAB Script

```
% Verification Mathematical Model RW system
% Author: Lillian Chen
% Assumptions:
% -RW is a cylinder
% -The body is seen as a rigid body
% -Mass of the RW is neglected to the overall body
% The body reference frame is not aligned with the principal axes
% Compare results against the simulation results

clear;clc;

% Initial Conditions of Spacecraft
m = 50;
a = 0.5;
V = 0.125;

A = [1 0 0; 0 1 0; 0 0 1];  % Wheel configuration

Ix = (1/6) * m * (a^2);
Iy = Ix;
Iz = Ix;

I = [Ix 0 0; 0 Iy 0; 0 0 Iz];

% Initial Conditions of Wheel
f = 20;
m_w = 0.5;
r_o = 0.05;
r_i = 0.04;
h = 0.04;

Iw_z = (1/2) * m_w * (r_o^2 + r_i^2);
Iw_xy = (1/12) * m_w * (3 * (r_o^2 + r_i^2) + h^2);

Iw = [Iw_z 0 0; 0 Iw_z 0; 0 0 Iw_z];

s = (f*2*pi)^2 * Iw_xy;

% Initial velocity of wheels
```

```
rpmw = [2000 0 0];
Ww_i = rpmw * (pi / 30);
aw = [0 0 0];
accw_i = [0 0 0];

% Initial velocity of satellite
deg_s = [0 0 0];
Ws = [0 0 0];
as = [0 0 0];
accs = [0 0 0];
theta = [0 0 0];

% Time frame
period = 70;
step = 0.1;
count = 1;
for t = 0:step:period

   if ((t > 0) && (t <= 10) && (count > 1))      % positive angular acceleration
      aw = [0 0 0];
      Ww(count, 1:3) = Ww(count-1, 1:3) + aw * (t - (t - step));
      accw(count, 1:3) = aw;

   elseif ((t > 20) && (t <= 30)&& (count > 1))     % negative angular acceleration
      aw = [0 0 0];
      Ww(count, 1:3) = Ww(count-1, 1:3) + aw * (t - (t - step));
      accw(count, 1:3) = aw;

   elseif ((t > 30) && (t <= 40)&& (count > 1))     % negative angular acceleration
      aw = [0 0 0];
      Ww(count, 1:3) = Ww(count-1, 1:3) + aw * (t - (t - step));
      accw(count, 1:3) = aw;

   elseif ((t > 40) && (t <= 50)&& (count > 1))     % negative angular acceleration
      aw = [0 0 0];
      Ww(count, 1:3) = Ww(count-1, 1:3) + aw * (t - (t - step));
      accw(count, 1:3) = aw;

   elseif ((t > 60) && (t <= 70)&& (count > 1))     % positive angular acceleration
      aw = [0 0 0];
      Ww(count, 1:3) = Ww(count-1, 1:3) + aw * (t - (t - step));
      accw(count, 1:3) = aw;
```

```
elseif (count == 1)
    Ww(1, 1:3) = Ww_i;
    accw(1, 1:3) = accw_i;

else                % no angular acceleration
    aw = [0 0 0];
    Ww(count, 1:3) = Ww(count-1, 1:3) + aw * (t - (t - step));
    accw(count, 1:3) = aw;

end

if (count > 1)
    H = I * Ws(count-1, 1:3)';
    H_dot = I * accw(count-1, 1:3)';

    Hw = Iw * Ww(count-1, 1:3)';
    Hww(count, 1:3) = Hw;
    Hw_dot = Iw * accw(count, :)';

    % Calculate the change in angular acceleration of spacecraft
    as = (cross(-Ws(count-1, 1:3), (I*Ws(count-1, 1:3)')) - (A*Hw_dot)' - cross(Ws(count-1, 1:3)', (A*Hw')))/ I;
    accs(count, 1:3) = as;

    Ws(count, 1:3) = Ws(count-1, 1:3) + as * step;
    theta(count, 1:3) = Ws(count-1, 1:3)*t + 0.5 * as * (t - (t - step))^2;

    % Calculate the generated torque Wheel 1
    ww1 = [Ww(count, 1) 0 0]';
    aw1 = [accw(count, 1) 0 0]';
    M1(count, 1:3) = (Iw*aw1) + cross(Ws(count-1, 1:3)', Iw(:,1).*ww1);
    T1(count, 1:3) = M1(count, 1:3) * s;

    % Calculate the generated torque Wheel 2
    ww2 = [0 Ww(count, 2) 0]';
    aw2 = [0 accw(count, 2) 0]';
    M2(count, 1:3) = (Iw*aw2) + cross(Ws(count-1, 1:3)', Iw(:,2).*ww2);
    T2(count, 1:3) = M2(count, 1:3) * s;

    % Calculate the generated torque Wheel 3
    ww3 = [0 0 Ww(count, 3)]';
    aw3 = [0 0 accw(count, 3)]';
    M3(count, 1:3) = (Iw*aw3) + cross(Ws(count-1, 1:3)', Iw(:,3).*ww3);
    T3(count, 1:3) = M3(count, 1:3) * s;
```

```
    end
    t = t + step;
    count = count + 1;

end

% Plot angular acceleration and angular velocity of reaction wheel
figure(1)
tiledlayout(3,1)

nexttile
plot((0:step:period), Hww(:, 1:3))
xlabel('time [s]'), ylabel('Angular Momentum [rad/s]')
legend('Wheel 1', 'Wheel 2', 'Wheel 3')
title('Angular momentum of Reaction Wheel vs Time')

nexttile
plot((0:step:period), Ww(:, 1:3))
xlabel('time [s]'), ylabel('Angular Velocity [rad/s]')
legend('Wheel 1', 'Wheel 2', 'Wheel 3')
title('Relative Angular velocity of Reaction Wheel vs Time')

nexttile
plot((0:step:period), accw(:, 1:3))
xlabel('time [s]'), ylabel('Angular Acceleration [rad/s^2]')
legend('Wheel 1', 'Wheel 2', 'Wheel 3')
title('Angular acceleration of Reaction Wheel vs Time')

% Plot angular acceleration and angular velocity of satellite
figure(2)
tiledlayout(3,1)

nexttile
plot((0:step:period), theta(:, 1:3)/(pi/180))
xlabel('time [s]'), ylabel('Angular Displacement [degree]')
legend('x-axis', 'y-axis', 'z-axis')
title('Anglular displacement of Satellite vs Time')

nexttile
plot((0:step:period), Ws(:, 1:3))
xlabel('time [s]'), ylabel('Angular Velocity [rad/s]')
legend('x-axis', 'y-axis', 'z-axis')
```

```
title('Angular velocity of Satellite vs Time')

nexttile
plot((0:step:period), accs(:, 1:3))
xlabel('time [s]'), ylabel('Angular Acceleration [rad/s^2]')
legend('x-axis', 'y-axis', 'z-axis')
title('Angular acceleration of Satellite vs Time')

% Plot the changes in the torque for wheel 1
figure(3)
tiledlayout(3,1)

nexttile
plot((0:step:period), M1(:, 1))
xlabel('time [s]'), ylabel('Momentum x-direction [Nm]')
title('Gyroscope Effect Wheel 1 (x-axis) vs Time')

nexttile
plot((0:step:period), M1(:, 2))
xlabel('time [s]'), ylabel('Torque y-direction [Nm]')
title('Gyroscope Effect Wheel 1 (y-axis) vs Time')

nexttile
plot((0:step:period), M1(:, 3))
xlabel('time [s]'), ylabel('Torque z-direction [Nm]')
title('Gyroscope Effect Wheel 1 (z-axis) vs Time')

% Plot the changes in the torque for wheel 2
figure(4)
tiledlayout(3,1)

nexttile
plot((0:step:period), M2(:, 1))
xlabel('time [s]'), ylabel('Torque x-direction [Nm]')
title('Gyroscope Effect Wheel 2 (x-axis) vs Time')

nexttile
plot((0:step:period), M2(:, 2))
xlabel('time [s]'), ylabel('Momentum y-direction [Nm]')
title('Gyroscope Effect Wheel 2 (y-axis) vs Time')

nexttile
plot((0:step:period), M2(:, 3))
```

```
xlabel('time [s]'), ylabel('Torque z-direction [Nm]')
title('Gyroscope Effect Wheel 2 (z-axis) vs Time')

% Plot the changes in the torque for wheel 3
figure(5)
tiledlayout(3,1)

nexttile
plot((0:step:period), M3(:, 1))
xlabel('time [s]'), ylabel('Torque x-direction [Nm]')
title('Gyroscope Effect Wheel 3 (x-axis) vs Time')

nexttile
plot((0:step:period), M3(:, 2))
xlabel('time [s]'), ylabel('Torque y-direction [Nm]')
title('Gyroscope Effect Wheel 3 (y-axis) vs Time')

nexttile
plot((0:step:period), M3(:, 3))
xlabel('time [s]'), ylabel('Momentum z-direction [Nm]')
title('Gyroscope Effect Wheel 3 (z-axis) vs Time')
```

Appendix B: Validation of Rigid Body Reaction Wheel Simulink Model MATLAB Script

```
% This script compares the result of the same input profile from a
% Mathematical model against the designed Simulink model for a rigid boday
% reaction wheel satellite configuration

% Intialise
clear
clc

Iw_xy = 5.79167e-4;

% Simulate the Rigid Body RW Configuration
deg_rigid = sim("Simulation_Rigid.slx", 30);
Time = deg_rigid.rigid.Time;
rigid = timeseries2timetable(deg_rigid.rigid);
rigid_quat = quaternion(rigid.Data);
rigid_rad = rotvec(rigid_quat);
rigid_rad = unwrap(rigid_rad, [], 1);
rigid_deg = rigid_rad * (180 / pi);

% MM
% Initial Conditions of Spacecraft
m = 100;
a = 0.5;
V = 0.125;

A = [1 0 0; 0 1 0; 0 0 1];  % Wheel configuration

Ix = (1/6) * m * (a^2);
Iy = Ix;
Iz = Ix;

I = [Ix 0 0; 0 Iy 0; 0 0 Iz];

% Initial Conditions of Wheel
m_w = 0.5;
r_o = 0.05;
r_i = 0.04;
h = 0.04;
```

```
Iw_z = (1/2) * m_w * (r_o^2 + r_i^2);
Iw_xy = (1/12) * m_w * (3 * (r_o^2 + r_i^2) + h^2);

Iw = [Iw_z 0 0; 0 Iw_z 0; 0 0 Iw_z];

% Initial velocity of wheels
rpmw = [0 0 0];
Ww_i = rpmw * (pi / 30);
aw = [0 0 0];
accw_i = [0 0 0];

% Initial velocity of satellite
deg_s = [0 0 0];
Ws = [0 0 0];
as = [0 0 0];
accs = [0 0 0];
theta = [0 0 0];

% Time frame
period = 30;
step = 0.001;
count = 1;

for t = 0:step:period

   if ((t > 0) && (t <= 10) && (count > 1))      % positive angular acceleration
      aw = [20.944 20.944 0];
      Ww(count, 1:3) = Ww(count-1, 1:3) + aw * (t - (t - step));
      accw(count, 1:3) = aw;

   elseif (count == 1)
      Ww(1, 1:3) = Ww_i;
      accw(1, 1:3) = accw_i;

   else                  % no angular acceleration
      aw = [0 0 0];
      Ww(count, 1:3) = Ww(count-1, 1:3) + aw * (t - (t - step));
      accw(count, 1:3) = aw;

   end

   if (count > 1)
```

```
        H = I * Ws(count-1, 1:3)';
        H_dot = I * accw(count-1, 1:3)';

        Hw = Iw * Ww(count-1, 1:3)';
        Hww(count, 1:3) = Hw;
        Hw_dot = Iw * accw(count, :)';

        % Calculate the change in angular acceleration of spacecraft
        as = (cross(-Ws(count-1, 1:3), (I*Ws(count-1, 1:3)')) - (A*Hw_dot)' - cross(Ws(count-1, 1:3)', (A*Hw)')) / I;
        accs(count, 1:3) = as;

        Ws(count, 1:3) = Ws(count-1, 1:3) + as * step;
        theta(count, 1:3) = Ws(count-1, 1:3)*t + 0.5 * as * (t - (t - step))^2;

    end
    t = t + step;
    count = count + 1;

end

% Plot the Movement of the satellite in both cases
figure(1)
plot(Time, rigid_deg(:, :), 'r')
hold on
plot((0:step:period), theta(:, 1:3)/(pi/180), 'b')

xlabel('Time [s]');
ylabel('Angular Displacement [deg]');
legend({'Rigid Model','','', 'Mathematical Model'}, 'Location', 'southeast');
title('Angular Displacement of Satellite with respect to Time');
grid on;

% Plot angular acceleration and angular velocity of satellite
figure(2)
tiledlayout(3,1)

nexttile
plot((0:step:period), theta(:, 1:3)/(pi/180))
xlabel('time [s]'), ylabel('Angular Displacement [degree]')
legend('x-axis', 'y-axis', 'z-axis')
title('Anglular displacement of Satellite vs Time')

nexttile
```

```
plot((0:step:period), Ws(:, 1:3))
xlabel('time [s]'), ylabel('Angular Velocity [rad/s]')
legend('x-axis', 'y-axis', 'z-axis')
title('Angular velocity of Satellite vs Time')

nexttile
plot((0:step:period), accs(:, 1:3))
xlabel('time [s]'), ylabel('Angular Acceleration [rad/s^2]')
legend('x-axis', 'y-axis', 'z-axis')
title('Angular acceleration of Satellite vs Time')

% Plot angular acceleration and angular velocity of reaction wheel
figure(3)
tiledlayout(3,1)

nexttile
plot((0:step:period), Hww(:, 1:3))
xlabel('time [s]'), ylabel('Angular Momentum [rad/s]')
legend('Wheel 1', 'Wheel 2', 'Wheel 3')
title('Angular momentum of Reaction Wheel vs Time')

nexttile
plot((0:step:period), Ww(:, 1:3))
xlabel('time [s]'), ylabel('Angular Velocity [rad/s]')
legend('Wheel 1', 'Wheel 2', 'Wheel 3')
title('Relative Angular velocity of Reaction Wheel vs Time')

nexttile
plot((0:step:period), accw(:, 1:3))
xlabel('time [s]'), ylabel('Angular Acceleration [rad/s^2]')
legend('Wheel 1', 'Wheel 2', 'Wheel 3')
title('Angular acceleration of Reaction Wheel vs Time')
```

Appendix C: Case Study (20 Hz and 4 Hz) MATLAB Script

```
% This script computes the angular displacement of the each wheels
% from the following case studies:
%
% 1. Extra Low Stiffness SoftSuspension (4Hz)
% 2. Low Stiffness SoftSuspension (20Hz)

% Intialise
clear
clc

Iw_xy = 5.79167e-4;



% Simulate the Rigid Body RW Configuration
deg_rigid = sim("Simulation_Rigid.slx", 30);
Time = deg_rigid.rigid.Time;

% Simunlate the 20Hz Soft-Suspension RW Configuration
f = 20;
s = (f*2*pi)^2 * Iw_xy; % Formula converting frequency to spring stiffness
d = 0.01;

deg_SS_20Hz = sim("Simulation_SS_20Hz.slx", 30);
wheel_1_20 = deg_SS_20Hz.wheel1.data;
wheel_2_20 = deg_SS_20Hz.wheel2.data;
wheel_3_20 = deg_SS_20Hz.wheel3.data;

% Simunlate the 4Hz Soft-Suspension RW Configuration
f = 4;
s = (f*2*pi)^2 * Iw_xy; % Formula converting frequency to spring stiffness
d = 0.01;

deg_SS_4Hz = sim("Simulation_SS_4Hz.slx", 30);

wheel_1_4 = deg_SS_4Hz.wheel1.data;
wheel_2_4 = deg_SS_4Hz.wheel2.data;
wheel_3_4 = deg_SS_4Hz.wheel3.data;

figure(1)
plot(Time, wheel_1_20)
hold on
```

```
plot(Time, wheel_2_20)
hold on
plot(Time, wheel_3_20)
hold off
xlabel('Time [s]');
ylabel('Angular Displacement [deg]');
legend({'wheel 1', 'wheel 2', 'wheel 3'}, 'Location', 'southeast');
title('Angular Displacement of each wheel in the y-axis of 20Hz RW with respect to Time');
grid on;

figure(2)
plot(Time, wheel_1_4)
hold on
plot(Time, wheel_2_4)
hold on
plot(Time, wheel_3_4)
hold off
xlabel('Time [s]');
ylabel('Angular Displacement [deg]');
legend({'wheel 1', 'wheel 2', 'wheel 3'}, 'Location', 'southeast');
title('Angular Displacement of each wheel in the y-axis of 4Hz RW with respect to Time');
grid on;
```

Appendix D: Pointing Error Comparison Between Different Reaction Wheel MATLAB Script

```
% This script compare the pointing error of the Satellite with different
% Reaction Wheels
% 1. Rigid Body
% 2. Extra Low Stiffness SoftSuspension (4Hz)
% 3. Low Stiffness SoftSuspension (20Hz)
% 4. High Stiffness SoftSuspension (200Hz)
%
% Time step: 0.001 [sec]
% Simulation Period: 30 [sec]

% Intialise
clear
clc

Iw_xy = 5.79167e-4;


% Simulate the Rigid Body RW Configuration
deg_rigid = sim("Simulation_Rigid.slx", 30);
Time = deg_rigid.rigid.Time;
rigid = timeseries2timetable(deg_rigid.rigid);
rigid_quat = quaternion(rigid.Data);
rigid_rad = rotvec(rigid_quat);
rigid_rad = unwrap(rigid_rad, [], 1);
rigid_deg = rigid_rad * (180 / pi);

% Simunlate the 20Hz Soft-Suspension RW Configuration
f = 20;
s = (f*2*pi)^2 * Iw_xy; % Formula converting frequency to spring stiffness
d = 0.01;

deg_SS_4Hz = sim("Simulation_SS.slx", 30);
SS_4 = timeseries2timetable(deg_SS_4Hz.ss);
SS_4_quat = quaternion(SS_4.Data);
SS_4_rad = rotvec(SS_4_quat);
SS_4_rad = unwrap(SS_4_rad, [], 1);
SS_4_deg = SS_4_rad * (180 / pi);

% Plotting the results of each simulation
figure(2)
```

```
tiledlayout(3,1)

nexttile
hold on;
plot(Time, SS_4_deg(:, 1), 'color', 'c');

nexttile
hold on;

plot(Time, SS_4_deg(:, 2), 'color', 'c');

nexttile
hold on;

plot(Time, SS_4_deg(:, 3), 'color', 'c');



% Simunlate the 4Hz Soft-Suspension RW Configuration
f = 4;
s = (f*2*pi)^2 * Iw_xy;     % Formula converting frequency to spring stiffness
d = 0;

deg_SS_4Hz = sim("Simulation_SS.slx", 30);
SS_4 = timeseries2timetable(deg_SS_4Hz.ss);
SS_4_quat = quaternion(SS_4.Data);
SS_4_rad = rotvec(SS_4_quat);
SS_4_rad = unwrap(SS_4_rad, [], 1);
SS_4_deg = SS_4_rad * (180 / pi);

% Simunlate the 20Hz Soft-Suspension RW Configuration
f = 20;
s = (f*2*pi)^2 * Iw_xy;     % Formula converting frequency to spring stiffness
d = 0;

deg_SS_20Hz = sim("Simulation_SS.slx", 30);
SS_20 = timeseries2timetable(deg_SS_20Hz.ss);
SS_20_quat = quaternion(SS_20.Data);
SS_20_rad = rotvec(SS_20_quat);
SS_20_rad = unwrap(SS_20_rad, [], 1);
SS_20_deg = SS_20_rad * (180 / pi);

% Simunlate the 200Hz Soft-Suspension RW Configuration
f = 200;
```

```
s = (f*2*pi)^2 * Iw_xy;     % Formula converting frequency to spring stiffness
d = 0;

deg_SS_200Hz = sim("Simulation_SS.slx", 30);
SS_200 = timeseries2timetable(deg_SS_200Hz.ss);
SS_200_quat = quaternion(SS_200.Data);
SS_200_rad = rotvec(SS_200_quat);
SS_200_rad = unwrap(SS_200_rad, [], 1);
SS_200_deg = SS_200_rad * (180 / pi);

% Finding the difference bewteen each simulation with rigid body
diff_x = rigid_deg(:, 1) - SS_20_deg(:, 1);
diff_y = rigid_deg(:, 2) - SS_20_deg(:, 2);
diff_z = rigid_deg(:, 3) - SS_20_deg(:, 3);

diff2_x = rigid_deg(:, 1) - SS_200_deg(:, 1);
diff2_y = rigid_deg(:, 2) - SS_200_deg(:, 2);
diff2_z = rigid_deg(:, 3) - SS_200_deg(:, 3);

diff3_x = rigid_deg(:, 1) - SS_4_deg(:, 1);
diff3_y = rigid_deg(:, 2) - SS_4_deg(:, 2);
diff3_z = rigid_deg(:, 3) - SS_4_deg(:, 3);

% Plot Graph
figure(1)
tiledlayout(3,1)

nexttile
hold on;
plot(Time, diff_x, 'color', 'r');
plot(Time, diff2_x, 'color', 'g');
plot(Time, diff3_x, 'color', 'b');
xlabel('Time [s]');
ylabel('Angular Displacement X-direction [deg]');
legend({'Rigid-20Hz', 'Rigid-200 Hz', 'Rigid-4Hz'}, 'Location', 'southeast');
title('Difference of Angular Displacement for each model with respect to Time (X-Direction)');
grid on;

nexttile
hold on;
plot(Time, diff_y, 'color', 'r');
plot(Time, diff2_y, 'color', 'g');
plot(Time, diff3_y, 'color', 'b');
```

```
xlabel('Time [s]');
ylabel('Angular Displacement Y-direction [deg]');
legend({'Rigid-20Hz', 'Rigid-200 Hz', 'Rigid-4Hz'}, 'Location', 'southeast');
title('Difference of Angular Displacement for each model with respect to Time (Y-Direction)');
grid on;

nexttile
hold on;
plot(Time, diff_z, 'color', 'r');
plot(Time, diff2_z, 'color', 'g');
plot(Time, diff3_z, 'color', 'b');
xlabel('Time [s]');
ylabel('Angular Displacement Z-direction [deg]');
legend({'Rigid-20Hz', 'Rigid-200 Hz', 'Rigid-4Hz'}, 'Location', 'southeast');
title('Difference of Angular Displacement for each model with respect to Time (Z-Direction)');
grid on;

% Plotting the results of each simulation
figure(2)
tiledlayout(3,1)

nexttile
hold on;
plot(Time, rigid_deg(:, 1), 'color', 'r');
plot(Time, SS_4_deg(:, 1), 'color', 'c');
plot(Time, SS_20_deg(:, 1), 'color', 'b');
plot(Time, SS_200_deg(:, 1), 'color', 'g');

xlabel('Time [s]');
ylabel('Angular Displacement [deg]');
legend('Rigid', '4Hz', '20 Hz', '200 Hz', 'Location', 'southeast')
title('Angular Displacement for each model with respect to Time (x-direction)');
grid on;

nexttile
hold on;
plot(Time, rigid_deg(:, 2), 'color', 'r');
plot(Time, SS_4_deg(:, 2), 'color', 'c');
plot(Time, SS_20_deg(:, 2), 'color', 'b');
plot(Time, SS_200_deg(:, 2), 'color', 'g');

xlabel('Time [s]');
ylabel('Angular Displacement [deg]');
```

```
legend('Rigid', '4Hz', '20 Hz', '200 Hz', 'Location', 'southeast')
title('Angular Displacement for each model with respect to Time (y-direction)');
grid on;

nexttile
hold on;
plot(Time, rigid_deg(:, 3), 'color', 'r');
plot(Time, SS_4_deg(:, 3), 'color', 'c');
plot(Time, SS_20_deg(:, 3), 'color', 'b');
plot(Time, SS_200_deg(:, 3), 'color', 'g');

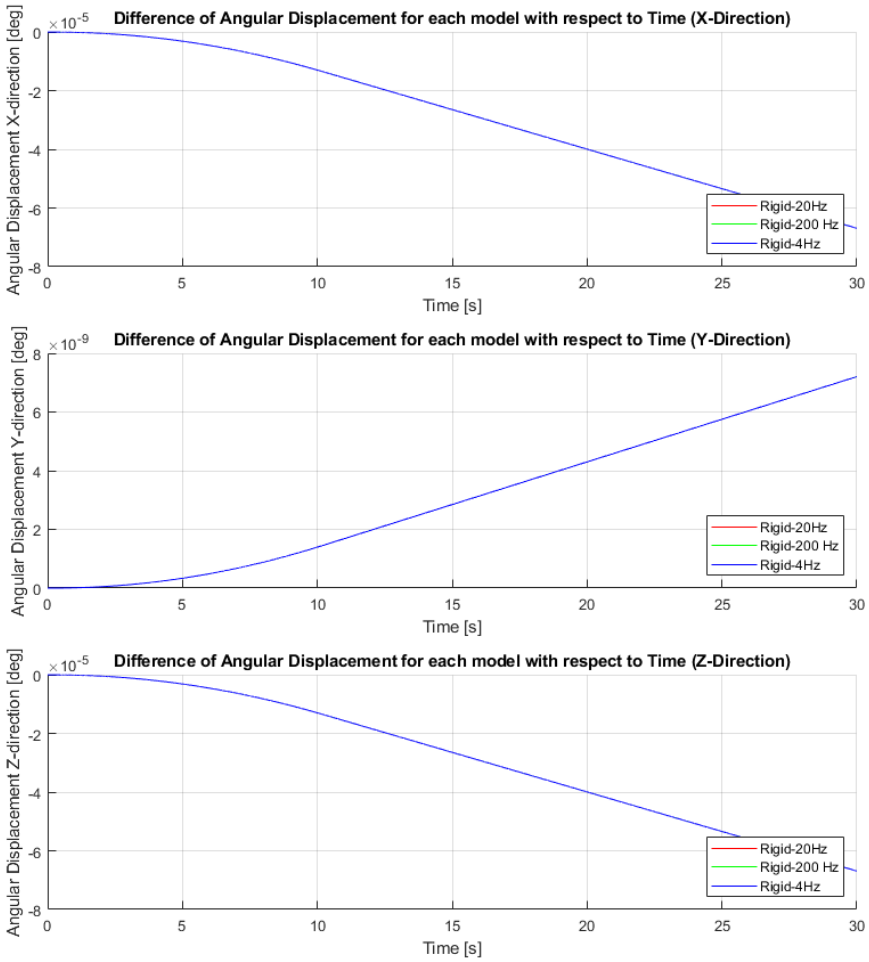
xlabel('Time [s]');
ylabel('Angular Displacement [deg]');
legend('Rigid', '4Hz', '20 Hz', '200 Hz', 'Location', 'southeast')
title('Angular Displacement for each model with respect to Time (z-direction)');
grid on;
```

Appendix E: Pointing Error Comparison Between Different Reaction Wheel Test Case 2

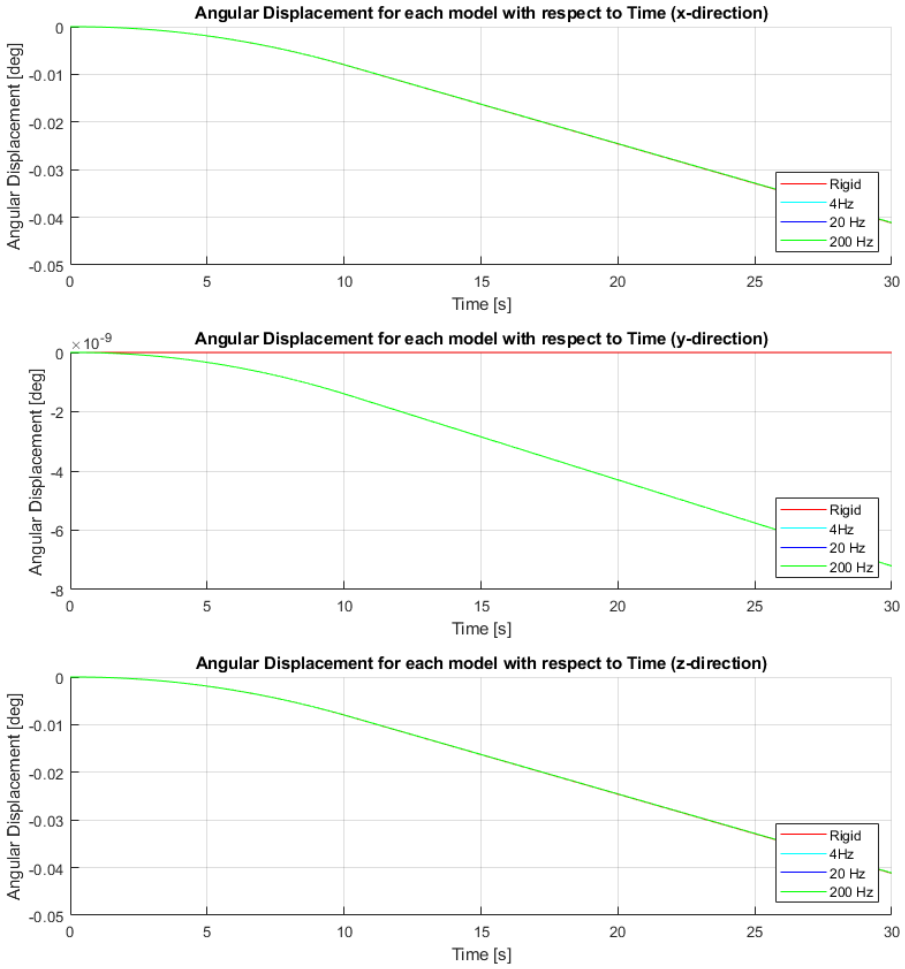
Initial Condition

	Value	Unit
Wheel 1 acceleration	0.01	rad/s^2
Wheel 2 acceleration	0	rad/s^2
Wheel 3 acceleration	0	rad/s^2
Satellite acceleration	0	rad/s^2
Wheel 1 velocity	0	rad/s
Wheel 2 velocity	0	rad/s
Wheel 3 velocity	0	rad/s
Satellite velocity	0	rad/s^2
Wheel 1 displacement	0	rad
Wheel 2 displacement	0	rad
Wheel 3 displacement	0	rad
Satellite displacement	0	rad

Results



Simualtion results of difference in angular displacement of the satellite with soft suspension reaction wheels (4 Hz, 20 Hz, 200Hz) with rigid body reaction wheels



Simualtion results of angular displacement of each of the satellite with soft suspension reaction wheels (4 Hz, 20 Hz, 200Hz) and rigid body reaction wheels

Appendix F: Pointing Error Calculation with Range of Different Frequencies MATLAB Script

```
            % This script compare the pointing error of the Satellite with different
% Reaction Wheels
% Compare the pointing error of a rigid body RW configuration satellite
% with the pointing error of different soft-supension RW configuration
% satellite (ranging from 1 Hz to 40 Hz with a step size of 1 Hz)
%
% Time step: 0.001 [sec]
% Simulation Period: 30 [sec]

% Intialise
clear
clc

Iw_xy = 5.79167e-4;

% Simulate the Rigid Body RW Configuration
deg_rigid = sim("Simulation_Rigid.slx", 30);
Time = deg_rigid.rigid.Time;
rigid = timeseries2timetable(deg_rigid.rigid);
rigid_quat = quaternion(rigid.Data);
rigid_rad = rotvec(rigid_quat);
rigid_rad = unwrap(rigid_rad, [], 1);
rigid_deg = rigid_rad * (180 / pi);

for f = 1:1:40
   hold on
   s = (f*2*pi)^2 * Iw_xy;     % Formula converting frequency to spring stiffness
   d = 0;

   % Simunlate the Soft-Suspension RW Configuration
   deg_SS = sim("Simulation_SS.slx", 30);
   SS = timeseries2timetable(deg_SS.ss);
   SS_quat = quaternion(SS.Data);
   SS_rad = rotvec(SS_quat);
   SS_rad = unwrap(SS_rad, [], 1);
   SS_deg = SS_rad * (180 / pi);

   % Finding the difference bewteen each simulation with rigid body
   diff_x = rigid_deg(:, 1) - SS_deg(:, 1);
   diff_y = rigid_deg(:, 2) - SS_deg(:, 2);
```

```
    diff_z = rigid_deg(:, 3) - SS_deg(:, 3);

    figure(1)

    hold on
    plot(Time, diff_x);
    xlabel('Time [s]');
    ylabel('Angular Displacement X-direction [deg]');
    title('Difference of Angular Displacement for each model with respect to Time (X-Direction)');
    grid on;

    figure(2)
    hold on
    plot(Time, diff_y);
    xlabel('Time [s]');
    ylabel('Angular Displacement Y-direction [deg]');
    title('Difference of Angular Displacement for each model with respect to Time (Y-Direction)');
    grid on;


    figure(3)
    hold on
    plot(Time, diff_z);
    xlabel('Time [s]');
    ylabel('Angular Displacement Z-direction [deg]');
    title('Difference of Angular Displacement for each model with respect to Time (Z-Direction)');
    grid on;

end

hold off
```

Appendix G: Study of Campbell Diagram MATLAB Script

```
% This script calculates the natural frequencies of the Soft-suspension
% reaction wheel at different rpm

clear all
close all
clc
```

Wheel Initialisation

```
m = 0.5;              % Wheel mass  [Kg]
r = 0.05;             % Wheel radius [m]
D = 0.025;            % shaft diameter [m]
```

Inertia wheel and properties

```
Iz = 0.001;               % vertical inertia of the wheel Kg/m^2
Ir = 5.7917e-4;           % radial inertia of the wheel Kg/m^2

f = 4;                    % frequency of the wheel
k = (f*2*pi)^2 * Ir;      % stiffness of the wheel

for w = 0:0.5:(2800*2*pi/60)

% Equation: x^4 - w*(Iz/Ir)*x^3 - ((k/m)+(k+k*D^2)/Ir)*x^2 + w*((k*Iz)/(m*Ir))*x + (k^2/(m*Ir));
   coefvct = [1 -w*(Iz/Ir) -((k/m)+(k+k*D^2)/Ir) w*((k*Iz)/(m*Ir)) (k^2/(m*Ir))];  % Coefficient Vector
   x = roots(coefvct);    % Solution
   x = abs(x);

   figure(1)
   plot(w/(2*pi/60), x/(2*pi),'.');hold on;
end

% Plotting the diagram
title('Campbell Diagram');
xlabel('Rotation [rpm]');
ylabel('Frequency [Hz]')
```

Appendix H: Controller gain Calculation and Simulation MATLAB Script

```
% This script runs the simulation of a three soft-suspension reaction wheel
% satellite configuration with a PID controller
% Author: Lillian Chen

close all
clear all
clc
```

Initialisation for satellite system

```
Iw_xy = 5.79167e-4;        % Inertia of the ss wheels
f = 20;                    % Frequency of the ss wheels
s = (f*2*pi)^2 * Iw_xy;    % Formula converting frequency to spring stiffness
d = 0;                     % Damping coefficient
```

Defining Gains - Ziegler-Nichols PID tuning method

```
Ku = 32;              % Ultimate Gain
Tu = 0.45;            % Ultimate Period

% PID controller variables
Kp = 0.6*Ku;
Ki = 1.2*Ku/Tu;
Kd = 0.075*Ku*Tu;

K_gain = -0.015;      % Tuned gain due to non-linearity of plant
```

Run Simulation

```
result = sim('Controller_Rigid.slx', 10);
time = result.tout;

% Rigid body simulation results
rigid = timeseries2timetable(result.Q_out);
rigid_quat = quaternion(rigid.Data);
rigid_rad = rotvec(rigid_quat);
rigid_rad = unwrap(rigid_rad, [], 1);
rigid_deg = rigid_rad * (180 / pi);
```

```
% Reference Tracjectory
ref = timeseries2timetable(result.ref);
ref_deg = ref.Data * (180 / pi);
```

Plot Results

```
figure(1)
plot(time, ref_deg, 'r'),
hold on
plot(time, rigid_deg, 'b')
xlabel('time [seconds]'),
ylabel('y-axis [deg]'),
legend('Reference Tracjectory','','', 'Actual Tracjectory - Rigid Body','', ''),
title('Evaluation of a PID controller performance to compensate pointing error');
grid on;
```